A Network Synthesis Based Approach for Frequency Dependent Network Equivalents

By

MEYSAM AHMADI

A Thesis submitted to the Faculty of Graduate Studies of
The University of Manitoba
in partial fulfillment of the requirements of the degree of

Doctor of Philosophy

Department of Electrical and Computer Engineering
University of Manitoba
Winnipeg, Manitoba

THE UNIVERSITY OF MANITOBA
FACULTY OF GRADUATE STUDIES
****
COPYRIGHT PERMISSION

"A Network Synthesis Based Approach for Frequency Dependent Network Equivalents"

By

MEYSAM AHMADI

A Thesis submitted to the Faculty of Graduate Studies of
The University of Manitoba
in partial fulfillment of the requirements of the degree of

Doctor of Philosophy

Department of Electrical and Computer Engineering
University of Manitoba
Winnipeg, Manitoba

Author's Declaration

I hereby declare that I am the sole author of this thesis. This is a true copy of the thesis, including any required final revisions, as accepted by my examiners. I understand that my thesis may be made available to the public electronically.

Abstract

Transient simulation of large electric power systems is resource-intensive and it is often prohibitive to model the entire network in the simulator. To save computational resources, only a part of the network is modelled in detail and the remainder is modelled as an equivalent from the point of connection. To derive this equivalent, a frequency scan of the network portion is obtained either through measurements made on the actual network or via measurements on a highly detailed simulation model; and stored as a table of frequency versus impedance (magnitude and phase). Such a model is called a Frequency Dependent Network Equivalent (FDNE). Using curve-fitting, the frequency scan is fitted by a rational function, which can then readily be converted into a time-domain simulation model. Using the FDNE instead of modelling a whole network in detail, greatly reduces the computer simulation time, which is critical, and reduces the cost of computing resources particularly in real-time simulators. One of the major challenges in the current state of the art in implementing FDNEs is that the fitted rational function is often not passive. In other words, the model generates energy in some ranges of frequencies which may lead to instability in the simulation.

In this work, a new method is explored to go directly from the frequency scan (tabulated function) to the time domain model without fitting the response by rational functions. In this technique, using network realization methods, an electric network made up of RLC branches and ideal transformers are used to fit the response while preserving the passivity of the network. Brune's realization method for the single-port network and Tellegen's extension for multi-port networks are adapted to implement numerically on tabulated functions. The most desirable feature of these techniques is that the realized network is always passive. So, unlike the current methods, there is no possibility whatsoever of violation of passivity in the resulted network.

Acknowledgments

First and foremost, *Allah SWT*, the almighty, shall be praised and thanked, for granting me the endless blessing and endowment, and countless knowledge and opportunities. *"This is by the grace of my Lord to test me whether I am grateful or ungrateful. And whoever is grateful, it is only for their own good. But whoever is ungrateful, surely my Lord is Self-Sufficient, Most Generous." The Holy Quran, 27:40.*

***

I would like to express my sincerest appreciation to my advisor, *Prof. Aniruddha Gole*, for his invaluable guidance and continuous supports throughout this work. I am very thankful to *Prof. José R. Martí* for carefully reading the thesis and providing very insightful comments. Also thanks to *Prof. Madjid Birouk* and *Prof. Shaahin Filizadeh* for being part of my Ph.D. examination committee and help me complete this journey.

I am also grateful to *Dr. Dharshana Muthumuni*, *Dr. Rohitha Jayasinghe*, and *Dr. Jeewantha De Silva* of Manitoba Hydro International for their help and technical supports.

In addition to my fellow Ph.D. and M.Sc. students, *Dr. Shengtao Fan* and *Dr. Huanfeng Zhao* should also be thanked for their great suggestions and fruitful discussions throughout the years.

Dedication

This work would have not been finished without the immense support and love of my family. Therefore, I would like to dedicate this thesis to my wife, *Zohreh* and my son *Sadra* for bearing with me during this endeavour. I am also thankful to my parents for their encouragement and prayers, without, I could never succeed.

This thesis is also dedicated to all the souls that were sacrificed to enlighten the path of truth and knowledge in the history of humanity.

Contents

List of Figures

List of Tables

List of Principle Symbols

s	Complex variable of Laplace transform
j	Complex number equal to $\sqrt{-1}$
ω	Angular frequency (*rad/sec*)
$z(s)$	's' domain scalar function of impedance
$y(s)$	's' domain scalar function of admittance
k_x	Residue of the pole of a scalar function at frequency ω_x
$z(j\omega)$	Tabular function of impedance
$y(j\omega)$	Tabular function of admittance
$\Re$	Real part of a function
$\Im$	Imaginary part of a function
ω_m	Frequency at which the minimum real part occurs
n	Number of ports and also size of the square matrix of multi-port functions
$Z(s)$	's' domain impedance matrix
$Y(s)$	's' domain admittance matrix
K_x	Matrix of residue of the pole of a multi-port function at frequency ω_x
$Z(j\omega)$	Tabulated function of $n \times n$ impedance matrix
$Y(j\omega)$	Tabulated function of $n \times n$ admittance matrix

Chapter 1

Introduction

In this chapter, an overview of the Frequency Dependent Network Equivalent (FDNE) concept, its background, and applications are illustrated through a literature review. Different methods of modeling FDNEs in Electromagnetic Transient (EMT) type programs are discussed and finally, gaps in the current methods and the core idea of this work are elaborated.

1.1 Background

Transient simulation of power systems has always been essential for an accurate study of a different phenomenon, e.g., over-voltages, switching capacitors or inductors, faults, lightning surges, inrush currents, High Voltage Direct Current (HVDC), and Flexible Alternative Current Transmission Systems (FACTS) devices, etc. [3–10] in the network. To get the exact and realistic simulation result, it is necessary to have tools that provide precise and stable models for every element in power systems.

Basic network elements, e.g., RLC branches, Lossless transmission lines, transformers, etc. were modeled by Dommel in [11] for Electromagnetic Transient (EMT) type programs. However, more complicated pieces of networks, e.g., lossy transmission lines and cables [12–14], FDNEs, etc. are still being under improvement. The intense focus on FDNEs in the literature shows that accurate modeling of FDNEs is still one of the most challenging

problems for the EMT programs [15–23].

1.1.1 FDNE Concept

In the transient simulation, FDNEs provide smaller and more compact equivalents of large electrical power systems to save computational resources [24]. They are also used to model pieces of networks given as a black-box [25]. One of the special applications of FDNEs is in real-time simulators where it is crucial to decrease the details of unnecessary parts of the network to both speeds up the simulation and reduce computation cost [26].

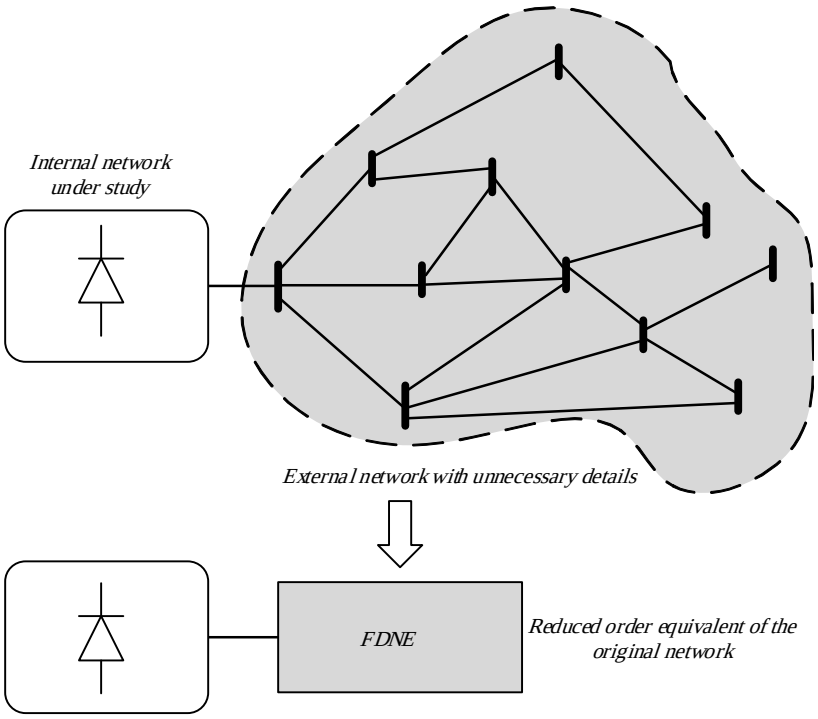

Figure 1.1: Conceptual representation of FDNE.

Figure 1.1 shows the conceptual representation of FDNE of an external highly detailed network connected to an internal network that is of interest. To build the FDNEs, a frequency scan of the network portion is performed either through measurement made on the actual network or via calculation on a highly detailed circuit model of the network.

1.1.2 Scanning the Detailed Network

A frequency scan of the network can be conducted by injecting a current (or voltage), which contains several frequencies, at the point of interest, and measuring the voltage (current). Then using the discrete Fourier series of the output voltage and taking the ratio of voltage by the current at each frequency, the impedance of the network can be calculated. In this method, the signal amplitude must be sufficiently small so that it will not interfere with the operating points of nonlinear parts of the network [27]. Alternatively, many EMT programs (e.g. PSCAD) are able to give the node admittance matrix of the whole network at each frequency, and then by removing the internal nodes with respect to the input terminals, the admittance matrix seen at the terminal can be calculated.

The PSCAD scan module considers the following situation when performing the scan of a network:

- Transformer saturation and arresters are assumed to be in their unsaturated region.
- All the power electronic devices are assumed to be in their OFF state.
- Synchronous and Induction Machines are represented as a grounded inductor.
- The 0-sequence impedance of an SVC is represented as the primary-delta leakage reactance of the transformer, and the $+/-$ sequence impedance is represented by the defined shunt loss conductance.
- The minimum frequency to calculate system impedance is 1 mHz. Therefore, DC resistance is not computed.

When the frequency scan is obtained, it is stored as a table of frequency versus impedance (magnitude and phase) as a tabulated function. Then, using fitting methods, the tabulated function is fitted with a smaller order RLC network [3–5, 9] approximating the frequency response or alternatively, a purely mathematical model using a rational function of the Laplace transform variable 's' and implemented as an impedance element in the EMT program [28, 29]. Finally, the reduced network or the rational function can readily be converted

into a time domain simulation model either by RLC branches or by means of recursive convolution of exponential terms. Therefore; a compact mathematical or circuit model of tabulated function can be used in the EMT program to mimic the transient behavior of those portion of the network.

It is worth mentioning that in this manuscript the term FDNE refers to a model for a Linear Time Invariant (LTI) network. Therefore any non-linearity in the network must be either small enough to be ignored (or linearized) or left outside of the FDNE model and considered as an external network connected to one of the inputs. The necessary and sufficient condition for a network to be LTI is that the scanned impedance from the terminal must be a Positive Real (PR) function. PR functions and their properties are explained in Appendix A.

In this work, it is assumed that the original scanned data is a PR impedance. However, it is possible sometimes that, particularly with the field measurement data, due to the measurement error, the scanned data itself is not PR at some frequency samples. This is usually not known as a priory but becomes evident when for example a negative resistor value is encountered in the synthesis. In such cases, a pre-processing step (e.g. uniform eigenvalue-shift perturbation, least diagonal perturbation, least-eigenvalue perturbation, least-norm perturbation) should be performed in order to rectify the issue on those frequency sample [30].

1.1.3 Earlier Methods on Modeling the FDNEs

Trying to model frequency dependency of the networks in power system transient simulations goes back to as early as 1970 when Hingorani fitted the frequency response plot of the original external network interconnected to HVDC links with several parallel RLC branches, whose combined impedance matches the driving point impedance [4]. Also, the need to have a more accurate equivalent network of power systems for switching surge studies made Clerici [5] do similar work using RLC approaches. Clerici used the fixed topology of the First type of Foster circuit [31] and computed the values for RLC branches to match the main resonances of the impedance of the original network [5].

Later in the '70s, Snelson [32] introduced a method based on traveling waves to model frequency-dependent transmission lines , Meyer and Dommel [33] used Fourier transformation , Marti in [34] used Foster I circuit synthesis [31], and Semlyen [35] used recursive convolution to consider frequency dependency of lossy transmission line for the EMT program.

In the 1980's, a wideband frequency model of transmission network equivalent was introduced by Morched [10] using RLC parallel branches, and considering series and parallel resonance in the network response scan. Que Do and Gavrilovic [7,8] have also tried to curve fit the FDNE model using iterative pole removal technique and least-squares fitting method and then implement through the RLC network realization in time domain .

In another approach to consider frequency dependency of power system network in time domain simulations Watson et al. [9] developed equivalent RLC branches for harmonic analysis. Using multi-variable optimization methods, the frequency responses of self and mutual impedances were fitted by an RLC network. The method only concentrated on voltage and current harmonics study at the HVDC terminals and was not accurate over a very wide range of frequencies.

The word FNDE seems to be firstly used by Morched et al. [3] where they developed a method to make a reduced-order model of a multi-port frequency-dependent network utilizing RLC equivalent circuit in which RLC branches are found through an optimization process. The same group of authors also presented a high-frequency transformer model by first approximating the admittance of the transformer by rational functions and then realized it in the form of an RLC network which could be directly used in EMT programs [6].

In a study [36], a *pi*-type network is used to realize a low order equivalent of the admittance matrix of a network which is first fitted using rational functions and non-constraint optimization program.

In the late 1990s, a mathematical method, Vector Fitting (VF) was introduced by Gustavsen and Semlyen in [28] and later improved by Gustavsen [37]. VF utilizes rational functions of the form (1.1) to fit the scanned data. With some techniques, VF changes the

equations of the unknowns to a linear form of $Ax = b$. Then the the unknowns, i.e., poles and residues can be found by solving a least-squares problem out of an over-determined linear problem.

$$Z(s) = \sum_{n=1}^{N} \frac{c_n}{s + a_n} + d + sh \tag{1.1}$$

The functionality of the VF method is also verified by accurate modeling of overhead transmission lines [38]. VF is also used for a universal model of transmission lines and cables [39]. Currently, VF is widely used in EMT programs and is developed extensively through several research work [1, 38–45].

The Modified Matrix Pencil method is another approach to determine the poles and residues of (1.1). In this approach, a frequency domain matrix pencil method is developed which, utilizes Vandermonde matrices and Moore–Penrose pseudoinverse technique to find poles, a_n, and QR decomposition to solve a least square problem for calculating residues, c_n [2].

The major issue with the mathematical approaches is the passivity problem. Sometimes the fitted function violates the passivity criteria which means the model can generate energy in some frequency ranges. This should not happen if the original network is passive. To overcome this problem, a further step is often applied in order to enforce the passivity to the mathematical function. This is addressed in the last section of this chapter.

1.2 FDNEs Applications

FDNEs can be used in several applications in transient simulation tools which are briefly explained in this section.

1.2.1 Reducing The Order of Electric Networks

In transient studies, it usually happens that a large linear electric network with too many details is connected to a nonlinear circuit such as a High Voltage Direct Current (HVDC) link,

or a switching time-varying circuit, etc. In such cases, using FDNEs, the original network can be simulated with accurate enough and smaller order model. Sometimes the model is limited to the range of frequencies of interest by ignoring those parts of the response at other frequencies. This will help to accelerate the simulation and lessen the complexity [1, 46–50].

1.2.2 Real Time Simulation

Transient simulations in real-time are becoming more popular especially for testing power system apparatus, e.g., relays and controllers in a semi-realistic situation. Currently, there are several real-time EMT tools such as HYPERSIM, OPAL-RT, and Real-Time Digital Simulator (RTDS) [51]. Real-time simulators finish all the necessary calculations within a single time step, synchronized with a real-world clock. In many cases, due to large network matrices and complicated calculations, e.g., large matrix inversion, it will become impossible to have all the network simulation done in a single step.

With the help of FDNEs, the network can become smaller and real-time simulation becomes possible. Besides, the larger network means more processing units in the simulator and this proportionally increases the cost [26]. Therefore, FDNEs can also reduce the monetary cost of the simulation.

1.2.3 Wide Band Transformer Modeling

Transformers have peculiar behavior at high frequencies phenomenon. So, it is vital to consider their wideband frequency response in transient studies. To create a wideband response of the transformers in EMT studies, they are modeled by a frequency dependent black-box and then fitted using a similar concept as of FDNEs [6, 29, 52].

1.2.4 Hybrid Simulations

In some applications, FDNEs are used to perform hybrid simulations like RTDS-TSA interconnections. In [21], real-time digital simulator simulates an HVDC, a transient stability

analysis (TSA) program models the ac side of the network, and FDNEs are used to model the frequency dependency of the ac part. Reference [5] shows another earlier example of hybrid simulation where a transient network analyzer (TNA) is connected with digital computers for switching surge studies. In [53] a seamless-link hybrid simulation of RTDS and a dynamic simulation system is studied.

1.3 Approaches in FDNE Modeling in EMT Programs

Modeling FDNEs in EMT programs can be generally categorized into two main approaches; "Network Fitting" and "Mathematical" approaches, which are explained in this section.

1.3.1 Network Fitting Approaches

Earlier methods for developing FDNEs were based on network fitting techniques where predetermined network elements are found so that the impedance fits the scanned data. In [4] a fixed parallel RLC structure is considered with the resonance frequencies matching those of the network scan. It was only proper for low order function, e.g., three to four parallel RLC branches. Clerici [5] used Foster Type I circuits as shown in Figure 1.2. Then by disregarding resistances, LC components are calculated based on specific resonance frequencies of the scanned network. Obviously, this method is only accurate on a few certain frequencies.

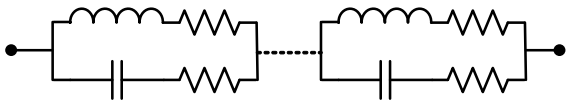

Figure 1.2: Foster Type I circuit.

Marti [34], used Bode's procedure [54] to model frequency dependent characteristic impedance of a transmission line in the time domain. The tabulated function is approximated by assigning zeros and poles at proper frequencies and a rational function is formed. Then it is expanded into partial fractions of the form (1.2).

$$Z_{eq}(s) = k_0 + \frac{k_1}{s + p_1} + \frac{k_2}{s + p_2} + \cdots + \frac{k_n}{s + p_n} \tag{1.2}$$

The partial fractions then can be readily realized utilizing series combination of parallel RC components using Foster I synthesis method. Figure 1.3 shows the equivalent circuit of the $Z_{eq}(s)$in which $R_0 = k_0, R_i = k_i/p_i$ and $C_i = 1/k_i$.

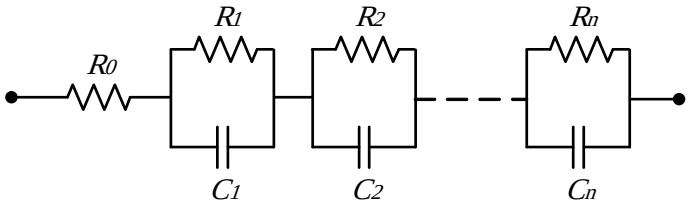

Figure 1.3: Foster I equivalent circuit for transmission line characteristic impedance.

The above-mentioned method works very well for smooth functions but will cause a large number of poles and zeros for the cases in which the frequency response has many resonance peaks (such as cable systems and filters). This effect will lower the simulation speed and make it inefficient.

Brune's network realization method [55] was also used in modeling microwave circuits by first utilizing vector fitting to create the "s" domain rational function and then realizing the rational functions [56–60]. Since in this approach the data is first fitted by VF, the passivity of the both function and the realized network remains as a concern.

1.3.2 Mathematical Fitting Approaches

One of the earliest mathematical approaches to model FDNEs was by Van Que Do [7] who used the least-square curve fitting with iterative pole removal technique. Gustavsen and Semlyen [37] introduced a straightforward mathematical approach to fit non-smooth frequency responses by means of Vector Fitting (VF). In vector fitting, the fitted function is assumed to be in the form of (1.3) and the problem of fitting becomes a linear least-square optimization. So, by relocating the poles and after some iteration, the function $Y_{eq}(s)$ will

be fitted to the tabulated function. VF is explained in Appendix C in more detail.

$$Y_{eq}(s) = \sum_{n=1}^{N} \frac{c_n}{s + a_n} + d + sh \tag{1.3}$$

Then the function in 1.3 can be implemented in the EMT type program by means of recursive convolution [35] as mentioned earlier in this chapter. Also, another way to implement the function $Y_{eq}(s)$ in the EMT program is using the equivalent RLC branches as shown in Figure 1.4 suggested in [61].

Modified Matrix Pencil Method is also another approach to find the poles and residues of the fitted function in (1.3) introduced in [2].

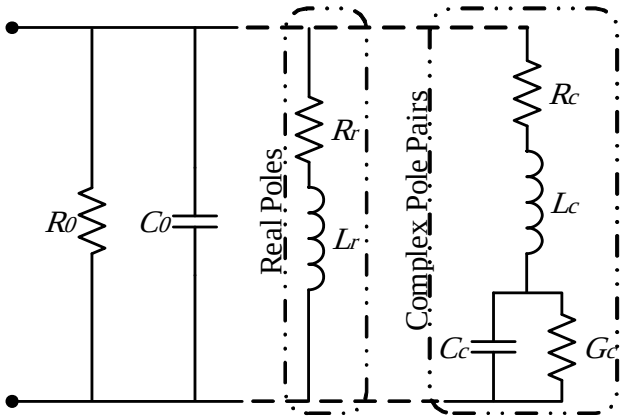

Figure 1.4: Realizing a network for partial fraction admittance function

1.4 Gaps in the Current Methods and Objective of this Work

The earlier methods of implementing FDNEs in EMT programs which were based on equivalent RLC branches are mostly able to only fit the resonance frequencies and do not always give an accurate fit over a wide band of frequencies. Also, they were meant to be used in very basic computers with limited processing capabilities. Thus their relevance is limited in current applications and also with much faster processing units that are available in the

market.

In contemporary simulation tools, vector fitting is used to derive a rational function approximation. As briefly mentioned in the previous sections, VF sometimes results in passivity violation which may cause unstable simulation. By definition, passive networks should not create energy if they do not contain any kind of power source. But, when fitting the impedance of the network (FDNEs) using mathematical functions, the fitted function in some range of frequencies may show non-passive behavior. It means the fitted function generates energy at those frequencies which is physically impossible. To avoid this, the fitting procedure must be closely monitored and modified if necessary to ensure that the fitted function is passive. However, this procedure is not always successful and results in either accuracy loss in the fitting or passivity violations in other regions of the spectrum. Several methods are introduced to do passivity enforcement. These methods have the cost of losing the accuracy of the fitting. Thus, there must be a compromise between the accuracy and passivity of the fitted function. [62–69]. Some of these passivity enforcement methods do not guarantee global passivity of the model while others require a large computational burden i.e. memory and processing units, thus are not efficient [15].

Although network synthesis was investigated mostly in the earlier part of the 20^{th} century, when computers were unavailable, but very little research has been done in the past quarter-century. As a general idea, looking back to the classical methods can help find possible benefits in combination with fast computation which is accessible via contemporary computers. This could solve some of the problems which arise in today's state of the art such as passivity issue in power system simulation tools.

The main objective of this work is to develop a new technique based on a network realization approach which intrinsically does not create passivity violation. Network realization approaches by Brune [55] and Tellegen [70] guarantees the passivity of the network and can fit any type of frequency responses over a wide band of frequencies with a minimum number of elements. Therefore, the new technique will also inherently preserve the passivity of the fitted networks. Also, RLC networks can be easily implemented in EMT type programs in

a compact way either by means of companion circuits or state-space models.

The main challenge of this work is that Brune and Telleng's ideas are developed for a given s-domain function, $Z(s)$, while in the cases of FDNEs only $Z(j\omega)$ is available at some sample points in form of a tabulated function.

1.5 Overview of the Thesis

There are six chapters in this dissertation. In Chapter 2, details of some renowned classical network realization methods and their properties are discussed and Brune's network synthesis approach is illustrated in more detail. Chapter 3 of this thesis is dedicated to adopting Brune's idea for the numerical implementation of tabulated functions. Also, simulation cases are provided to confirm the functionality of the new approach. Multi-port networks application using modified Tellegen's approach is also discussed in Chapter 4. Chapter 5 includes the time-domain implementation of the proposed realization-based approach. Chapter 6 summarizes the contributions of the thesis and provides the conclusion and some suggestions for future work.

Chapter 2

Review of Classical Network Realization Methods

The core idea of this work is to develop a network synthesis based approach to model FDNEs such that the passivity is preserved. To do so, a search has been carried out among the classical network realization methods and their characteristics. The methods are also investigated and examined for having the following properties in order to be feasible to serve in the intended scheme of this work:

- The realization method must preserve the passivity.
- It must be capable of being applied to the tabulated function.
- The algorithm should be feasible for computerization.
- The preferred method should realize a circuit with a minimum number of elements.

This chapter includes a brief survey on several methods with a focus on the above-mentioned properties. Brune's realization method is seen to satisfy all the conditions stated above for the purpose of this work. Thus, details of Brune's original idea is explained in this chapter. The modification and numerical application on the tabulated functions will be discussed in the next chapter.

2.1 Review: Classical Network Realization Methods

Classical network realization methods can be categorized in different ways such as type of elements used in the network, the number of ports, class of functions, and their canonical network type that include Series, Parallel, Lattice, Tandem, Ladder. Some of the well-known methods are described below.

2.1.1 Foster Synthesis

Foster used combinations of series anti-resonant circuits (Type I) and parallel resonant circuits (Type II) to construct networks for realizing a driving point impedance (or admittance) function as shown in Figure 2.1 [31]. Although Foster's idea was to realize a resistance-less reactance network (only containing L and C), Cauer [71] extended it to RC and RL networks. Given the admittance or impedance function and considering its resonant and anti-resonant points, elements of the network are calculated by partial fraction expansion of the function.

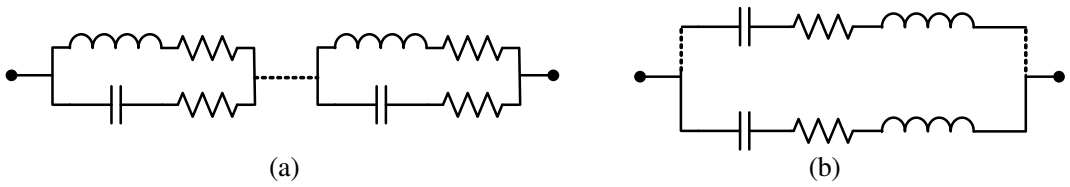

Figure 2.1: Foster Type I (a) and type II (b) circuits.

Although this is inherently passive and gives the minimum number of elements [31], it can not be applied to tabulated functions as it was developed for synthesizing transfer functions $N(s)/D(s)$. The method needs to create the partial fractions of the s domain impedance (or admittance) function to calculate the elements. Also, it is limited to single port networks only.

2.1.2 Cauer Synthesis

Cauer [71] used ladder networks to realize single port driving point impedance $z(s)$. He first converted the function $z(s)$ in the form of a continued fraction expansion as shown in (2.2),

then the impedances and admittances z_1, y_2, z_3, y_4 are realized via the elements labeled in the Figure 2.2.

$$z(s) = z_1 + \cfrac{1}{y_2 + \cfrac{1}{z_3 + \cfrac{1}{y_4 + \ldots}}} \tag{2.1}$$

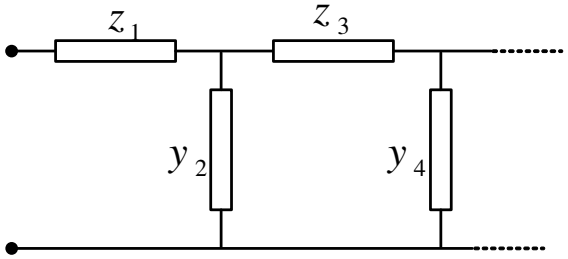

Figure 2.2: Ladder network used in the Cauer realization method.

As in the case of Foster and Cauer, this kind of expansion can only be applied to s domain rational function and not to tabulated functions. Therefore no matter what other properties has this method, it can not be used in the scheme of this work.

2.1.3 Darlington Synthesis

Darlington used a two-port lossless network terminated in a resistance as shown in Figure 2.3 to realize an impedance function $z(s) = P(s)/Q(s)$. Then using some mathematical decompositions and manipulations, he shows how to realize the lossless network [72].

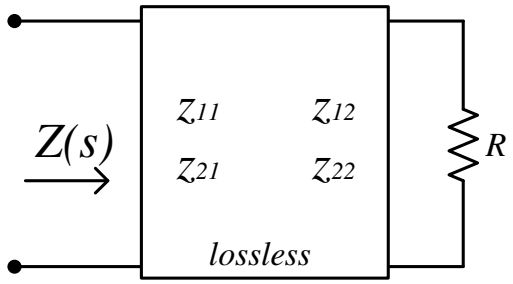

Figure 2.3: Darlington network.

Consider $P(s) = m_1 + n_1$ and $Q(s) = m_2 + n_2$ in which $m_{1,2}$ are the real part and $n_{1,2}$ are the imaginary part of the corresponding functions. In order to realize the lossless

network, Darlington uses m_1/n_2, m_2/n_2 and $\sqrt{m_1.m_2 - n_1.n_2}/n_2$ functions for z_{11}, z_{22} and z_{12} respectively. Obviously this type of decomposition is not possible in case of tabulated functions, thus can not be applied directly to such functions.

2.1.4 Bode Synthesis

Bode uses lattice type of network to realize a two port network for the given function $z(s)$ as shown in Figure 2.4 in which $z_a = z_{11} - z_{12}$ and $z_b = z_a = z_{11} + z_{12}$. Then realization of each one of z_a and z_b is done via partial fraction expansion similar to what Cauer did [54]. Thus for the same reason not applicable to tabulated functions.

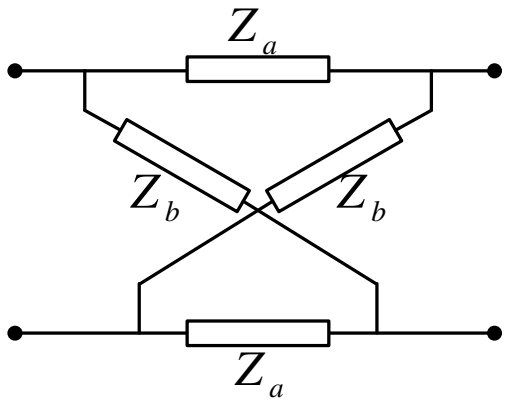

Figure 2.4: Lattice network.

2.1.5 Bott-Duffin Synthesis and Other Methods

Bott-Duffin [73] proved that any impedance function given in the form of a PR function can be realized by only RLC elements without the need for transformers. In a part of their synthesis approach, they defined the mathematical function in (2.2) to find the variable k which is necessary to proceed.

$$R(s) = \frac{kz(s) - sz(k)}{kz(k) - sz(s)} \tag{2.2}$$

The function $R(s)$ can not be made out of tabulated function. Thus this method is also not proper for the scope of this work.

Reza [74], Miyata [75], McMillan [76], Westcott [77], Ozaki [78], Onno [79], Weinberg [80] and others in the literature also used approaches which are to some extent similar to the above mentioned methods. But the key property needed for this work, that is being applicable to the tabulated function, is missing in all of them.

2.2 Brune's Realization Method

Otto Brune [55] in 1931 showed that the necessary and sufficient condition for the function $z(s)$ to be the impedance (or admittance) of a passive RLC circuit is to be Positive Real (PR). That means $z(s)$ must be real when 's' is real and the real part of it must be positive when the real part of 's' is positive. A detailed overview of PR functions and their properties is given in Appendix A.

Brune's method of realization results in a network with a minimum number of energy storing elements (i.e capacitors and inductances) [70]. The number of elements comes out as p, the highest power of 's' in the function $z(s)$. Besides, Brune's method results in the minimum number of elements (i.e. capacitors, inductances, resistances, and ideal transformers) which would be $(2p + 1)$ independent elements. [70].

Due to the analogy between mechanical and electrical networks in which force and velocity are equivalent to current and voltage respectively, (and damper, spring, and inerter are equivalent to resistance, inductor, and capacitor respectively), the Brune realization is also used in the synthesis of mechanical systems [81]. Brune's method was also used in modeling microwave circuits by first utilizing vector fitting and then realizing the rational functions [56–60].

Brune's realization procedure includes four steps, all of which use RLC elements to realize a portion of the passive network that represents the given PR function. The procedure ends when no further circuit is left to be realized. Positive realness of the remainder function is always preserved as all the steps are based on properties of PR functions as listed in Appendix A.2.

The preliminary steps to realize the PR function $z(s)$ is removing all imaginary axis poles

and zeros and then removing Brune's cycle which is described as follows.

2.2.1 Step One: Imaginary Axis Pole Removal

At the first step of Brune's procedure, all the poles of $z(s)$ on imaginary axis should be removed. These poles can be removed from the $z(s)$ in the form of (2.3). In this equation, k_∞, k_0 and k_j are the residues of the poles at infinity, zero and ω_j respectively.

$$z_1(s) = z(s) - k_\infty s - \frac{k_0}{s} - \sum_{j=1}^{n} \frac{2k_j s}{s^2 + \omega_j^2} \tag{2.3}$$

The imaginary axis poles can then be represented by a series network as depicted in Figure 2.5, terminated by the remainder $z_1(s)$ which is still a PR function.

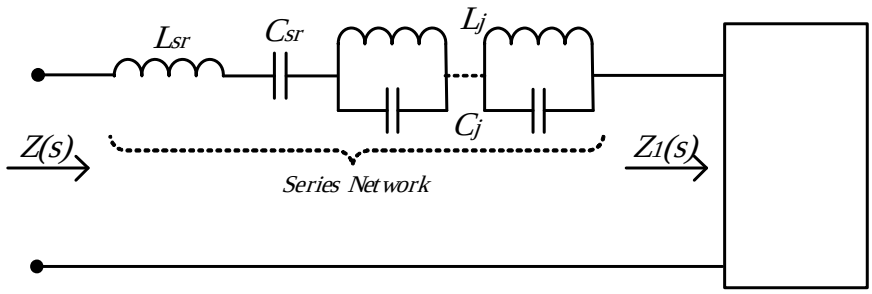

Figure 2.5: Series network removing imaginary axis poles in Brune's procedure

Where comparing (2.3) and Figure 2.5 , it can be found that;

$$L_{sr} = k_\infty \quad , \quad C_{sr} = \frac{1}{k_0} \quad , \quad C_j = \frac{1}{2k_j} \quad , \quad L_j = \frac{1}{C_j \omega_j^2} \tag{2.4}$$

After this step, there will be no more imaginary axis pole in the remainder function $z_1(s)$.

2.2.2 Step Two: Imaginary Axis Zero Removal

Second step of Brune's procedure is to remove the imaginary axis zeros from the remainder function $z_1(s)$.

It is clear that zeros of the $z_1(s)$ are the poles of function $y_1(s) = 1/z_1(s)$. Therefore, removing poles of $y_1(s)$ is the same as removing zeros of $z_1(s)$ which can be done in the same manner as done in the previous part.

Poles of $y_1(s)$ can be removed as shown in (2.5) where $k_{\infty 1}$, k_{01} and k_i are the residues of the poles at infinity, zero and ω_i respectively.

$$y_2(s) = y_1(s) - k_{\infty 1}s - \frac{k_{01}}{s} - \sum_{i=1}^{n} \frac{2k_i s}{s^2 + \omega_i^2} \tag{2.5}$$

Poles of $y_1(s)$, or in another word zeros of $z_1(s)$, shall be realized by shunt components as Figure 2.6 shows. Again by comparing Equation (2.5) and Figure 2.6, it can be found that;

$$C_{sh} = k_{\infty 1} \quad , \quad L_{sh} = \frac{1}{k_{01}} \quad , \quad L_i = \frac{1}{2k_i} \quad , \quad C_i = \frac{1}{L_i \omega_i^2} \tag{2.6}$$

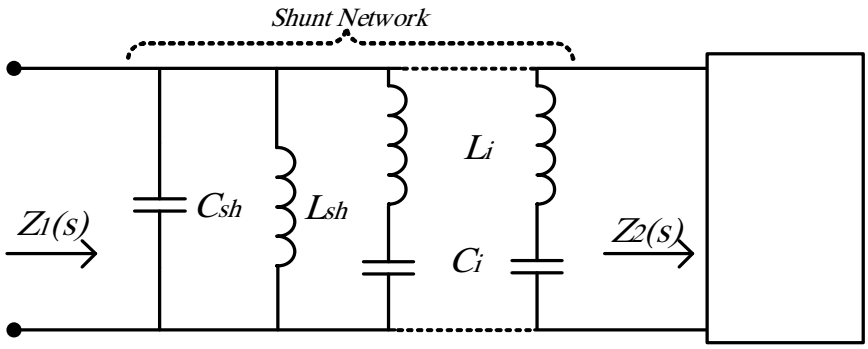

Figure 2.6: Shunt network removed as imaginary axis zeros in Brune's procedure

The first 2 steps shall be repeated until there are no more imaginary axis poles and/or zeros. The remainder function, which has no poles and/or zeros is called a minimum reactance - minimum susceptance function.

2.2.3 Step Three: Minimum Resistance Removal

In the third step of the Brune's realization, a zero is made on imaginary axis. To do so, first, the minimum of the real part of the function $z_2(j\omega)$ is removed. This will realize a series

resistance called R_{min} as shown in Figure 2.7.

$$z_3(s) = z_2(s) - R_{min} \tag{2.7}$$

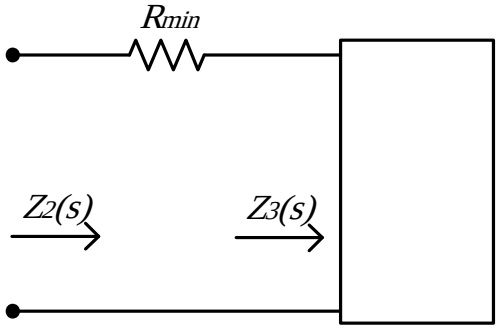

Figure 2.7: Removing the minimum resistance in Brune's procedure

If the minimum of the real part happens at frequencies $\omega = 0$ or $\omega = \infty$, it means a zero will be created there. That is because the imaginary part of the function was also already removed at zero and infinity. Therefore, this zero should be removed in the form of shunt elements L_z or C_z in the same way as mentioned in step 2.

If the minimum of the real part happens at some finite frequency ω_m, then the function $z_3(s)$ is purely imaginary at this frequency. The function $z_3(s)$ is referred to as "minimum function".

2.2.4 Step Four: Brune's Cycle Removal

The fourth step of the procedure referred to as"Brune's cycle" has some smaller steps which are explained in this part. As mentioned before, z_3 at ω_m is pure imaginary. So;

$$z_3(j\omega_m) = jX \tag{2.8}$$

The reactance X can be positive or negative. Therefore, depending on the value of X, further reduction is possible following two directions;

Direction 1: $X < 0$

The reactance X should be removed in form of series inductance $L_1 = X/\omega_m$. Therefore,

$$z_4(s) = z_3(s) - sL_1 \tag{2.9}$$

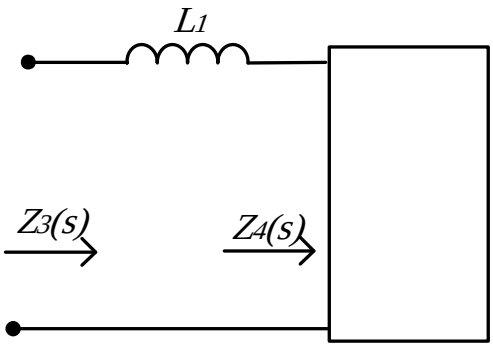

Figure 2.8: Removing the inductance L_1 in Brune's cycle

This reduction will make a zero in $z_4(s)$ at ω_m which is then removed in form of a pole of $y_4(s)$ by a shunt LC component as depicted in Figure 2.9.

$$y_5(s) = y_4(s) - \frac{s/L_2}{s^2 + \omega_m^2} \tag{2.10}$$

where L_2 and C_2 are given by (2.11):

$$1/L_2 = \frac{s^2 + \omega_m^2}{2s} y_4(s) \mid_{at\ s=j\omega_m} \qquad C_2 = 1/(L_2\omega_m^2) \tag{2.11}$$

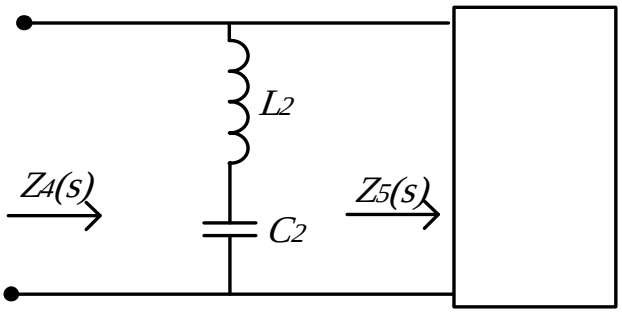

Figure 2.9: Removing the zero created at ω_0 in Brune's cycle

Finally, the imaginary axis pole which has been created at infinity should be removed. This pole is also removed in form of series inductance L_3 as shown by (2.12) and depicted in Figure 2.10.

$$z_6(s) = z_5(s) - sL_3 \tag{2.12}$$

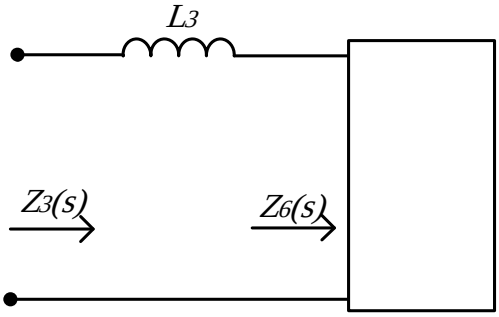

Figure 2.10: Removing the inductance L_3 in Brune's cycle

It can be proved that the relation (2.13) is always true for the inductances L_1, L_2 and L_3.

$$L_3 = \frac{-L_1 L_2}{L_1 + L_2} \tag{2.13}$$

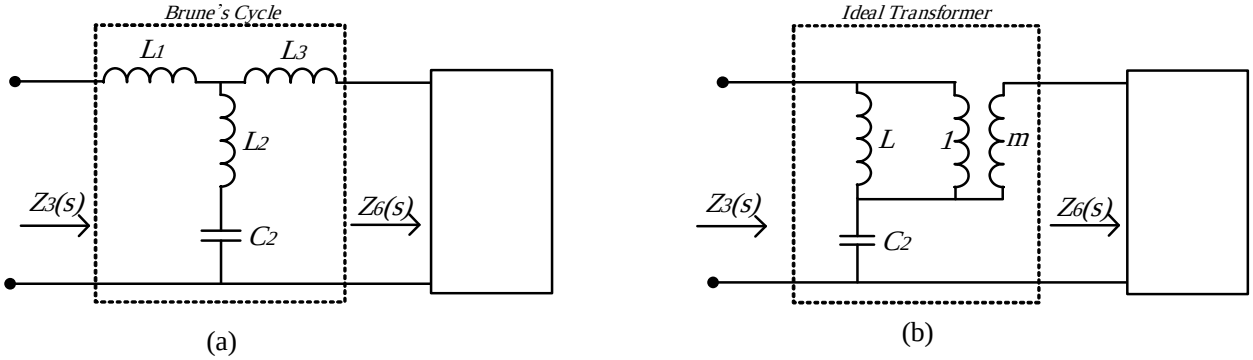

Figure 2.11: (a) Brune's cycle and (b) equivalent ideal transformer of the 'Tee' connection

Considering Equation (2.13), although exactly one of L_1 or L_3 will be negative, the circuit is still physically realizable with all positive elements. This is feasible by replacing the "Tee"

connection of inductors with two coupled inductor L_A and L_B and mutual inductance of M as given by (2.14).

$$L_A = L_1 + L_2, \quad L_B = L_2 + L_3, \quad M = L_2 \tag{2.14}$$

As the coupling coefficient ($k = |M|/\sqrt{L_A L_B}$) is unity, the "Tee" connection can be implemented with a real network having by an ideal transformer with turns ratio of $m = M/L_A$ and $L = L_1 + L_2$. Figure 2.11 shows (a) the Brune's cycle and (b) the equivalent ideal transformer together.

Direction 2: $X > 0$

If the reactance X is positive, the procedure continues in form of capacitive network. Thus, it should be removed in the form of series capacitance C_1 which is given by:

$$jX = 1/(j\omega_m C_1) \quad \Rightarrow \quad C_1 = -\frac{1}{X\omega_m} \tag{2.15}$$

The capacitor C_1 is removed as (2.16);

$$z_4(s) = z_3(s) - \frac{1}{sC_1} \tag{2.16}$$

This will make a zero in $z_4(s)$ at ω_m which is removed in form of a pole of $y_4(s)$ by a series LC component.

$$y_5(s) = y_4(s) - \frac{s/L}{s^2 + \omega_m^2} \tag{2.17}$$

in which L and C_2 are found as below;

$$1/L = \frac{s^2 + \omega_m^2}{2s} y_4(s) \mid_{at\ s=j\omega_m} \qquad C_2 = 1/(L\omega_m^2) \tag{2.18}$$

And finally, the capacitive pole created at zero is removed by C_3 as given by:

$$z_6(s) = z_5(s) - \frac{1}{sC_3} \tag{2.19}$$

It has been also proved [82] that there is a relation between C_1, C_2 and C_3 which is shown in (2.20).

$$C_3 = -(C_1 + C_2) \tag{2.20}$$

The network realization of Brune's cycle for the situation $X > 0$ is shown in Figure 2.12.A. By equating the impedance matrices of the 2-terminal networks in Figure 2.12.A corresponding to $X > 0$ and Figure 2.12.B which is corresponding to $X < 0$, it is proved that these networks are equivalents with the relations given by (2.21).

$$\begin{aligned} C &= \frac{C_1 C_2}{C_1 + C_2} \\ L_1 &= \frac{C_1 + C_3}{C_1} L \\ L_2 &= -\frac{C_3}{C_1} L \\ L_3 &= \frac{C_3(C_1 + C_3)}{C_1^2} L \end{aligned} \tag{2.21}$$

Therefore, even with $X > 0$, the process can move on considering Direction 1, and the reduced impedance after removing Brune's cycle would be the same as if Direction 2 were selected. In other words, there is no need to consider the above mentioned different directions in realizing Brune's cycle.

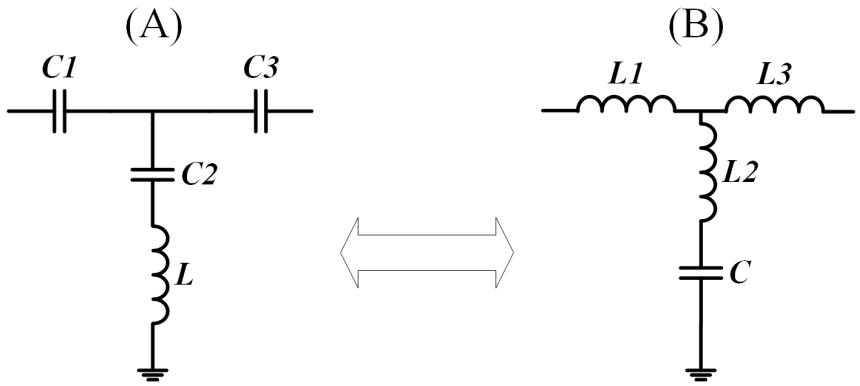

Figure 2.12: (A) Brune's cycle for $X > 0$ which is equivalent to network (B) that is corresponding to $X < 0$

2.2.5 Continuation and Termination

The above 4 steps of Brune's procedure (i.e., removing imaginary axis poles and zeros, removing minimum resistance and Brune's cycle) are again applied to $z_6(s)$ to further reduce the order of the remainder. The process is continued till the order of the resulting impedance is zero, i.e., all that remains is a resistor (named as R_{end}). Then the network will be terminated in the resistance R_{end}.

It is worth mentioning that the remainder function $z_6(s)$ is still a PR function because all the manipulation made on the original function always preserved the positive realness of the remainder. Also, all the elements of the realized network are positive (or can be made to be positive with an ideal transformer), thus yields a guaranteed passive network.

The discussion so far assumed that the impedance was available in the form of a positive real transfer function in the Laplace domain. The next chapter will introduce an approach for its application to an impedance represented by tabulated data (real and imaginary components as a function of frequency or alternatively magnitude and phase as a function of frequency).

2.3 Tellegen's Extension to Multi-port Networks

Brune's realization method was only introduced for single port networks. Using steps analogous to Brune's Method, Tellegen was able to realize a multi-port network represented by an impedance matrix $Z(s)$ [70]. Note that for multi-port networks, the impedance representation becomes a matrix $Z(s)$ instead of the scalar $z(s)$.

Similar to Brune's idea, a matrix $Z(s)$ can be realized if it is a PR matrix. A matrix $Z(s)$ is PR if and only if [36];

- All the coefficients of $Z(s)$ are real when "s" is real.
- All the coefficients of $Z(s)$ are analytic in the right-half "s" plane.

- Poles on the $j\omega$ axis are simple and their matrix of residues is a positive semi-definite matrix.
- The Hermitian part of $Z(j\omega)$, $Z_H(j\omega) = Z(j\omega) + Z^{*T}(j\omega)$, is positive semi-definite for all ω. In case of symmetric matrices (as in this paper), the Hermitian matrix is the real part of $Z(j\omega)$, i.e. $\Re\{Z(j\omega)\}$.

A detailed overview of the multi-port PR functions and their properties is provided in Appendix A.1.2.

Analogous to the Brune Synthesis in Section 2.2, Tellegen's realization procedure for a multi-port network also includes 4 steps as explained below;

2.3.1 Step One: Removing Imaginary Axis Poles

If at least one element of the impedance matrix $Z(s)$ has a pole at a certain frequency (e.g. $s = 0$, ∞, ω_{jp}), it is considered as the pole of the whole matrix. The pole at $s \to \infty$ yields the residue matrix of $K_{\infty p}$, the pole at $s \to 0$ results in residue matrix of K_{0p} and finally, K_{jp} represents the residue matrix of the pole at frequency $s \to \omega_{jp}$. These constant matrices are found as in (2.22).

$$K_{\infty p} = \lim_{s\to\infty} \frac{Z(s)}{s} \quad , \qquad K_{0p}^{-1} = \lim_{s\to 0} sZ(s) \quad , \qquad K_{jp} = \lim_{s\to\omega_{jp}} \frac{s^2+\omega_{jp}^2}{2s} Z(s) \tag{2.22}$$

The residue matrices of the poles, $K_{\infty p}$, K_{0p} or K_{jp} are each realized by an impedance and $n-1$ ideal transformers as given by (2.23) with the assumption that all three are rank one matrices.

$$\begin{aligned}
&L_{sr} = K_{\infty p}(1,1), \quad t_{\infty p}^m = \frac{K_{\infty p}(1,m)}{K_{\infty p}(1,1)} \quad m = 2,3,..,n \\
&C_{sr} = \frac{1}{K_{0p}(1,1)}, \quad t_{0p}^m = \frac{K_{0p}(1,m)}{K_{0p}(1,1)} \quad m = 2,3,..,n \\
&C_{jp} = \frac{1}{2K_{jp}(1,1)}, L_{jp} = \frac{1}{C_{jp}\omega_{jp}^2} \quad t_{jp}^m = \frac{K_{jp}(1,m)}{K_{jp}(1,1)} \quad m = 2,3,..,n
\end{aligned} \tag{2.23}$$

The block named "Series Network" in Figure 2.13 shows the imaginary poles, corresponding to $K_{\infty p}$, K_{0p} and K_{jp}.

The matrices of poles are then removed from $Z(s)$, to yield the remainder function of $Z_1(s)$ as shown in (2.24);

$$Z_1(s) = Z(s) - sK_{\infty p} - \frac{1}{s}K_{0p}^{-1} - \sum_{jp=1}^{np} \frac{2s}{s^2 + \omega_{jp}^2} K_{jp} \tag{2.24}$$

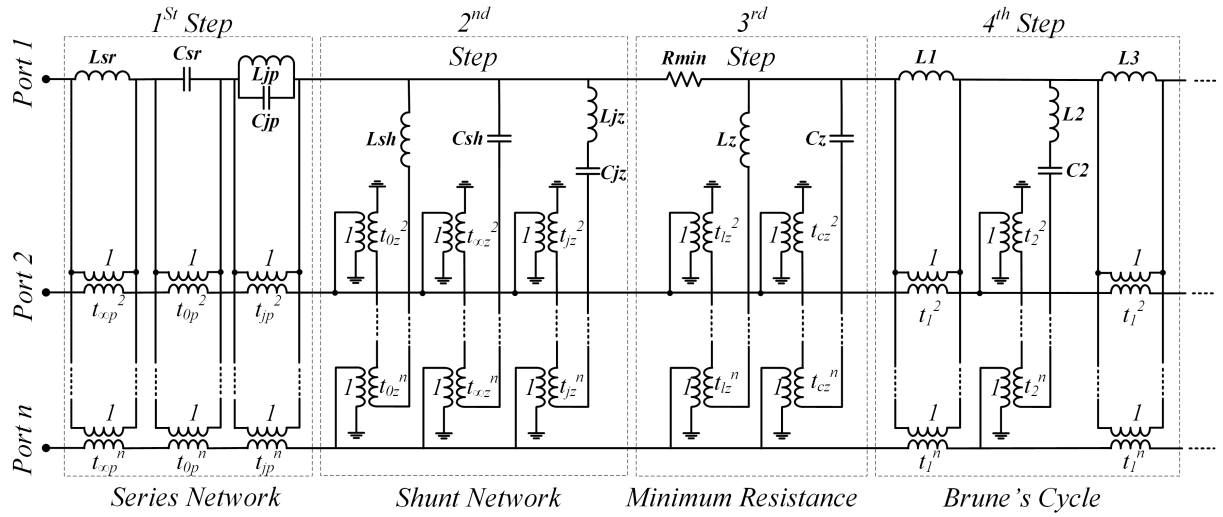

Figure 2.13: The whole possible n-port network in one round of Tellegen's realization

2.3.2 Step Two: Removing Imaginary Axis Zeros

If the determinant $|Z_1(s)| = 0$ at a certain frequency, it implies that there is a zero at that frequency. As was done with the scalar functions with the Brune method, the zeros of the matrix $Z_1(s)$ are removed in form of poles of $Y_1(s) = Z_1^{-1}(s)$ and realized as a shunt network.

Residues of the poles of $Y_1(s)$ are labeled as $K_{\infty z}$, K_{0z} and K_{jz} represent the residues of the poles at frequencies $s \to \infty$, $s \to 0$ and $s \to \omega_{jz}$ respectively and found by (2.25).

$$K_{\infty z} = \lim_{s\to\infty} \frac{Y_1(s)}{s} \quad , \quad \underset{=}{K_{0z}^{-1}} \lim_{s\to 0} sY_1(s) \quad , \quad K_{jz} = \lim_{s\to\omega_{jz}} \frac{s^2 + \omega_{jz}^2}{2s} Y_1(s) \tag{2.25}$$

The residue matrices of zeros are realized using a shunt network of one impedance and $n-1$ transformers given by (2.26).

$$
\begin{aligned}
C_{sh} &= K_{\infty z}(1,1), \quad t^m_{\infty z} = \frac{K_{\infty z}(1,m)}{K_{\infty z}(1,1)} \quad m = 2,3,..,n \\
L_{sh} &= \frac{1}{K_{0z}(1,1)}, \quad t^m_{0z} = \frac{K_{0z}(1,m)}{K_{0z}(1,1)} \quad m = 2,3,..,n \\
C_{jz} &= \frac{1}{2K_{jz}(1,1)}, \quad L_{jz} = \frac{1}{C_{jz}\omega^2_{jz}} \quad t^m_{jz} = \frac{K_{jz}(1,m)}{K_{jz}(1,1)} \quad m = 2,3,..,n
\end{aligned} \tag{2.26}
$$

In Figure 2.13, the block labeled "Shunt Network" shows the realization of the imaginary zeros corresponding to the residues, $K_{\infty z}$, K_{0z} and K_{jz} assuming that they are rank one matrices.

The poles of $Y_1(s)$ are then removed as shown in (2.27) which results in the remainder matrix $Y_2(s)$.

$$
Y_2(s) = Y_1(s) - sK_{\infty z} + \frac{1}{s}K^{-1}_{0z} + \sum_{jz=1}^{nz} \frac{2s}{s^2 + \omega^2_{jz}} K_{jz} \tag{2.27}
$$

The first two steps are repeated until there are no more poles or zeros in the matrix $Z_2(s)$.

2.3.3 Step Three: Removing the Minimum Real Part

Let $A(\omega) = \Re\{Z_2(j\omega)\}$ the real part of the matrix $Z_2(s)$. The minimum resistance, R_{min}, is then defined by (2.28) in which $\Delta_{11}(\omega)$ is the $(1,1)$ minor of $A(\omega)$.

$$
R_{min} = \min\{\Lambda(\omega)\} \qquad , \qquad \Lambda(\omega) = \frac{|A(\omega)|}{\Delta_{11}(\omega)} \tag{2.28}
$$

If ω_m is the frequency at which the minimum of $\Lambda(\omega)$ happens, then by subtracting the resistance R_{min} from $Z_2(s)$, a zero is created at ω_m in the real part of the function $\Re\{Z_2(j\omega)\}$. This means $|\Re\{Z_3(j\omega_m)\}| = 0$ or the real part of matrix $Z_3(s)$ will become rank deficient at ω_m.

As suggested by Tellegen, the resistance R_{min} is only realized at port one of the network and then removed from the function $Z_2(s)$ as given by (2.29):

$$Z_3(s) = Z_2(s) - \begin{pmatrix} R_{min} & 0 & \cdots & 0 \\ 0 & 0 & \cdots & 0 \\ \vdots & \vdots & \ddots & \vdots \\ 0 & 0 & \cdots & 0 \end{pmatrix} \tag{2.29}$$

In case $\omega_m = \infty$ or $\omega_m = 0$, removing the resistance R_min creates a zero at the corresponding frequency. This is due to the fact that both imaginary and real part of the function becomes zero at that corresponding frequency. Thus, the zero is removed in the form of a pole of $Y_3(s)$ by means of the shunt network consisting of L_Z, C_Z and ideal transformers with the turns ratio t_{lz} and t_{cz} as shown in Figure 2.13.

2.3.4 Step Four: Removing Tellegen's Extension of Brune Cycle

If the frequency at which the minimum resistance, R_{min} happens is a finite frequency ω_m, i.e., $0 < \omega_m < \infty$ then a step analogous to Brune's cycle is required to lower the order of the impedance matrix by two.

In the previous step, the real part of the matrix $Z_3(s)$ became rank deficient at ω_m, and by definition there exists a vector β such that;

$$\Re\{Z_3(j\omega_m)\}\beta = 0 \tag{2.30}$$

in which the vector β is called the null vector, i.e. the eigenvector corresponding to the zero eigenvalue.

Then, the imaginary part, $X = \Im\{Z_3(j\omega_m)\}$ should also become rank deficient at ω_m with the same vector β. Therefore, there is a rank one symmetric matrix H such that;

$$(X - H)\beta = 0 \qquad , \qquad X = \Im\{Z_3(j\omega_m)\} \tag{2.31}$$

While any real symmetric rank one matrix of H can be written as a product of a real vector h and a constant α;

$$H = \alpha h h^T \qquad , \qquad \alpha = \pm 1 \tag{2.32}$$

where the value of α is determined by (2.33).

$$X\beta = \alpha h h^T \beta \qquad \Rightarrow \qquad \beta^T X \beta = \alpha (h.\beta)^2 \qquad \Rightarrow \qquad \alpha = \frac{(h.\beta)^2}{\beta^T X \beta} \tag{2.33}$$

The vector h can also be determined by (2.34)

$$h = \frac{1}{\sqrt{\alpha \beta^T X \beta}} X\beta \tag{2.34}$$

Similar to Brune's approach for scalar functions, there will be two possible directions to continue the procedure for multi-port functions which depend on the value of the α.

Direction 1: $\alpha < 0$

Now, the rank one matrix H is normalized with respect to H_{11} in order to create the inductance $L_1 = H_{11}/\omega_m$. Then the inductance is removed from $Z_3(s)$ as shown in (2.35) in which t_1 is the vector of the ideal transformer turns ratio.

$$Z_4(s) = Z_3(s) - sL_1 t_1 t_1^T \qquad , \qquad t_1 = \frac{1}{H_{11}} h \tag{2.35}$$

Then, the zero of $Z_4(s)$ which is created at ω_m is removed in form of pole of $Y_4(s)$ as shown in (2.36).

$$Y_5(s) = Y_4(s) - \frac{sK_m}{s^2 + \omega_m^2} \qquad , \qquad K_m = \frac{1}{L_2} t_2 t_2^T \quad , \quad C_2 = \frac{1}{L_2 \omega_m^2} \tag{2.36}$$

The reside K_m is a rank one matrix which is normalized with respect to the first element, i.e. (1,1) to calculate L_2, and t_2 is the vector of transformer turns ratio connecting the L_2C_2 branch to the other ports.

Eventually, the inductance L_3 is removed from the function $Z_5(s) = Y_5^{-1}(s)$ as;

$$Z_6(s) = Z_5(s) - sL_3 t_1 t_1^T \tag{2.37}$$

It was proved by Tellegen [70] that L_3 uses the same set of transformer turns ratio as L_1. Also, similar to what Brune did, Tellegen proved that there is a relation between the inductances L_1, L_2 and L_3 as in (2.38).

$$L_3 = \frac{-L_1 L_2}{F^2 L_1 + L_2} \qquad , \qquad F = t_1.t_2 \tag{2.38}$$

Analogous to Brune's realization for single port networks, L_2 is always positive, and exactly one of L_1 or L_3 is always negative. However, this arrangement is physically implementable as it represents an ideal transformer. This is shown in Figure 2.14.A and its equivalent network with positive inductance L and transformers turns ratio, m^i, are calculated by (2.39) and are shown in Figure 2.14.B.

$$\begin{aligned} L &= F^2 L_1 + L_2 \\ m^1 &= \frac{F(F-1)L_1 + L_2}{L} \\ m^i &= -\frac{F L_1 t_1^i}{L} \quad , \quad i = 2, 3, 4, ... \end{aligned} \tag{2.39}$$

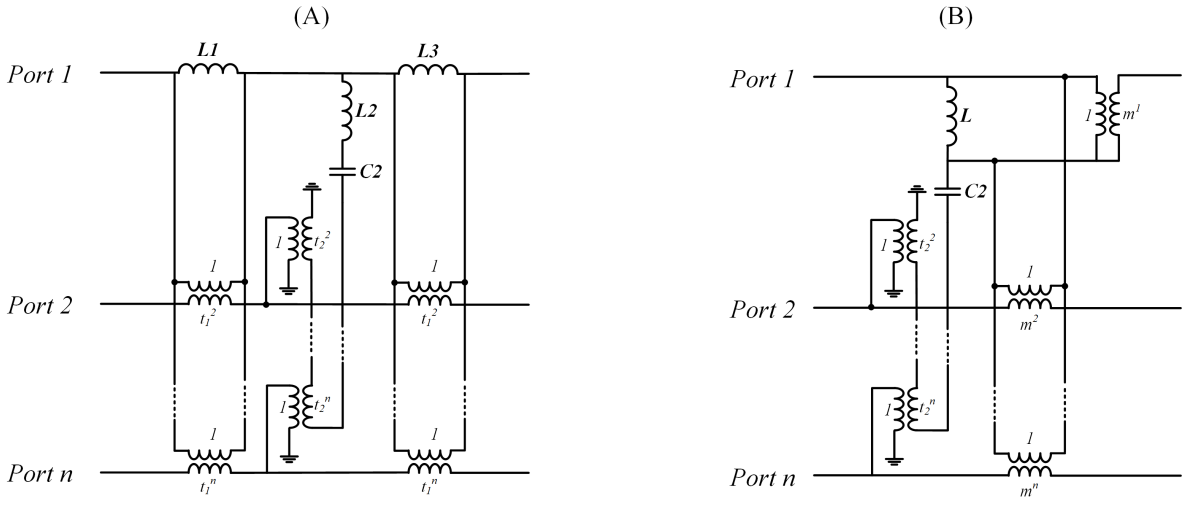

Figure 2.14: (A) The extended Brune's cycle for the case of $\alpha < 0$ and (B) its equivalent network with only positive elements.

Direction 2: $\alpha > 0$

If α is positive, a capacitive network is realized instead of the inductive network. The rank one matrix H is normalized with respect to H_{11} in order to create the capacitance $C_1 = -1/(\omega_m H_{11})$. The capacitance C_1 is subtracted from $Z_3(s)$ as given by (2.40) where t_1

is the vector of the transformer turns ratio.

$$Z_4(s) = Z_4(s) - \frac{1}{sC_1} t_1 t_1^T \qquad , \qquad t_1 = \frac{1}{H_{11}} h \tag{2.40}$$

The zero of $Z_4(s)$ at ω_m is then removed in form of pole of $Y_4(s)$ as shown in (2.41).

$$Y_5(s) = Y_4(s) - \frac{sK_m}{s^2 + \omega_m^2} \qquad , \qquad K_m = \frac{1}{L_2} t_2 t_2^T \qquad , \quad C_2 = \frac{1}{L_2 \omega_m^2} \tag{2.41}$$

Finally, the capacitance C_3 is removed from the function $Z_5(s) = Y_5^{-1}(s)$ as given by (2.42);

$$Z_6(s) = Z_5(s) - \frac{1}{sC_3} t_1 t_1^T \tag{2.42}$$

It is also proved that C_1, C_2, and C_3 are related by (2.43).

$$C_3 = -(C_1 + F^2 C_2) \qquad , \qquad F = t_1 . t_2 \tag{2.43}$$

Figure 2.15.A shows the realized capacitive network for $\alpha > 0$. Here also one of C_1 or C_3 becomes negative, but with the similar approach as before, the "Tee" connection of the capacitors can be converted into ideal transformers and a positive Capacitor C which is shown in Figure 2.15.B. Calculations to find Capacitor C and the corresponding transformer ratio are in (2.44).

$$\begin{aligned} C &= \frac{C_1 C_2}{F^2 C_1 + C_2} \\ m^1 &= \frac{C(F(F-1)C_2 + C_1)}{C_1 C_2} \\ m^i &= -\frac{FCt_1^i}{C_1} \quad , \quad i = 2, 3, 4, ... \end{aligned} \tag{2.44}$$

2.3.5 Continuation and Termination

The next round of reduction may be applied to $Z_6(s)$ to reduce its order further. The realization procedure continues until the residual network is a constant matrix i.e. R_{end}.

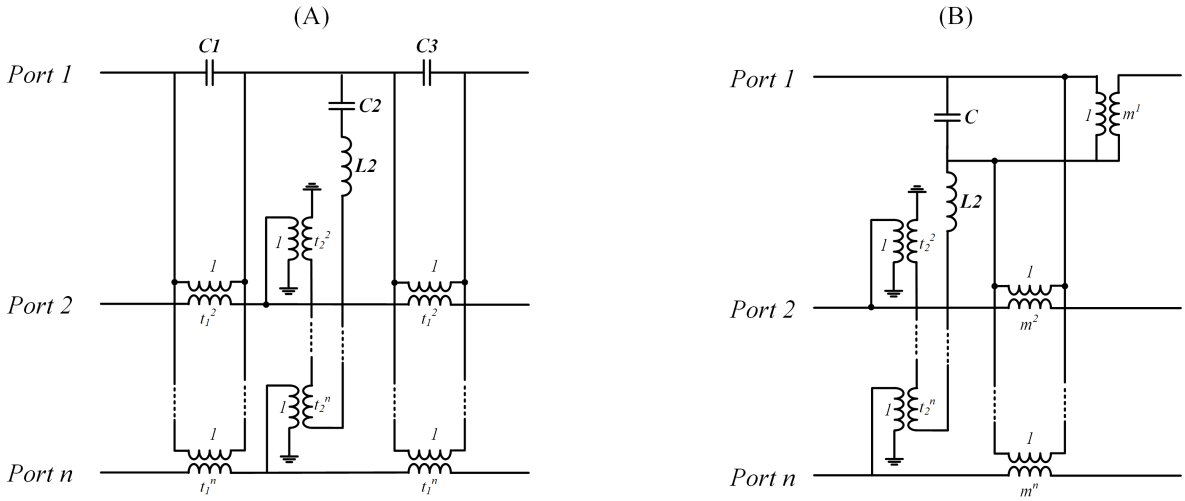

Figure 2.15: (A) The extended Brune's cycle for the case of $\alpha > 0$ and (B) its equivalent network with only positive elements

Figure 2.13 shows the overall possible network which might be realized after one round of performing four steps of the Tellegen's procedure. When the realization process is completed, the sub-circuits are connected in cascade and terminated in resistive network R_{end} which is the remainder constant matrix at the end of the realization process.

2.4 Summary

In this chapter, an overview of several classical network realization methods was conducted. This review aimed to find an appropriate realization method that could be used as an alternative way to fit FDNEs with guaranteed passivity. The methods were investigated to have certain properties such as preserving the passivity, being applicable to the tabulated functions, feasibility for computerization, and providing a network with a minimum number of elements. Brune's realization approach and its extension to multi-port networks by Tellegen were found to be very suited for this purpose. Hence, these methods were discussed in more detail in this chapter. adaptation of Brune and Tellegen methods to work with tabulated data are the subject of the following chapters.

Chapter 3

Adapting Brune's Realization for Tabulated Functions

This chapter develops an approach so that Brune's synthesis method, described in Chapter 2, can be adapted in order to create a time-domain model of FDNEs directly from the tabulated functions. The method realizes a circuit with the same frequency response as that of the original network. In this approach, a network with all passive elements is realized. Now, any circuit built by connecting purely passive elements is also always passive [83]. This guarantees the passivity of the realized FDNE model.

In case of FDNEs, the impedance function is not available in s-domain $z(s)$. Therefore, it should be first proven that it is possible to do the realization process with only $z(j\omega)$. Then, some modifications will be necessary to apply Burne's idea to tabulated function, $z(j\omega)$. (Note that in the use of symbols, a lower case i.e., $z(s)$ indicates a scalar function and later in the next chapter, the capital $Z(s)$ represents a matrix.)

At the end of this chapter, some simulation case studies are provided to verify the proposed method.

3.1 Theorem: Realization Procedure on Imaginary Axis

The classical Brune method works with an impedance function $z(s)$ which is a rational function in the 's' (Laplace variable) domain. But it is observed that all the steps in the Brune realization method are done on the $j\omega$ axis. Therefore, information of $z(s)$ on the $j\omega$ axis must be sufficient. Before adapting the Brune realization, it must be proved that having a tabulated function $z(j\omega)$ rather than a rational polynomial function $z(s)$ is enough for performing the realization. Hence, the following theorem is proved in the thesis.

Theorem:

"A lumped, passive circuit can be derived from a table of impedance, $z(j\omega)$, versus the frequency."

Proof:

- Referring to the 's' domain Brune synthesis in Section 2.2, step one removes the poles, and step two removes the zeros of the impedance function which are located "on the imaginary or $j\omega$ axis". Therefore knowing function $z(j\omega)$ is enough to perform these two steps. For example, the series inductance in Brune's first step will be $Lsr = z(j\omega_\infty)/\omega_\infty$ and the residual function $z_1(j\omega) = z(j\omega) - j\omega L_{sr}$ can be used for the further synthesis steps. Similarly, the remaining poles and zeros can be calculated which are explained in detail in the next section. Of course, it is necessary that the table include asymptotic values of $z(j\omega)$ at sufficiently low and high frequencies.

- Let the residue function from the step 2 be $z_2(j\omega)$. Step 3 involves removal of the minimum real part, realized as R_{min}. This can be achieved by investigating the table of $z_2(j\omega)$ and identifying the frequency $\omega = \omega_m$ where $\Re\{z_2(j\omega)\}$ has the smallest value. Then $R_{min} = \Re\{z_2(j\omega_m)\}$, and the residual function for the next synthesis step becomes $z_3(j\omega) = z_2(j\omega) - R_{min}$.

- In step four, values of the elements in Brune's cycle are also similarly calculated:

- ☐ L_1 is calculated by the fraction $\frac{X}{\omega_m}$, where $X = z_3(j\omega_m)$ the imaginary part of z_3 at the frequency $s = j\omega_m$ where the minimum real part is extracted. Therefore information of $z_3(j\omega_m)$ is necessary and sufficient for calculating L_1. Removal of L_1 results in the residual function $z_4(j\omega) = z_3(j\omega) - j\omega L_1$. By removing both real and imaginary part of function at ω_m, $z_4(j\omega_m) = 0$.

- ☐ L_2 and C_2 are found by calculating the residue of the zero which is created in $z_4(j\omega)$ (or pole of $y_4(j\omega) = z_4(j\omega)^{-1}$) at frequency ω_m. Thus, $y_4(j\omega)$ should have a factor of $-\omega^2+\omega_m^2$ in denominator to represent the pole at $\pm j\omega_m$. This is shown in (3.1) by $y_4(j\omega) = y_4'(j\omega)/(-\omega^2+\omega_m^2)$, in which $-\omega^2+\omega_m^2$ factors are canceled.

$$1/L_2 = \frac{-\omega^2+\omega_m^2}{2j\omega} y_4(j\omega) \mid_{at\ w=\omega_m} = \frac{1}{2j\omega_m} y_4'(j\omega_m) \qquad C_2 = 1/(L_2\omega_m^2) \quad (3.1)$$

  So it can be concluded that having $z_4(j\omega)$ is sufficient.

- ☐ $L_3 = -L_1L_2/(L_1 + L_2)$ is then calculated via the relation between the three inductors.

- The above steps are repeated until only a resistive element remains (i.e., the tabulated function is essentially a real constant). This constant value represents the termination resistance.

3.2 Adaptation of Brune's Procedure

This section illustrates the analogous "numerical" steps to be taken corresponding to each "analytical" step in Brune's procedure described in the previous Chapter to adapt the idea for tabulated function $z(j\omega)$. Note that due to the data granularity, the tabulated function will have a collection of points in frequency samples, i.e., it may not be available as a continuous function of $j\omega$. Figure 3.1 shows the whole network that is possible to be realized in one round of the Brune procedure. Each of the four steps realizes a set of elements (or a single element), leaving behind a remainder impedance for further realization in the next steps.

3.2.1 Step 1: Reduction of the network by removal of imaginary axis poles

The presence of poles on the imaginary axis can be determined by observing the phase angle of the tabulated function, $z(j\omega)$, in the following way.

If the phase angle of $z(j\omega)$ at very high frequency, ω_∞, is close to $+90^\circ$, it means there is a pole at infinity. This pole is synthesized in the form of a series inductance. This is achieved automatically by comparing the angle at very high frequency sample points against a threshold. L_{sr}, the residue of the pole at infinity, can be calculated using the imaginary part of the impedance at very high frequency, ω_∞, as shown in Eq. (3.2).

$$L_{sr} = \frac{\Im\{z(j\omega_\infty)\}}{\omega_\infty} \tag{3.2}$$

Similarly, if the phase angle of the tabulated function $z(j\omega)$ at very low frequency, ω_0, is very close to -90°, it means there is a pole at zero. Therefore, it is synthesized in the form of series capacitance C_{sr} as given by (3.3).

$$C_{sr} = \frac{\Im\{1/z(j\omega_0)\}}{\omega_0} \tag{3.3}$$

To find the poles at any finite and non-zero frequency, ω_j, it is necessary to look into the table for a sudden change in the phase angle from $+90^\circ$ to -90°. Then the residue of this pole should be calculated as

$$k_j = \frac{-\omega^2 + \omega_j^2}{2j\omega} z(j\omega)|_{at\ \omega=\omega_j} \tag{3.4}$$

C_j and L_j of the corresponding branches can be found from k_j and ω_j as mentioned in (2.6). It is worth mentioning that usually, such poles are very rare in power system networks.

After calculating the residues, the imaginary axis poles reduction from the tabulated function is computed at each sample frequency as shown in (3.5). Consequently, one is left with function;

$$z_1(j\omega) = z(j\omega) - j\omega L_{sr} + \frac{1}{j\omega C_{sr}} + \sum_{j=1}^{n} \frac{2j\omega k_j}{-\omega^2 + \omega_j^2} \tag{3.5}$$

3.2.2 Step 2: Reduction of the network by removal of imaginary axis zeros

In the same manner as done for the poles, by observing the phase angle of tabulated function at a very high frequency (ω_∞) and a very low frequency (ω_0), the presence of zeros can be determined. If the phase angle of $z_1(j\omega)$ at very high frequency ω_∞ is close to -90°, it means there is an imaginary zero at infinity. On the other hand, if the phase angle of $z_1(j\omega)$ at very low frequency ω_0 is close to $+90^\circ$, it means there is an imaginary zero at zero.

It was mentioned in the previous chapter that the imaginary axis zeros of $z_1(j\omega)$ will be removed in form of poles of $y_1(j\omega) = 1/z_1(j\omega)$. This can be done with the same procedure as mentioned in the previous step by investigating the behaviors of phase angle at very high and very low frequencies and also sudden changes from $+90^\circ$ to -90°. Then these poles can be removed numerically at each frequency sample point as shown in Eq. (3.6).

$$y_2(j\omega) = y_1(j\omega) - j\omega C_{sh} + \frac{1}{j\omega L_{sh}} + \sum_{i=1}^{m} \frac{2j\omega k_i}{-\omega^2 + \omega_i^2} \tag{3.6}$$

3.2.3 Step 3: Reduction of the network by removal of minimum resistance

The Minimum of the real part of function $z_2(j\omega)$, i.e. $\Re\{z_2(j\omega)\}$, is found by looking into the tabulated function which then synthesized in the form of a series resistance R_{min}, giving a remainder function on its removal as in Eq. (3.7).

$$z_3(j\omega) = z_2(j\omega) - R_{min} \tag{3.7}$$

Let the frequency at which R_{min} occurs be ω_m. In the case that ω_m happens to be very close to 0 or ∞, the function $z_3(j\omega)$ will have a zero at that corresponding frequency. This is due to the fact that both imaginary and real parts of the function became zero at ω_m. Note that the imaginary poles and zeros at 0 and ∞ were removed in Step 1 and Step 2, so at 0 and ∞, the imaginary part of the function $z_3(j\omega)$ was already zero. Now, if the real part is also removed at $\omega_m \to 0$ or $\omega_m \to \infty$, $z_3(j\omega_m)$ will become zero, thus creating a zero

in the function $z_3(j\omega)$ at that corresponding frequency. Consequently, the zero of $z_3(j\omega)$ is realized in the form of shunt element L_z for the case of $\omega_m \to 0$ or C_z for the case $\omega_m \to \infty$. This can be performed in the same manner as done in Step 2.

If ω_m is neither 0 nor ∞, it will be a finite non-zero value in which $z_3(j\omega_m)$ is "purely imaginary". This is because $\Re\{z_3(j\omega_m)\} = 0$ after subtracting R_{min} in (3.7). Then the procedure goes to the next step.

3.2.4 Step 4: Brune's cycle for further network reduction

Similar to the analytical approach in Chapter 2, Brune cycle elements can be synthesized numerically. Firstly, as $z_3(j\omega_m)$ is purely imaginary, the value of L_1 is determined by (3.8) and then is removed from $z_3(j\omega)$ to yield the remainder function $z_4(j\omega)$ as in (3.9).

$$z_3(j\omega_m) = jX \quad \Rightarrow \quad L_1 = \frac{X}{\omega_m} \tag{3.8}$$

$$z_4(j\omega) = z_3(j\omega) - j\omega L_1 \tag{3.9}$$

Removing L_1 in (3.9) creates a zero in $z_4(j\omega)$ at ω_m, since both real and imaginary parts are removed at this frequency. The zero of $z_4(j\omega)$ is then synthesized as a shunt branch of L_2 in series with C_2. L_2 is found by calculating the residue of the pole of $y_4(j\omega)$ shown in (3.10) and the value of C_2 is determined from the fact that the realized LC circuit is resonant at ω_m.

$$L_2 = \frac{2j\omega}{-\omega^2 + \omega_m^2} z_4(j\omega) \mid_{at\ \omega=\omega_m} \qquad C_2 = 1/(L_2\omega_m^2) \tag{3.10}$$

Note that (3.10) gives an indeterminate value (0/0) at $\omega = \omega_m$, because $z_4(j\omega_m) = 0$, and also $-\omega^2 + \omega_m^2 = 0$. To resolve it, one can compute (3.10) for ω slightly less than ω_m , and again slightly more than ω_m , and interpolate in between to ω_m . This is the numerical equivalent of using L'Hopital's[1] rule in calculating a ratio where both numerator

[1] "Analyse des Infiniment Petits pour l'Intelligence des Lignes Courbes" by Guillaume-François-Antoine Marquis de l'Hôpital, 1696.

and denominator become zero at the point where the ratio is being evaluated. It should also be noted that the residue value of the interpolated point must be purely real, because it represents an inductor.

Note that $z_4(j\omega)$ has a zero at ω_m. To remove this zero, we consider $y_4(j\omega) = 1/z_4(j\omega)$ which has a pole at ω_m. The remainder function after we remove shunt L_2C_2 branch will be an admittance $y_5(j\omega)$ as in (3.11).

$$y_5(j\omega) = y_4(j\omega) - \frac{j\omega/L_2}{-\omega^2 + \omega_m^2} \tag{3.11}$$

At the end of the Brune cycle, $L_3 = -L_1L2/(L_1 + L_2)$ is calculated and removed from $z_5(j\omega)$.

$$z_6(j\omega) = z_5(j\omega) - j\omega L_3 \tag{3.12}$$

Figure 3.1 shows the entire set of possible elements that may be realized in one round of performing the 4 steps of Brune's procedure. Of course, some of these elements may not be present in the same round of realization. For instance, it is not possible to have pole at infinity (L_{sr}) and at the same round also a zero at infinity (C_{sh}), i.e., if L_{sr} is nonzero, $C_{sh} = 0$.

The next round of reduction will be applied to $z_6(j\omega)$ and continued till achieving a constant impedance which is called R_{end} in the Figure 3.1.

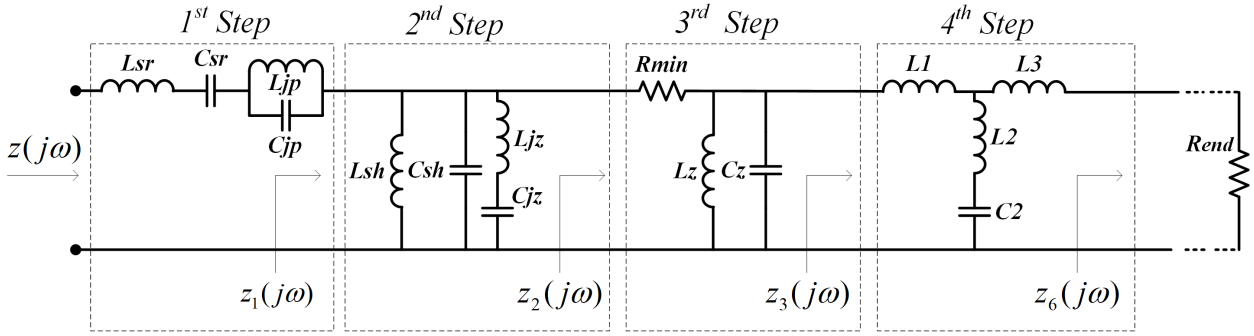

Figure 3.1: The whole possible network in one round of the Brune realization method

3.2.5 Continuation and Eventual Termination of the Process

In order to determine if further rounds of realization are needed or whether the procedure should be terminated, the phase angle of the remainder tabulated function $z_6(j\omega)$ is considered. If the phase angle is zero (smaller than a threshold, e.g. here 5 deg. was found to be reasonable) all over the frequency range, it means that $z_6(j\omega)$ is a real constant (which is R_{end}) and must be terminated.

In the case of networks with transmission lines and/or cables, the order of the function is infinite. Therefore, other than the above-mentioned criteria for stopping the process, a maximum number of rounds of realization can be set (e.g. 20) so that the process will not go on forever. A flowchart for the numerical implementation of the Brune synthesis is shown in Figure 3.2.

In the next section, some examples are provided in order to clarify the steps in this method and a flowchart of how to implement the algorithm. Case studies and simulation results will also be provided to verify the feasibility of the proposed method.

3.3 Case Studies and Simulation Results

The functionality of the proposed method of fitting is investigated via case studies. Simulations show the numerical implementation and that of the proposed method provides a good fitting and always guarantees the passivity of the realized network.

3.3.1 Simple PR Function

As mentioned earlier, any PR function can be realized as a passive network. Therefore, the first case study is a simple PR function given in (3.13). To show that the proposed "numerical" adaptation of Brune's method works the same as the "analytical" one, the function is realized using both approaches. To do so, the function is calculated at a range of frequencies and tabulated.

$$z(s) = \frac{12s^4 + 18s^3 + 31s^2 + 39s + 1}{4s^3 + 4s^2 + 4s} \tag{3.13}$$

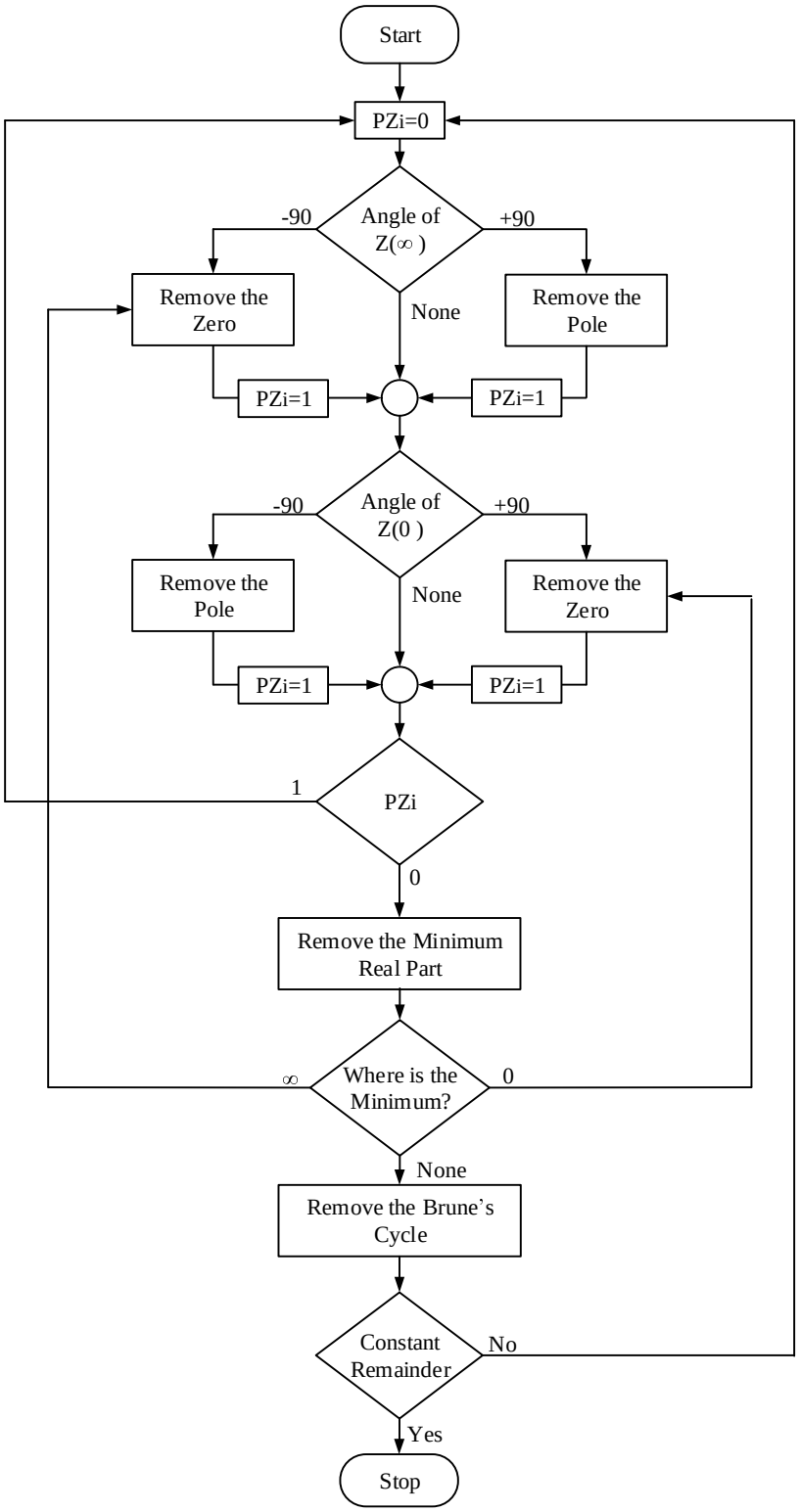

Figure 3.2: Flowchart of the algorithm for numerical implementation on Brune's procedure

Analytical Approach

The PR function in this example is simple enough for an analytical solution by the classical Brune method. This analytical realization can then be used as a template for checking whether the numerical procedure is correct.

Step 1: Pole at $s = \infty$ is found by by taking limit of the function $z(s)/s$ as shown in (3.14).

$$L_{sr} = \lim_{s\to\infty} \frac{1}{s} z(s) = 3\ H \tag{3.14}$$

The pole at zero is also found by computing the limit of the following function;

$$C_{sr} = \lim_{s\to 0} \frac{1}{s} \frac{1}{z(s)} = 4\ F \tag{3.15}$$

These poles are removed in $z_1(s)$ as given by (3.16);

$$z_1(s) = \frac{12s^4 + 18s^3 + 31s^2 + 39s + 1}{4s^3 + 4s^2 + 4s} - 3s - \frac{4}{s} = \frac{1.5s^2 + 4.5s + 9.5}{s^2 + s + 1} \tag{3.16}$$

Step 2: The function $z_1(s)$ has no zero at any frequency. So we move to the next step.

Step 3: In this step the minimum real part of $z_2(s)$ is found and removed. This is achieved by writing the analytical form of $\Re\{z_1(j\omega)\}$, and differentiating w.r.t. ω, and equating to zero. This yields $R_{min} = 0.5\ \Omega$, occurring at $\omega = \omega_m = \sqrt{3}$. On removing this resistance, we get the residual impedance $z_3(s)$ as in (3.17).

$$z_3(s) = \frac{1.5s^2 + 4.5s + 9.5}{s^2 + s + 1} - 0.5 = \frac{s^2 + 4s + 9}{s^2 + s + 1} \tag{3.17}$$

Step 4: Next is to remove L_1 of the Brune cycle.

$$L_1 = \frac{z_3(j\sqrt{3})}{j\sqrt{3}} = \frac{1}{j\sqrt{3}} \frac{(j\sqrt{3})^2 + 4j\sqrt{3} + 9}{(j\sqrt{3})^2 + j\sqrt{3} + 1} = -2\ H \tag{3.18}$$

The inductance L_1 is removed from $z_3(s)$ as follows;

$$z_4(s) = \frac{s^2 + 4s + 9}{s^2 + s + 1} - (-2s) = \frac{2s^3 + 3s^2 + 6s + 9}{s^2 + s + 1} \tag{3.19}$$

Then the zero of $z_4(s)$ created at ω_m should be removed in the form of a pole of $y_4(s)$ and to do this, it is needed to calculate the residue of the pole at this frequency.

$$\frac{1}{L_2} = \frac{s^2+\omega_m^2}{s} y_4(s) \mid_{s=j\omega_m} \Rightarrow \frac{1}{L_2} = \frac{1}{s}\frac{s^2+s+1}{2s+3} \mid_{s=j\sqrt{3}} \Rightarrow L_2 = 3\ H \tag{3.20}$$

$L_2 = 3\ H$ will result $C_2 = 1/L_2\omega_m^2 = 1/9\ F$. Now this pole can be removed from $Y_4(s)$.

$$y_5(s) = y_4(s) - \frac{s/L_2}{s^2+\omega_0^2} = \frac{1}{6s+9} \tag{3.21}$$

Last part of step 4 is to remove L_3 that using (2.13) results in a 6 H inductor. In the end, a constant impedance remains which is realized by a 9 Ω resistance as R_{end}.

$$z_6(s) = z_5(s) - 6s = 9\ \Omega \tag{3.22}$$

The resulting circuit is shown in Figure 3.5.

Note that if one realizes the Step 4 using "Direction 2" (i.e. capacitive network), a network of the type shown in 2.12.A. with the elements $C_1 = 1/6\ F$, $C_2 = 1/3\ F$, $L_2 = 1\ H$, $C_3 = -1/2\ F$ and $R_{end} = 1\ \Omega$ will result which has identical response to that of the above-mentioned inductive network.

Numerical Approach

To realize the tabulated function, the phase angle should be investigated. Observing the phase angle at very low and very high frequencies in Figure 3.5, it can be seen that the phase angle at very high frequencies reaches to $+90^\circ$, meaning that there is a pole at $\omega = \infty$ which can be realized by $L_{sr} = \Im\{z(j\omega_\infty)\}/\omega_\infty = 3.0000\ H$. Also, the phase angle at very low frequency is -90° which indicate the presence of a pole at $\omega = 0$, thus it can be realized as $C_{sr} = \Im\{1/z(j\omega_0)\}/\omega_0 = 3.9988\ F$.

Note that the capacitance of 3.9998 F is quite large, but this is merely an example to show how the process is applied, and results due to "nice" numbers used in the analytical expression in (3.17). Realistic values will of course occur in practical problems to be shown later.

In step 2, observing the phase angle at very low and very high frequencies indicates no zeros at both very low and very high frequencies. So the Step 2 of Brune's procedure does not realize any element for this particular function.

The next step can easily be done by looking into the table for the minimum real part which results in $R_{min} = 0.5000$ at $\omega_m = 1.732 \approx \sqrt{3}$.

Step 4 begins with calculating the value of $L_1 = z_3(j\omega_m)/j\omega_m = -2.0001H$. Then the shunt branch L_2 and C_2 can be found by calculating the residue at ω_m which gives $3.0001H$ and $0.1111F$ respectively. At the end L_3 is be calculated as $6.0014H$ and removed from the function. The remainder turns out to be 9.0000Ω resistance which is labeled as R_{end} earlier.

Figure 3.3 illustrates the numerical realization procedure with plots of the remainder functions after each step.

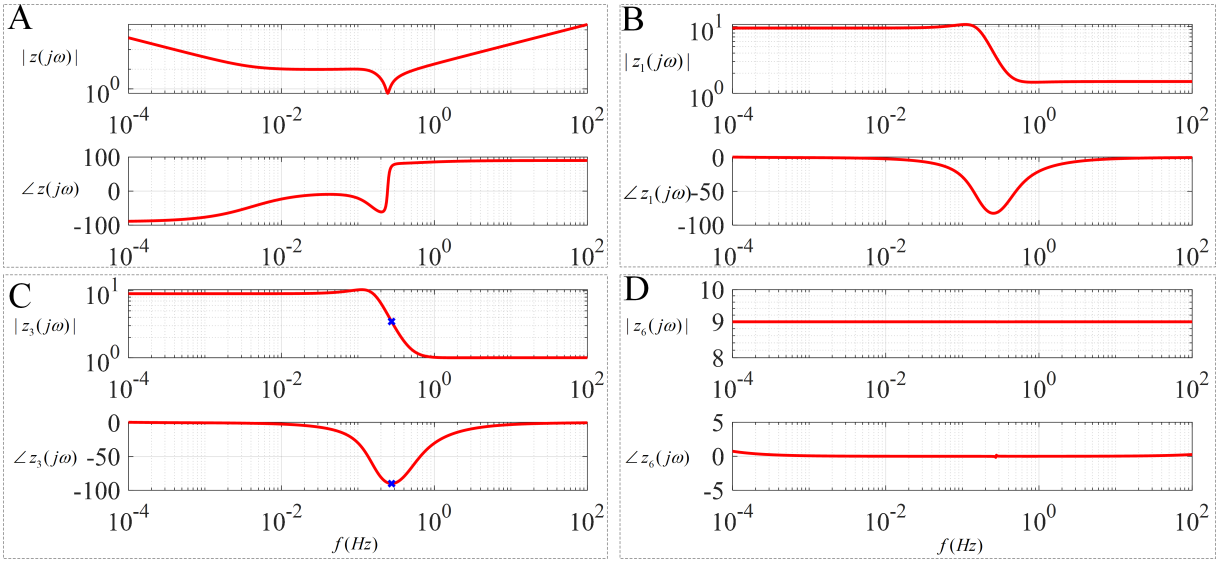

Figure 3.3: Amplitude and phase angle versus frequency of (A) Original function, (B) After removing poles in step 1, (C) After removing minimum resistance in step 3 and (D) The constant remainder after removing Brune's cycle of step 4.

Figure 3.4 shows the RLC circuit where those elements are calculated by analytical and numerical solutions of Brune's procedure. It can be seen that the values of the elements are well matched. with a maximum error of less that 0.03% for the $4F$ capacitor.

Frequency responses of the two above circuits are depicted in Figure 3.5 which shows

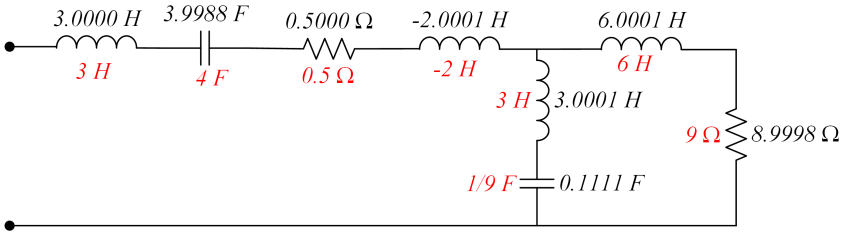

Figure 3.4: The fitted circuit using analytical (red) and the proposed method (black)

a wide-band match across all the frequencies. It has to be mentioned that the maximum deviation, in this case, is less than 0.03%.

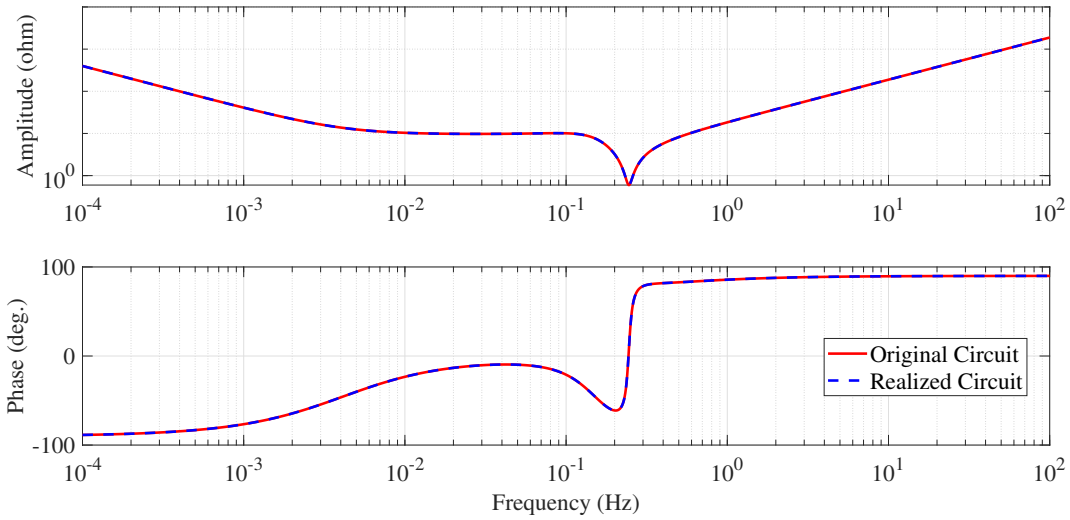

Figure 3.5: Frequency response of the original function and the fitted circuit

Accuracy versus Number of Samples

The proposed realization method is a successive procedure that fits the tabulated function by synthesizing a network whereas other fitting methods such as vector fitting which is an iterative procedure. Therefore, for this approach, there is no chance of iteration to change the values of the elements or relocate the minimum points in order to reduce the error. Since the tabulated data provides a limited number of samples, there is always a possibility of missing the exact minimum points. Thus, more samples provide better information of the

tabulated function and make the minima points closer to their actual location and hence closer fit. Also, for poles and zeros asymptotic to $\omega = 0$ or $\omega = \infty$, samples very close to these frequencies will give a more accurate calculation of their corresponding residues.

Table 3.1 shows different scenarios for sampling the function (3.13) and their fitting errors. This verifies the above-mentioned fact that the more number of samples and closer samples to $\omega = 0$ or $\omega = \infty$, i.e. scenario 3, results in more accurate fitting.

Table 3.1: Fitting error versus number of sample points

Scenario #	**1**	**2**	**3**	**4**
Number of Samples	10^3	10^3	10^5	10^5
Min & Max Frequencies (Hz)	10^{-4} & 10^1	10^{-6} & 10^3	10^{-6} & 10^3	10^{-4} & 10^1
Max Deviation (Ω)	0.1158	0.0073	0.0012	0.1165
Max Error (%)	0.8659	0.6710	0.0029	0.0293
RMS Error (Ω)	0.0322	0.0071	2.0023×10^{-4}	0.0260
L_{sr} (H)	2.9993	3.0000	3.0000	2.9993
C_{sr} (F)	3.9988	4.0000	4.0000	3.9988

3.3.2 High Order PR Function

To further examine the proposed method, a much higher order PR function is investigated in this case study. Consider the 17^{th} order rational function in the form of (3.23) is chosen with the poles and residues as given in Table (3.2).

$$z(s) = \sum_{n=1}^{N} \frac{c_n}{s + a_n} + d + sh \tag{3.23}$$

The above-mentioned function is calculated at 10^6 logarithmically spaced points in a range of frequencies $f = [10^{-3}, 10^8]$ Hz to convert it into a form of a tabulated function. Then the tabulated function is realized as a driving point impedance of a circuit using the proposed method.

The resultant network has 10 blocks in the form of Figure 3.1 connected in cascade and finally terminated in resistance R_{end} which is the constant remainder. Table D.1 in Appendix D.1, gives the values of the elements in each of the 10 blocks. In this table some of

Table 3.2: Poles and Residue of the 17^{th} order PR function

Poles (rad/s)		**Residues (Ω.rad/s)**	
-4500		$+3000$	
-120	$\pm j1500$	-250	$\pm j18$
-300	$\pm j45000$	-6000	$\pm j155$
-70	$\pm j50$	-50	$\pm j70$
-500	$\pm j9000$	-1400	$\pm j60$
-90	$\pm j1000$	-1550	$\pm j31000$
-80000	$\pm j5000$	-5000	$\pm j70000$
-40000	$\pm j450$	-800	$\pm j150000$
-20000	$\pm j5000$	-10000	$\pm j1500000$
$d = 0.2$ *and* $h = 0$			

the elements of Figure 3.1 are missing which means their corresponding steps did not occur in the process.

Figure 3.6 shows the frequency response of the original PR function comparing the realized network with the proposed method. It can be seen that the two responses are well-matched in both magnitude and phase angle. The maximum relative error of the fitted response is 0.002355 (equivalent to $\approx 1\%$) which happens at $11.5Hz$. The order of the realized circuit is also 17, which is exactly the same order as the PR function.

3.3.3 Realizing FDNE of a Portion of Electric Network

To get closer to the needs of power system simulation tools, a more realistic example is investigated and the proposed method is applied to it. In Figure 3.7 a single-phase 22kV distribution feeder is shown utilizing a 100km cable to feed a remote load. A filter bank also is installed at the sending end. Detailed information of the network including filter bank, loads, and the cable are given in Appendix D.2.

The study is made on the portion of the network from the Bus 2 point of view which is included in the box shown in Figure 3.7 in order to see the fault behavior which is applied on Bus 2. To do so, a frequency scan of the network is done looking into Bus 2. The scan is performed using a time-domain simulator (PSCAD™) scanning module. Then, applying the

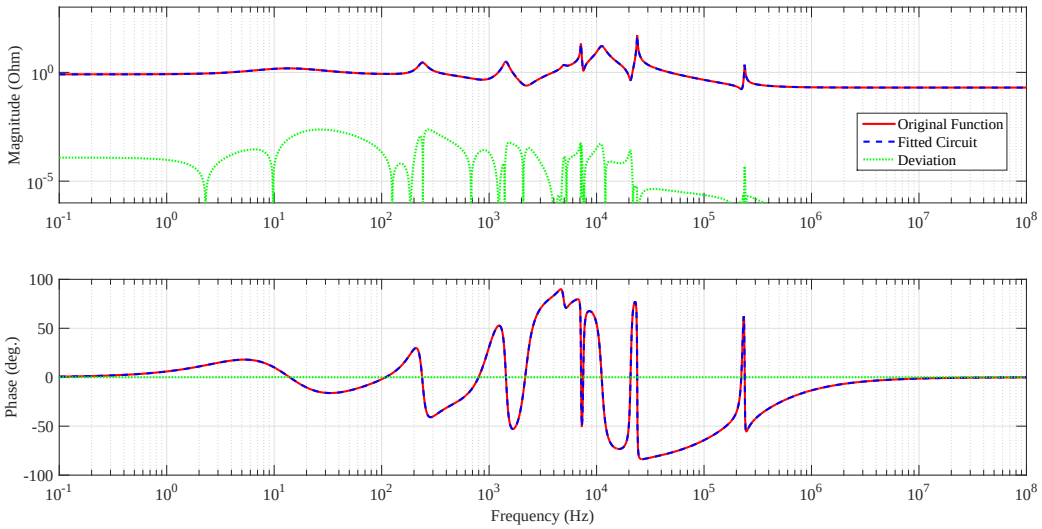

Figure 3.6: Frequency responses of the original function, the fitted circuit and their deviation

proposed method, a FDNE is realized with an equivalent circuit.

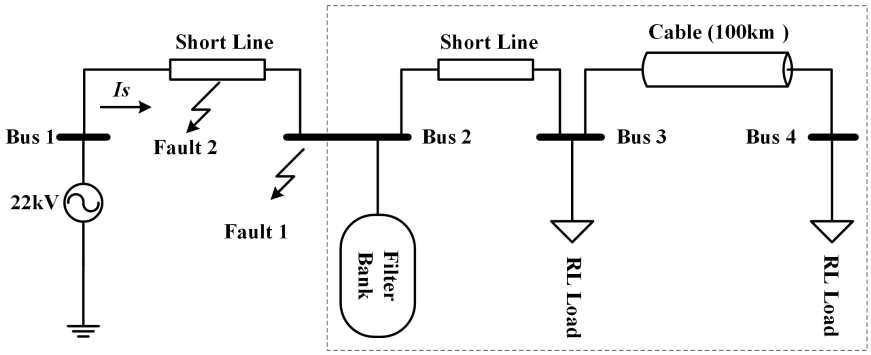

Figure 3.7: The portion of network scanned in the simulator from fault location and current I_s.

Figure 3.8 shows the frequency responses of the original circuit compared with the realized circuit as well as the deviation. The two responses match very well in both magnitude and phase angle. The maximum magnitude error, in this case, is about 0.05 which happens at very high frequencies.

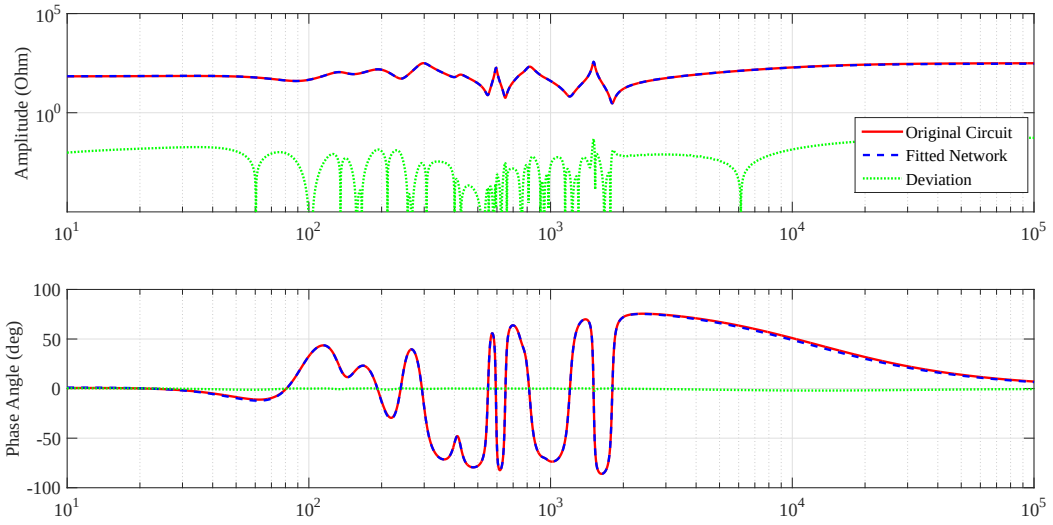

Figure 3.8: The frequency response comparison of the original network vs. realized circuit.

The realized circuit has 13 blocks of the type shown in Figure 3.1 where all elements are given in Table D.2 in Appendix D.2. In this case, also there are many missing elements that did not arise in the process of realization.

Investigating Rounds of Realization

Figure 3.9 shows the frequency response of the realized network versus the original FDNE response if the realization process is terminated after rounds 1, 2, 3, 4, 5, 8, 10, and 13. It can be seen that even after round 10, the fitting is acceptable but because of the 5° threshold defined in the algorithm as an exit criterion, the process goes on and exits after round 13. This shows that the procedure can be stopped at any round of realization even without reaching an exact constant remainder and still get a passive network realized.

Time Domain Comparison

The realized network is built in time-domain simulation. In the time-domain simulation, the network given in Table D.2 is modeled in the EMT simulator as well as the original network

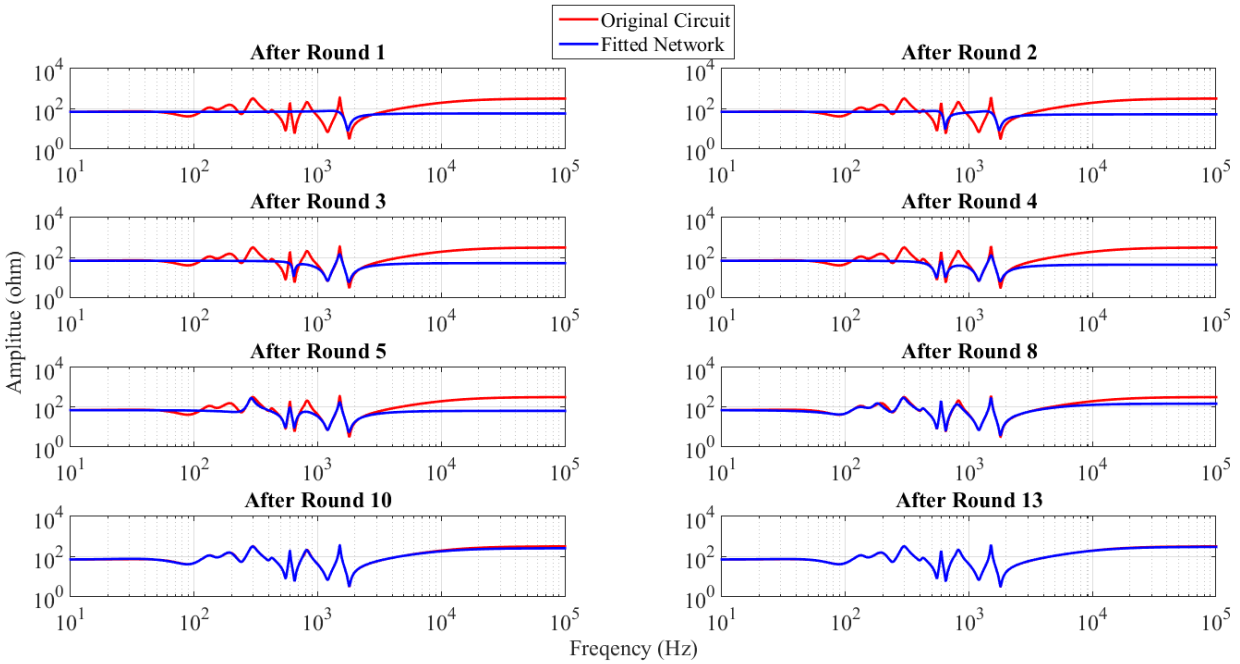

Figure 3.9: Frequency responses of the original function versus the fitted circuit stopped at different rounds of realization.

in Figure 3.7. Then a fault is applied at Bus 2 at 0.12 s and cleared at 0.18 s. Figure 3.10 shows the two circuit's responses (the current I_s) before, during, and after the fault period which indicates they are well matched.

It can be seen that the response is essentially identical both in the transient period (right after when the fault is cleared) as well as the steady-state.

Also, it is expected to have a faster time-domain simulation when reducing the circuit order with a FDNE. In this special example it is noted that the CPU run-time for the original network was 577 ms while the fitted circuit simulation is reduced to only 124 ms which is a gain of 4.65.

The author has published these results in [84].

In this chapter, frequency domain comparisons and examination results are only illustrated. Simple cases, that result in a few Brune's blocks can be manually built in EMT simulators but when it comes to much higher order fitting and consequently larger resultant network, a systematic technique is necessary to build the EMT model of the realized

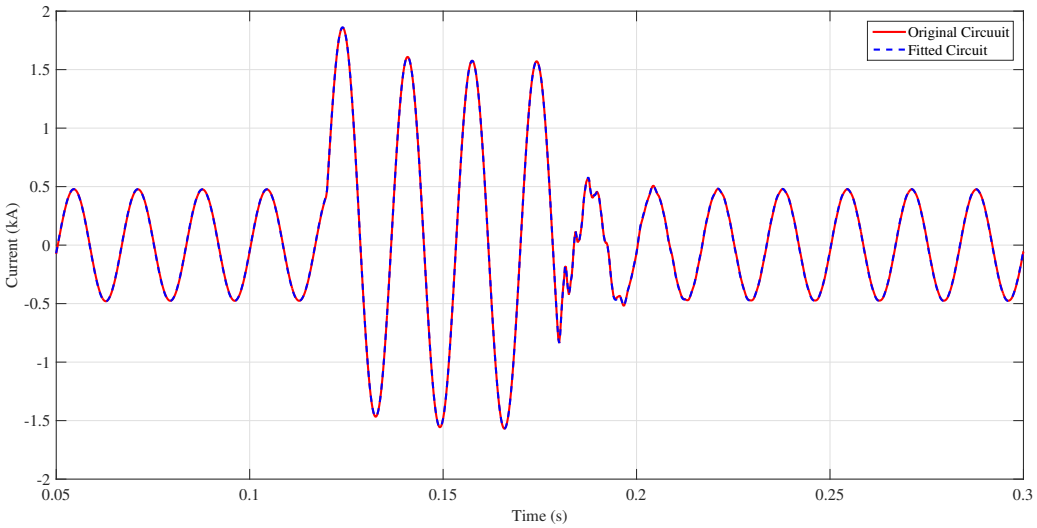

Figure 3.10: Sending end current I_s of the original circuit comparing to the fitted circuit during and after applying fault.

network. Chapter 5 explains how to implement networks with cascaded sub-circuits on an EMT simulator.

3.4 Summary

In this chapter, Brune's realization approach was adapted in order to be applied to the tabulated functions, $z(j\omega)$. To do so, firstly it was proved that unlike the Brune's original form which needs $z(s)$ to realize its network, only $z(j\omega)$ is necessary and sufficient. Then, analogous steps to that of Brune were introduced to perform the realization procedure in a numerical manner on tabulated functions using an automated program. The proposed approach was validated at the end of this chapter via examples where fitting and simulation results showed a very good match in the frequency domain as well as transient response. It was also shown via an example that the proposed approach provides a more accurate fitting if a higher resolution of data is given.

Chapter 4

Adapting Tellegen's Approach for Realization of Multi-port Networks from Tabulated Functions

Brune's realization method was only introduced for single port networks, while in typical power system analysis, multi-port networks are of interest.

As was discussed in Section 2.3, using steps similar to Brune's method, Tellegen extended the idea to realize a multi-port network for a given impedance matrix $Z(s)$. Note that for multi-port networks, the impedance representation becomes a matrix $Z(s)$ instead of the scalar $z(s)$.

Similar to Brune's approach, all steps of Tellegen's procedure [70] can also be done directly from tabulated frequency response data, i.e., $Z(j\omega)$ except that $Z(j\omega)$ is now a multi-port impedance matrix. Thus, to perform the realization process, knowing the tabulated frequency response data of function $Z(j\omega)$ is sufficient and there is no need for having $Z(s)$.

In this chapter, Tellegen's procedure is adapted in order to be applied to the tabulated function, $Z(j\omega)$, which is an $n \times n$ matrix for an n-port network. Then case studies and simulations are presented to verify the functionality of the method. Throughout the case studies, it was found that the Tellegen's method did not work in some special cases and thus

not possible to be applied to very high order FDNEs. Therefore the realization process is also modified so that it can work on any type of tabulated function, particularly the FDNE obtained for power system networks.

4.1 Tellegen's Multi-port Networks Procedure for Tabulated Data

This section illustrates the "numerical" steps to be taken for realizing the n-port network in Tellegen's procedure as were taken for the single port with Brune's method in Chapter 3. Here also before starting the procedure, the following theorem for the, $Z(j\omega)$, a $n \times n$ PR function is proved which will be used later.

Theorem:

" If $Z(j\omega)$ has a pole on $j\omega$ axis, its residue matrix has at least one non-zero diagonal element."

Proof:

" If all the diagonal elements of the residue matrix, K_x, are zero, then the matrix will not be positive semi-definite (Assuming K_x is not a zero matrix). This is because of the fact that the summation of all the eigenvalues of K_x is equal to the trace of K_x, i.e. sum of its diagonal elements. Therefore, as the trace of the matrix is zero, the sum of eigenvalues will also be zero. This means that one of the following two must be true:

I. All the eigenvalues are zero which is a contradiction, as it is assumed that K_x is not a zero matrix.

II. Some of the eigenvalues are positive and some are negative but the summation of all is zero. This is also in contradiction with the fact that the residue matrices of the imaginary axis poles of PR functions should be positive semi-definite and thus can not have negative eigenvalues.

Therefore, it is impossible to have the residue matrix of a pole of a PR function with all zero diagonal elements and this proves any pole of the matrix must appear on at least one of the diagonal elements."

One of the outcomes of the above-mentioned theorem is that in looking for poles of matrices, investigating the diagonal elements is sufficient. This reduces the number of elements to be checked for poles from n^2 to n for a n-port matrix.

4.1.1 Step 1: Reduction of the network by removal of the imaginary axis poles

As explained in Section 2.3, if at least one element of the tabulated function $Z(j\omega)$ has a pole at a certain frequency, it is considered as the pole of the whole matrix. Based on the above-mentioned theorem, the presence of poles is found by only investigating the phase angle of the "diagonal elements" of the matrix $Z(j\omega)$. An asymptotic phase angle of $+90^\circ$ as the frequency goes to infinity indicates a pole at $\omega \to \infty$, and thus yields the residue matrix of $K_{\infty p}$. A low frequency phase angle of -90° in any of the diagonal elements reveals the pole at $\omega \to 0$ and enables calculation of the residue matrix of K_{0p}. Finally, K_{jp} represents the residue matrix of the pole at frequency ω_{jp} which is found by sharp changes in phase angles from $+90^\circ$ to -90°. These constant matrices are found as shown in (4.1).

$$K_{\infty p} = \frac{\Im[Z(j\omega_\infty)]}{\omega_\infty} \quad , \qquad K_{0p} = \frac{1}{\Im[Z(j\omega_0)]\omega_0} \quad , \qquad K_{jp} = \frac{-\omega^2 + \omega_{jp}^2}{2j\omega} Z(j\omega)|_{at\ \omega=\omega_{jp}} \quad (4.1)$$

Now, if the residue matrices $K_{\infty p}$, K_{0p} or K_{jp} are rank one matrices, the corresponding pole will be represented by an impedance and $n-1$ ideal transformers as labeled in Figure 4.1 by "Series Network".

Otherwise, if the residue matrix is of higher rank, say M, it is broken into sum of rank one matrices. This is shown in (4.2) for a general matrix K_x in which it is assumed that the set $\{\lambda_1, \lambda_2, \lambda_3, ...\lambda_M, 0, 0, ..., 0\}$ are the eigenvalues of K_x and t_i , $i \in \{1, 2, 3, ..., M\}$ are their corresponding eigenvectors those are normalized with respect to the first row. The series rank M network is depicted in Figure 4.2.

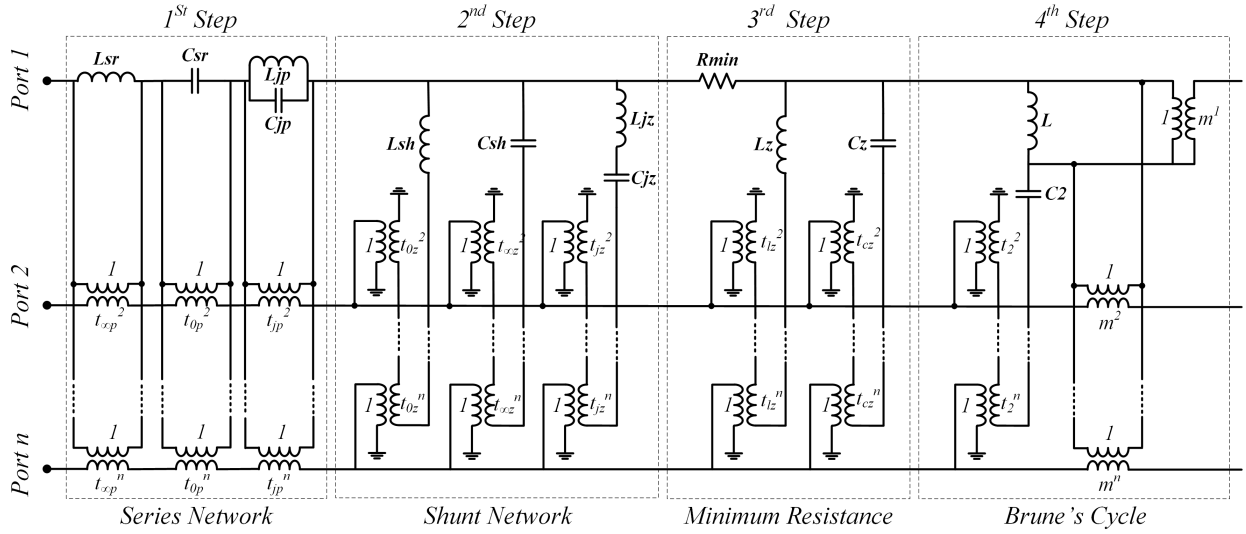

Figure 4.1: The whole possible n-port network in one round of the Tellegen's realization

$$K_x = \sum_{i=1}^{M} t_i \lambda_i t_i^T \qquad , \qquad t_i = \begin{bmatrix} 1 \\ t_{2i} \\ \vdots \\ t_{ni} \end{bmatrix} \tag{4.2}$$

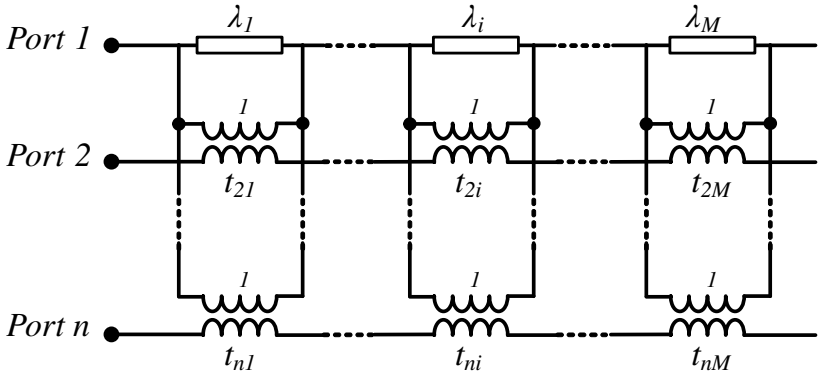

Figure 4.2: Series network realization of rank M impedance matrix

The matrices of poles are then subtracted as shown in (4.3) and realized in the form of

a series impedance network.

$$Z_1(j\omega) = Z(j\omega) - j\omega K_{\infty p} - \frac{1}{j\omega}K_{0p} - \sum_{jp=1}^{np} \frac{2j\omega}{-\omega^2 + \omega_{jp}^2} K_{jp} \tag{4.3}$$

4.1.2 Step 2: Reduction of the network by removal of the imaginary axis zeros

The determinant of the tabulated function $Z_1(j\omega)$, i.e. $|Z_1(j\omega)| = 0$ at a certain frequency implies that there is a zero at that frequency. As was done with the scalar function $z_1(j\omega)$, the zeros of the matrix $Z_1(j\omega)$ are similarly removed in the form of poles of $Y_1(j\omega) = Z_1^{-1}(j\omega)$ and realized as a shunt network. Similar to the previous step, the presence of the zeros of $Z_1(j\omega)$ (or poles of $Y_1(j\omega)$) by investigating the phase angle of the tabulated function. Residues of the poles of $Y_1(j\omega)$ are $K_{\infty z}$, K_{0z} and K_{jz} representing the poles at frequencies $\omega \to \infty$, $\omega \to 0$ and ω_{jz} respectively and found by (4.4).

$$K_{\infty z} = \frac{\Im[Y_1(j\omega_\infty)]}{\omega_\infty} \quad , \quad K_{0z}^{-1} = \frac{\Im[Y_1(j\omega_0)]}{\omega_0} \quad , \quad K_{jz} = \frac{-\omega^2 + \omega_{jz}^2}{2j\omega} Y_1(j\omega)|_{at\ \omega=\omega_{jz}} \tag{4.4}$$

The poles of $Y_1(j\omega)$ are removed as shown in (4.5) and remains the matrix $Y_2(j\omega)$. Similar to the residue matrix of the poles, the residue matrix of zeros is realized using rank one networks but in this case, using shunt networks as depicted in Figure 4.3.

$$Y_2(j\omega) = Y_1(j\omega) - j\omega K_{\infty z} - \frac{1}{j\omega}K_{0z}^{-1} - \sum_{jz=1}^{nz} \frac{2j\omega}{-\omega^2 + \omega_{jz}^2} K_{jz} \tag{4.5}$$

The first two steps are repeated until there are no more poles or zeros in the matrix $Z_2(j\omega)$.

The block named as "Shunt Network" in Figure 4.1 shows the imaginary zeros with the residues, $K_{\infty z}$,K_{0z} and K_{jz} are realized by a n-port network assuming that all of them are rank one matrices.

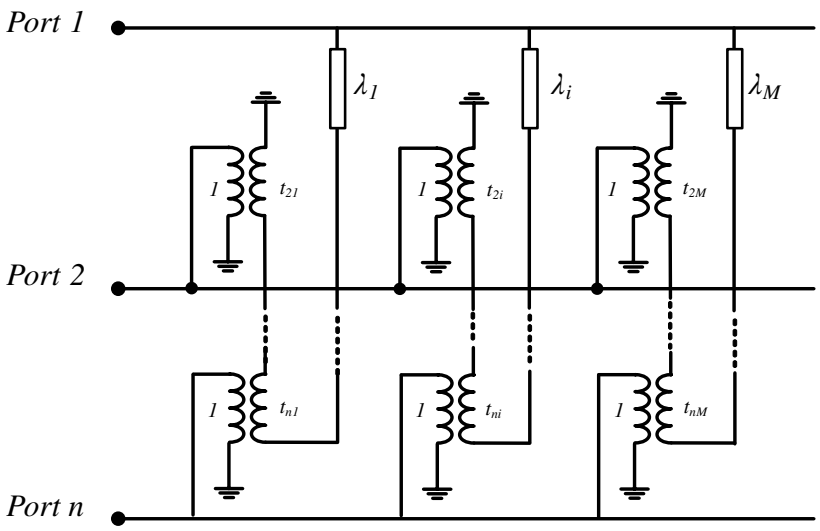

Figure 4.3: Shunt network realization of rank M admittance matrix

4.1.3 Step 3: Reduction of the network by removal of minimum resistance

Let $A(\omega) = \Re\{Z_2(j\omega)\}$ the real part of the tabulated matrix $Z_2(j\omega)$. The minimum resistance, R_{min}, is then defined by (4.6) in which $\Delta_{11}(\omega)$ is the $(1,1)$ minor of $A(\omega)$.

$$R_{min} = \min\{\Lambda(\omega)\} \qquad , \qquad \Lambda(\omega) = \frac{|A(\omega)|}{\Delta_{11}(\omega)} \tag{4.6}$$

Function $\Lambda(\omega)$ can be calculated at every sample point in tabulated form and thus, finding its minimum only needs looking up the table.

Let ω_m be the frequency at which the minimum resistance occurs. Then by subtracting the resistance R_{min} from $Z_2(j\omega)$, a zero is created at ω_m in $\Re\{Z_2(j\omega)\}$. This means $|\Re\{Z_3(j\omega_m)\}| = 0$ or the real part of matrix $Z_3(j\omega)$ will become rank deficient at ω_m. The resistance R_{min} is only realized at port one of the network. Therefore, the function $Z_3(j\omega)$ can be written by (4.7):

$$Z_3(j\omega) = Z_2(j\omega) - \begin{pmatrix} R_{min} & 0 & \cdots & 0 \\ 0 & 0 & \cdots & 0 \\ \vdots & \vdots & \ddots & \vdots \\ 0 & 0 & \cdots & 0 \end{pmatrix} \tag{4.7}$$

It is worth mentioning that in general, one can remove the resistance R_{min} from any port i, considering that the resistance must be calculated using the corresponding principal minor, Δ_{ii} in (4.6). This will be further discussed later in this chapter.

As mentioned in Chapter 2, in a case $\omega_m = \infty$ or $\omega_m = 0$, subtracting the resistance creates a zero in $Z_3(j\omega)$ at the corresponding frequency. This is because both imaginary and real part of the function becomes zero at that corresponding frequency. Thus, the zero is removed in the form of a pole of $Y_3(j\omega)$ by means of the shunt network consisting of L_Z, C_Z and ideal transformers with the turns ratio t_{lz} and t_{cz} as shown in Figure 4.1.

4.1.4 Step 4: Extended Brune's cycle for further network reduction

If R_{min} happens at a finite frequency, i.e., $0 < \omega_m < \infty$ then a step analogous to Brune's cycle is required to lower the order of the impedance matrix by two. This step can be done in a numerical manner on the tabulated function as explained below.

In the previous step, the real part of the matrix $Z_3(j\omega)$ became rank deficient at ω_m, and by definition there exists a vector β such that;

$$\Re\{Z_3(j\omega_m)\}\beta = 0 \tag{4.8}$$

in which the vector β is called the null vector, i.e. the eigenvector corresponding to the zero eigenvalue.

Then, the imaginary part, $X = \Im\{Z_3(j\omega_m)\}$ should also become rank deficient at ω_m with the same vector β. Therefore, there is a rank one symmetric matrix H such that;

$$(X - H)\beta = 0 \qquad , \qquad X = \Im\{Z_3(j\omega_m)\} \tag{4.9}$$

While any real symmetric rank one matrix of H can be written as a product of a real vector h and a constant α;

$$H = \alpha h h^T \qquad , \qquad \alpha = \pm 1 \tag{4.10}$$

In which the value of α is determined by (4.11).

$$X\beta = \alpha h h^T \beta \qquad \Rightarrow \qquad \beta^T X \beta = \alpha (h.\beta)^2 \qquad \Rightarrow \qquad \alpha = \frac{(h.\beta)^2}{\beta^T X \beta} \tag{4.11}$$

With some manipulations, the vector h can also be determined by (4.12)

$$h = \frac{1}{\sqrt{\alpha \beta^T X \beta}} X\beta \tag{4.12}$$

Similar to Brune's approach for scalar functions, depending on the value of α, there will be two possible directions to continue the procedure for multi-port functions as following:

Direction 1: $\alpha < 0$

Now, the rank one matrix H is normalized with respect to H_{11} in order to create the inductance $L_1 = H_{11}/\omega_m$. Then the inductance is removed from $Z_3(j\omega)$ as shown in (4.13) in which t_1 is the vector of the ideal transformer turns ratio.

$$Z_4(j\omega) = Z_3(j\omega) - j\omega L_1 t_1 t_1^T \qquad , \qquad t_1 = \frac{1}{H_{11}} h \tag{4.13}$$

Next, the zero which is created at ω_m is removed from $Z_4(j\omega)$ in form of pole of $Y_4(j\omega)$ as given by (4.14).

$$Y_5(j\omega) = Y_4(j\omega) - \frac{j\omega K_m}{-\omega^2 + \omega_m^2} \qquad , \qquad K_m = \frac{1}{L_2} t_2 t_2^T \quad , \quad C_2 = \frac{1}{L_2 \omega_m^2} \tag{4.14}$$

where the reside K_m is a rank one matrix which is normalized with respect to the first element, i.e. (1,1) to calculate L_2, and t_2 is the vector of transformer turns ratio connecting the L_2C_2 branch to the other ports.

Note that to calculate L_2 in (4.14), the residue matrix K_m is indeterminate at exactly ω_m. This is because $Z_4(j\omega)$ has a zero at ω_m, and so $Y_4(j\omega) = Z_4(j\omega)^{-1}$ has a pole at ω_m. This means $Y_4(s)$ has a factor $1/(-\omega^2 + \omega_m^2)$, and therefore using (4.14) to calculate $K_m = Y_4(j\omega)(-\omega^2 + \omega_m^2)/s$ at $s = \omega_m$, would give an indeterminate answer, i.e., 0/0. To

avoid this, K_m is calculated as a limit by evaluating and averaging the samples at frequencies immediately before and immediately after ω_m as was done at a similar stage in Brune Synthesis in Section 3.2.4.

Lastly, the inductance L_3 must be removed from the function $Z_5(j\omega) = Y_5^{-1}(j\omega)$ in order to finish the cycle as;

$$Z_6(j\omega) = Z_5(j\omega) - j\omega L_3 t_1 t_1^T \tag{4.15}$$

Tellegen [70] showed that to couple L_3 to other ports, it uses the same set of transformer turns ratio as L_1. Also, he proved that the relation (4.16) between the inductances L_1, L_2 and L_3 is always true:

$$L_3 = \frac{-L_1 L_2}{F^2 L_1 + L_2} \qquad , \qquad F = t_1^T t_2 \tag{4.16}$$

Direction 2: $\alpha > 0$

In case of a positive α, the procedure will continue by realizing a capacitive network. The rank one matrix H is normalized with respect to H_{11} in order to create the capacitance $C_1 = -1/(\omega_m H_{11})$. Then the capacitance is removed from $Z_3(j\omega)$ as shown in (4.17) in which t_1 is the vector of the ideal transformer turns ratio.

$$Z_4(j\omega) = Z_4(j\omega) - \frac{1}{j\omega C_1} t_1 t_1^T \qquad , \qquad t_1 = \frac{1}{H_{11}} h \tag{4.17}$$

Then, the zero which is created at ω_m is removed from $Z_4(j\omega)$ in form of pole of $Y_4(j\omega)$ as given by (4.18).

$$Y_5(j\omega) = Y_4(j\omega) - \frac{j\omega K_m}{-\omega^2 + \omega_m^2} \qquad , \qquad K_m = \frac{1}{L_2} t_2 t_2^T \qquad , \quad C_2 = \frac{1}{L_2 \omega_m^2} \tag{4.18}$$

Eventually, the capacitance C_3 is removed from the function $Z_5(j\omega) = Y_5^{-1}(j\omega)$ as shown in 4.19 ;

$$Z_6(j\omega) = Z_5(j\omega) - \frac{1}{j\omega C_3} t_1 t_1^T \tag{4.19}$$

It is also proved that C_3 can be calculated by (4.20).

$$C_3 = -(C_1 + F^2 C_2) \qquad , \qquad F = t_1.t_2 \tag{4.20}$$

Here also one of C_1 or C_3 becomes negative, but with a similar approach as before, the "Tee" connection of the capacitors can be converted into ideal transformers and a positive capacitor.

Similar to Brune's method, networks realized in "Direction 2" and "Direction 1" are equivalent, although one or the other may give more convenient values when a physical realization is desired. However, for implementation in a digital computer-based EMT solver, no matter what is the value of α, one can proceed by choosing any of the two "Directions" and achieve networks with exactly the same frequency response. In this thesis, we always choose Direction 1 regardless of the value of α.

4.1.5 Continuation and Termination

The next round of reduction is applied to $Z_6(j\omega)$ to further reduce its order and continues until the residual network is a constant matrix i.e. R_{end}. Numerically this termination is flagged when the diagonal elements have a very small phase angle (Threshold of 5° is used in this thesis).

Figure 4.1 shows the overall possible network which might be realized after one round of performing four steps of the Tellegen's procedure. After finishing the realization rounds, these blocks will be connected in cascade and finally terminated in a resistive network given by matrix R_{end}.

4.2 Case Studies and Need for Improving the Procedure

In this section case studies are provided showing the application of the proposed method for the multi-port network. Also, through the case studies, a critical issue with the Tellegen's

approach when applied to tabulated data is identified and then a solution to that is suggested.

4.2.1 Two Port RLC Network

Figure 4.4 shows the 2 ports network which has been scanned and tabulated. This tabulated data is then used as a first example, to demonstrate the Tellegen's synthesis procedure, for multi-port FDNE realizations.

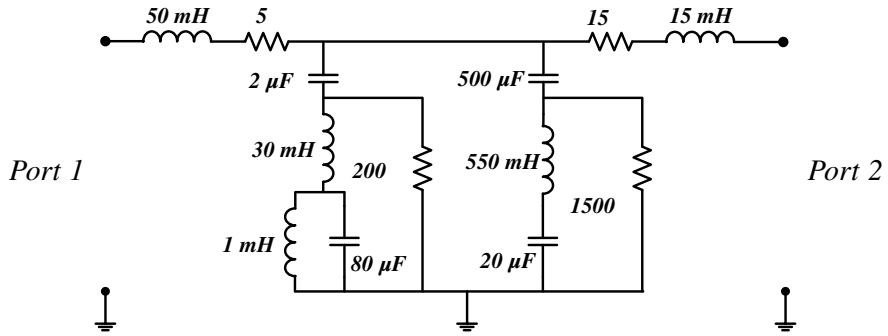

Figure 4.4: The simple two ports RLC network under study

Figure 4.5 shows the frequency response of the driving point impedance of the original circuit and the realized two-port network. The result shows a very good match both in amplitude and phase angle with the maximum deviation of 0.08% in amplitude which occurs at *1 Hz* for all three plots. The Figure shows the diagonal and off-diagonal elements as labeled.

The realized network elements are given in Table D.3 of Appendix D.

4.2.2 Impact of Linear versus Logarithmic Sampling of Data Points

It is worth mentioning that the tabular data samples used to synthesize the circuit could be either linearly or logarithmically spaced. Table 4.1 shows different scenarios for sampling the network in Figure 4.4 and the resulting error. With both linearly and logarithmically spaced samples, accuracy improves as the number of samples is increased. In comparison, the linearly spaced samples result in somewhat poorer fitting accuracy. As Figure 4.5 shows, although the sample range extends to 100,000 Hz, the significant poles appear to be at

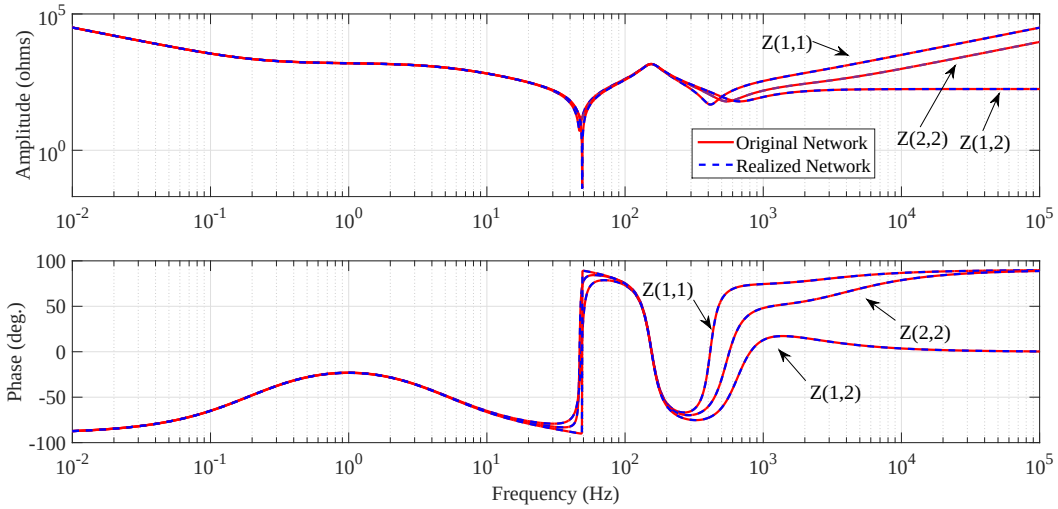

Figure 4.5: Frequency response of the original circuit and the realized two ports network

or below 1000 Hz. Logarithmically spaced samples result in more closely spaced samples at lower frequencies than at higher frequencies. This results in closer spaced sampling in the frequency range where the poles are located in comparison to linear spacing. Hence the logarithmic spacing is more accurate in this situation. On the other hand, if the poles were clustered nearer the higher frequency range, linear spacing between samples may have resulted in better accuracy.

Table 4.1: Accuracy of the fitting versus type of spacing in sampling

Scenario #	**1**	**2**	**3**	**4**
Number of Samples	10^3	10^5	10^3	10^5
Min & Max Frequencies (Hz)	10^{-3} & 10^5	10^{-3} & 10^5	10^{-3} & 10^5	10^{-3} & 10^5
Type of Spacing	Linear	Linear	Logarithmic	Logarithmic
Max Error (%)	0.6184	0.0013	0.0508	0.0009
RMS Error (Ω)	10.7751	0.6471	5.3054 $\times 10^{-4}$	0.1944

4.2.3 Three Port RLC Network and Implementation Challenges

After investigating several different cases with tabulated data, it was found that Tellegen's original procedure in some cases does not realize the correct network. As an example,

consider the three-port as in Figure 4.6, which was frequency scanned and tabulated, and the resulting data was used for FDNE synthesis with Tellegen's realization process.

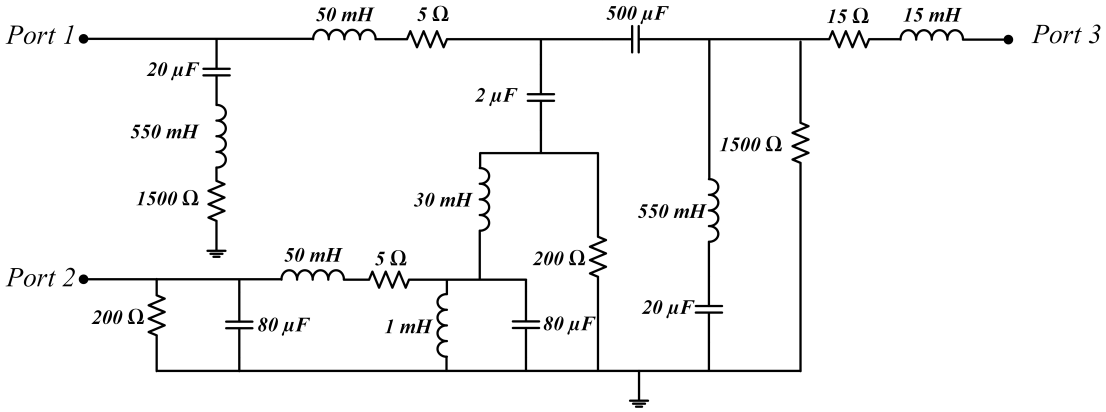

Figure 4.6: The three ports RLC network under study

The frequency response of the impedance matrix of the above mentioned three-ports network is shown in Figure 4.7.

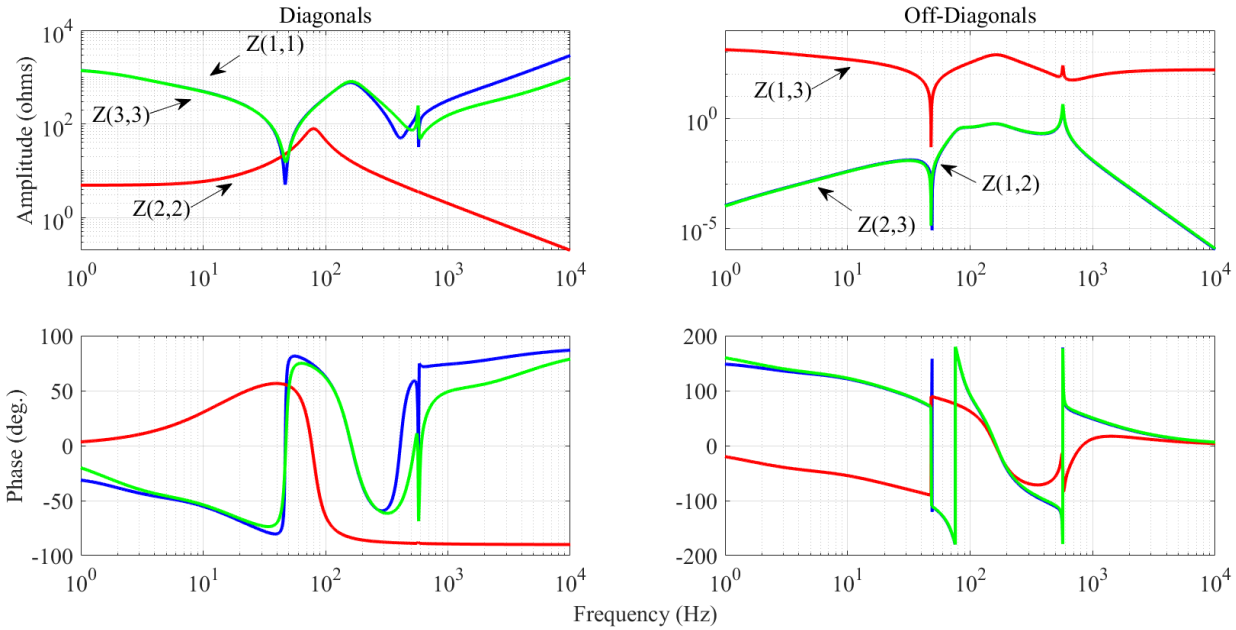

Figure 4.7: Frequency response of the three ports RLC network under study

After completing 7 rounds of the realization procedure, the frequency response of the remainder impedance matrix, i.e. $Z_2(j\omega)$, is shown in Figure 4.8.

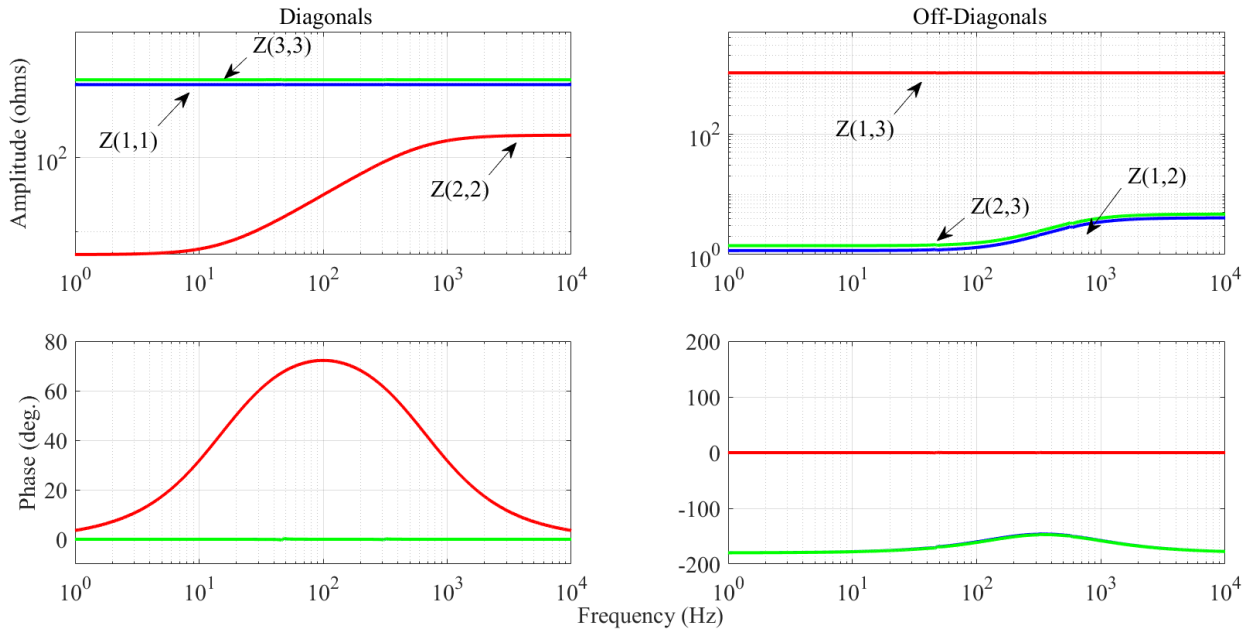

Figure 4.8: Frequency response of the three ports RLC network after 7 rounds

As Figure 4.8 shows, after 7 rounds of realization, the impedances Z_{11} and Z_{33} become constant while Z_{22} still remains to be further realized. As Z_{11} is constant, this means the idea of realizing the network on port one and coupling it to the other ports via the transformer is not possible. Furthermore, if the procedure continues on port one, the function $\Lambda(\omega)$ in (4.6) will also be a constant as shown in Figure 4.9 while $\Lambda(\omega)$ on port 2 is not.

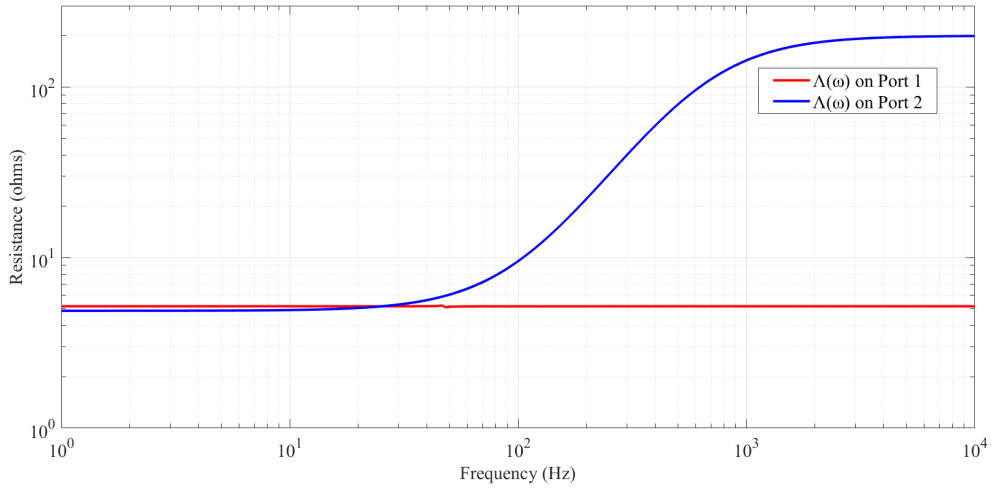

Figure 4.9: Function $\Lambda(\omega)$ on port 1 and port 2 after 7 rounds of realization

Furthermore, removing the constant $\Lambda(\omega)$ of port 1 as minimum resistance, R_{min}, will not create a zero on $Z_3(j\omega)$ (or a pole on $Y_3(j\omega)$ as shown in Figure 4.10) anywhere on the frequency span, therefore the algorithm can neither realize L_z and C_z nor a Brune's cycle. Thus, it will halt without finishing the realization correctly.

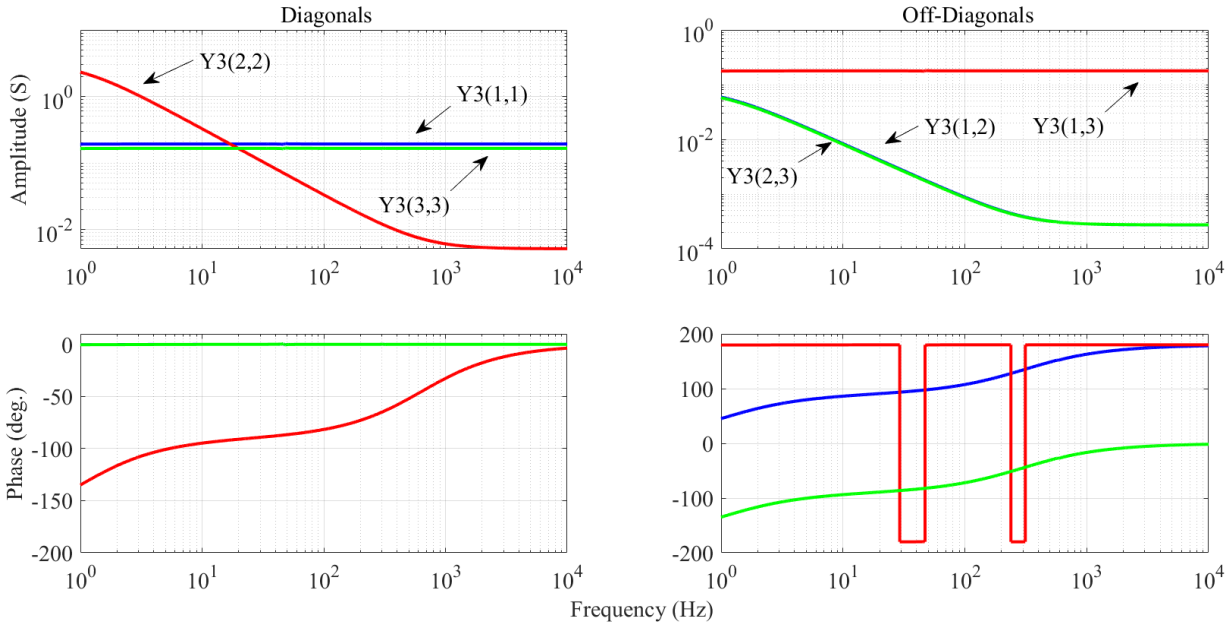

Figure 4.10: Frequency response of $Y_3(j\omega)$ showing no pole after removing the constant resistance

This indicates that when port one has reached a constant, other ports need to be monitored to make sure the realization moves ahead symmetrically for all ports. It becomes critical when facing very high order functions (e.g. transmission lines and cables) as the realization procedure never reaches a constant. This problem is investigated further in the next section and modification is proposed to overcome the issue.

4.3 Improvement of Tellegen's Method for Tabulated Data

In order to introduce the modification on Tellegen's approach, the following properties are to be clarified:

I. In both Brune's and Tellegen's realization approaches, after each round of realization (e.g. removing poles, zeros, minimum resistance, and the Brune's cycle), the remainder function is still a PR function [85]. Therefore, the remainder itself can be coped with an independent new PR function to be realized.

II. Tellegen's realization approach originally defines that the elements corresponding to the poles, zeroes, minimum resistance, etc. should be connected on port 1 and coupled to the other ports using ideal transformers. Investigating the four steps shows that instead of port 1, without loss of generality, at any round of realization, one might select any other port, e.g. port i, $i \in \{1, 2, ..., n\}$ to continue the realization process.

Considering the above mentioned two key facts, Tellegen's procedure was modified with the addition of the following:

1. "The realization process starts by connecting the elements on port 1 (which is referred to as the *realization port*). If nothing left to be realized on port 1, port 2 is selected as the realization port for the next round, and so on, with the realization port spanning across network ports in sequence until the resistive residual network remains."

   Therefore, the stop criterion should be that all Z_{ii}, $i \in \{1, 2, ..., n\}$ reach to a constant value. This can be performed by comparing the phase angle of each element against a small threshold (5° in this thesis). The reason for only investigating the diagonal elements stems from the theorem at the beginning of this chapter.

   Using this modification, the previous three-port case study can be completed with one more round of realization on port 2. The fitting result is shown in Figure 4.11 comparing

the diagonal and off-diagonal elements of the impedance matrix of the realized network and the original one.

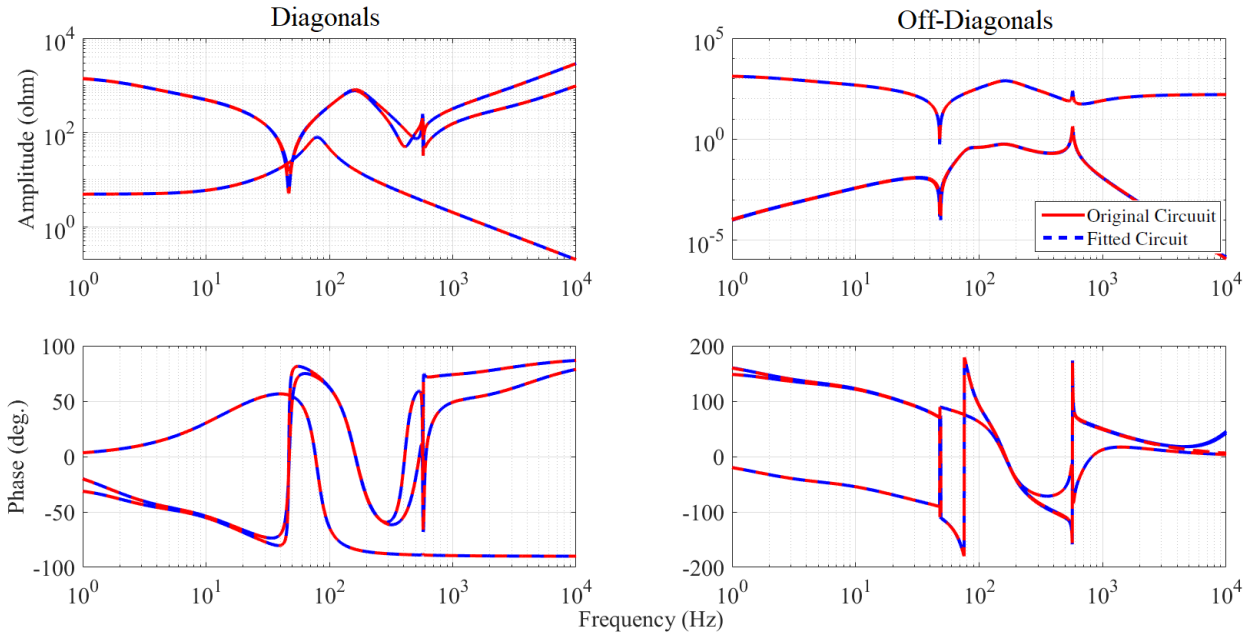

Figure 4.11: Frequency response of the three ports RLC network versus the realized network

2. "Furthermore; in case of very high order FDNEs (e.g. networks containing transmission lines and cables), it is found that if port 1 was selected as the *realization port*, poorer fitting was sometimes observed on other ports i.e. Z_{ij}, $i, j \in \{2, 3 \dots n\}$ although Z_{1i}, $i \in \{1, 2, 3 \dots n\}$ was fitted well. That is because the real network being converted to an FNDE could be of infinite order if distributed parameter elements such as cables or transmission lines are present, and therefore the reduction never reaches an exact final constant. For that reason, and considering the above-mentioned properties, the implementation of Tellegen's algorithm modifies the port order (from port 1 to 2, 3 ...) at each round of realization. This allows the procedure to reduce the order of FDNE in a balanced manner across all ports as it goes on.

   Of course, due to the inherent property of Brune and Tellegen's realization approaches, the remainder is still a positive real function after each round of realization. Thus, changing

the realization port in each round retains the passivity of the final network, as the overall network is constructed by the cascade connection of several passive sub-circuits.

4.4 Modelling a 20 kV Distribution Network with Proposed Approach and Comparison with Traditional Vector Fitting Approach

In this example, the proposed method is utilized for FDNE realization of a 20 kV distribution network shown in Figure 4.12 (adapted from [2]). Accuracy and passivity comparison with the popular vector fitting (VF)approach is also carried out for this example. The network contains very short overhead lines and underground cables. This means a very small time step is required (e.g 0.1 μs) to simulate the network and therefore a wider range of frequency response is necessary to capture same transient behaviour in its FDNE model. To do so, the network is scanned using the harmonic impedance component in PSCAD with a user-defined range of frequency (i.e. 0.01 Hz to 150 kHz). Figure 4.13 shows the configuration of the overhead lines and underground cables. Cable conductor data is provided in Table 4.2.

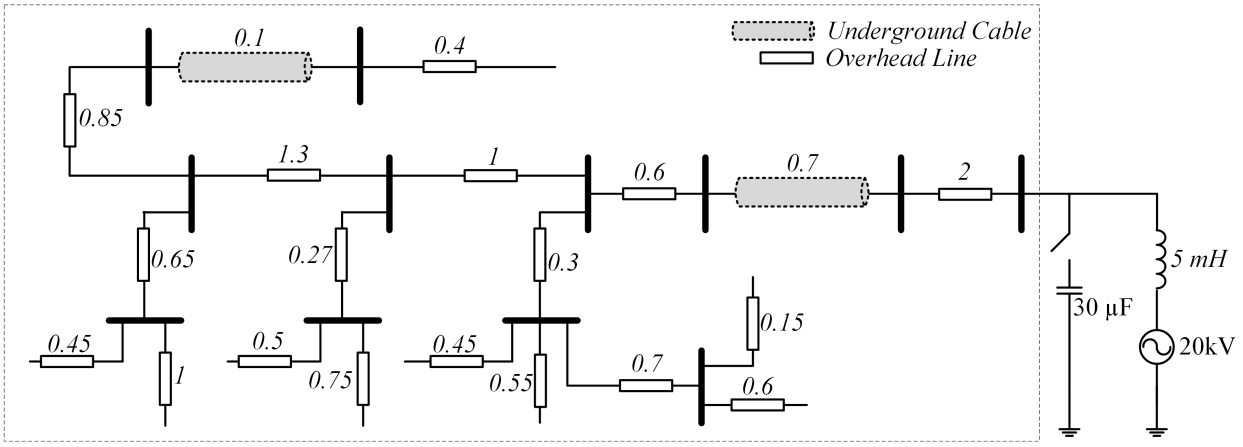

Figure 4.12: 20 kV distribution network (length of lines and cables are in kilometers) adapted from [1].

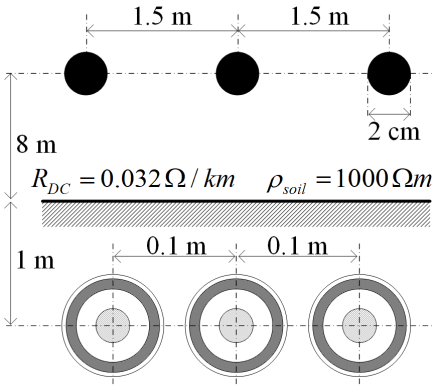

Figure 4.13: Configuration of the overhead lines and underground cables in the 20 *kV* distribution network.

Table 4.2: Cable data

Item	Outer radius (m)	Property
Core	0.022	$\rho = 1.68 \times 10^{-8}\ \Omega m$
Insulation	0.0395	$\varepsilon_r = 4.1$
Sheath	0.044	$\rho = 2.2 \times 10^{-7}\ \Omega m$
Jacket	0.0475	$\varepsilon_r = 2.3$

Eigenvalues of the real part of the scanned impedance matrix are plotted in Figure 4.14. As explained in Appendix A.1.2, eigenvalues of the real part of the positive semi-definite matrix should be non-negative in order to represent a passive network. It is found that in this example, the original scanned data incorrectly shows passivity violations while the network is passive. It can be seen that one of the eigenvalues becomes negative at frequencies in the neighborhood of 104 kHz. Therefore, this example shows how the proposed method works on imperfect scanned data.

Also, in this case study, a comparison between the proposed method and the well-known vector fitting method from literature [37] is made.

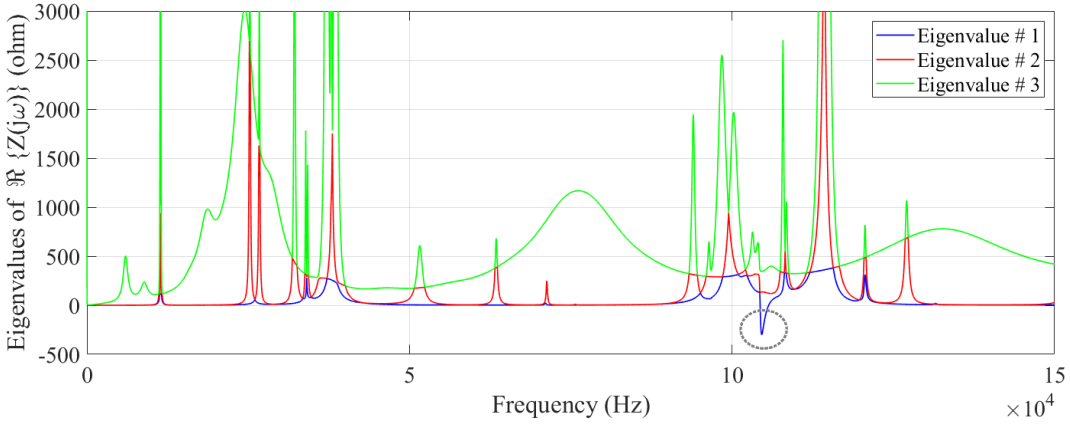

Figure 4.14: Eigenvalues of $\Re\{Z(j\omega)\}$ of the scanned network.

The proposed method used 35 rounds of realization (network order of 70) while the order of approximation by VF is also kept at 70 in order to compare them in the same order of fitting.

Figures 4.15 and 4.16 show the frequency responses of original network, realized network and vector fitting for Z_{11} and Z_{12} respectively. It can be seen that in some frequency range the proposed method shows better performance while in some other parts VF is better. Figures 4.17 and 4.18 show the fitting errors for the realized network and VF from the original tabulated frequency response for Z_{11} and Z_{12} respectively. In some frequency ranges VF based FDNE has a smaller error and in other ranges, the proposed FDNE has a smaller error.

However, as Figure 4.19 shows, VF results in non-passive fitting in this case (in the vicinity of the 104 kHz) which necessitates a further process of passivity enforcement.

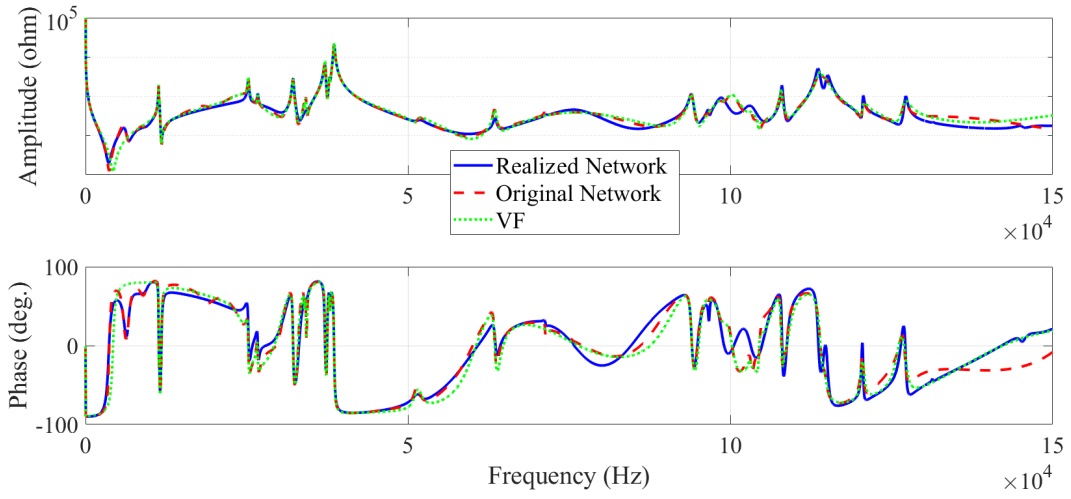

Figure 4.15: Frequency response comparison of the original distribution network versus fitted circuit and VF. (Z_{11}).

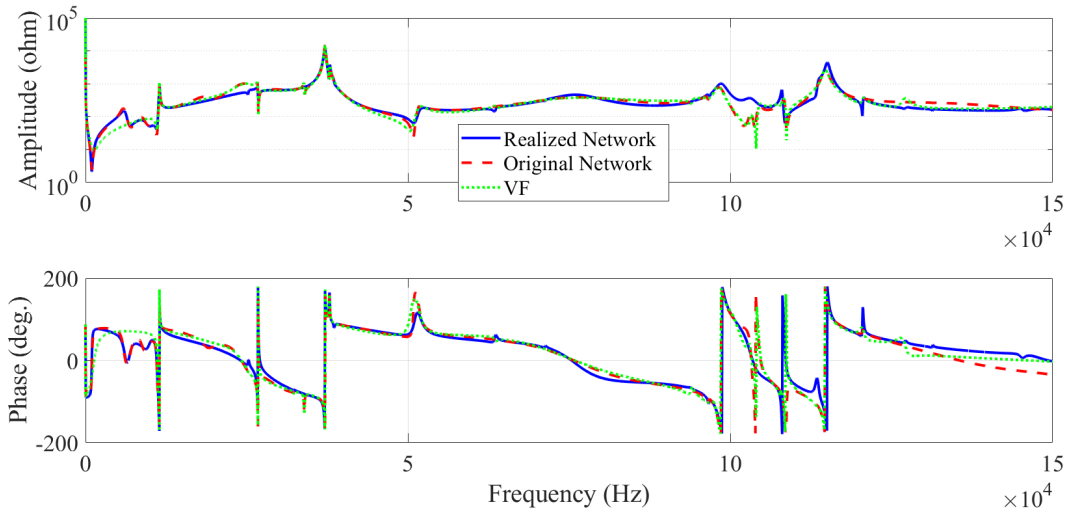

Figure 4.16: Frequency response comparison of the original distribution network versus fitted circuit and VF. (Z_{12}).

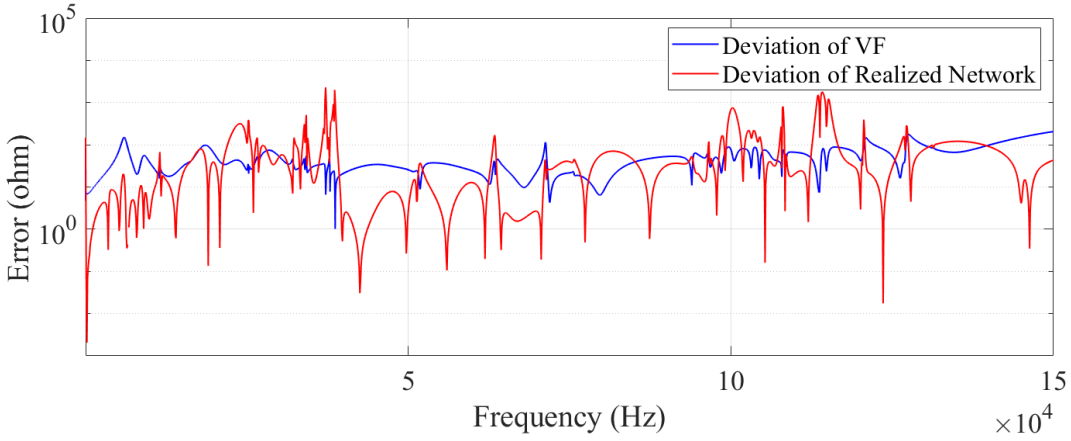

Figure 4.17: Fitting errors for the realized network and VF from the original tabulated frequency response (Z_{11}).

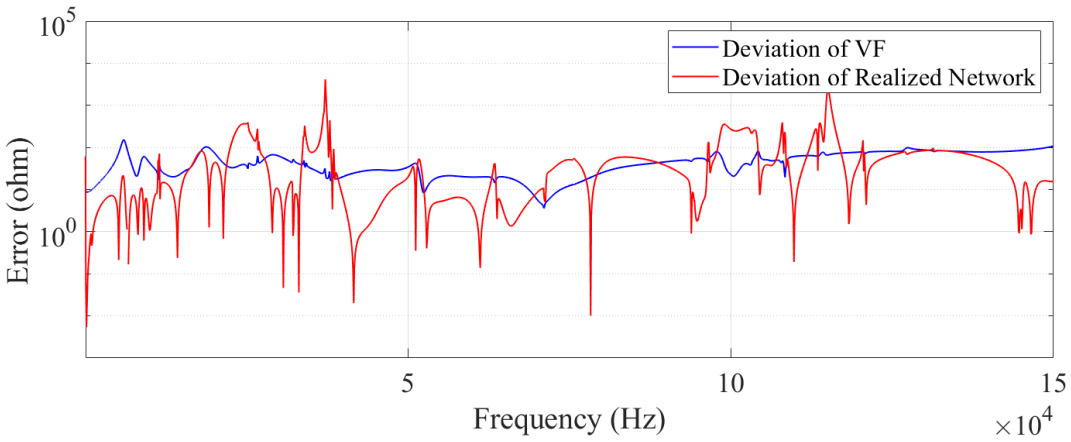

Figure 4.18: Fitting errors for the realized network and VF from the original tabulated frequency response. (Z_{12}).

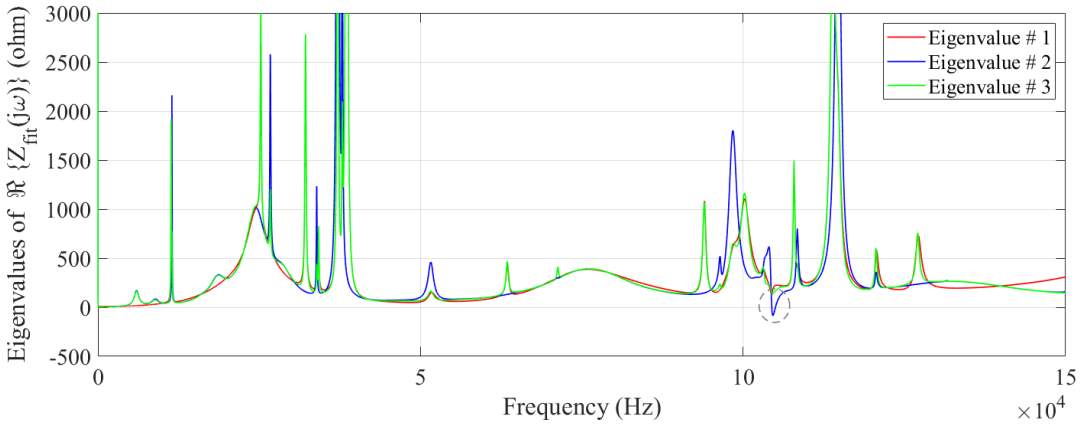

Figure 4.19: Eigenvalues of $\Re\{Z_{fit}(j\omega)\}$, fitted by VF method showing passivity violation.

4.5 Modelling a 230 *kV* Power Transmission Network with Proposed Approach and Comparison with Traditional Vector Fitting Approach

In order to apply the proposed approach to a very high order FDNE, tabulated data obtained by scanning the frequency response of a portion of a high voltage power transmission network containing several transmission lines are considered. This case shows the performance of the proposed network realization approach on very long transmission lines with distributed parameter. Accuracy comparison with the popular vector fitting (VF) approach is also carried out in this case.

The 230 kV network from which tabulated data was obtained is shown in Figure 4.20 and has 9 buses and 11 transmission lines. All the lines have the same configuration as shown in Figure 4.21, with 3 phase conductors and 2 grounding wires located on the height of 30 m above a lossy ground whose resistivity is 1000 Ωm.

The network is scanned looking into the 230 kV bus and fitted using the proposed approach. In this case, 80 rounds of realization are used. Figures 4.22 and 4.23 respectively show the diagonal (Z_{11}) and off-diagonal (Z_{12}) elements of the impedance function of the

fitted network using the proposed method versus VF and the original network. The fitting shows a good agreement between the two frequency responses. Although the VF in this specific example shows slightly better fitting to the original network, in other situation it may not. Also, the passivity issue in VF may compromise the accuracy in time domain simulation. Limitations of the proposed method against VF are discussed in the next section. This example proves that a network with distributed parameters (i.e. long transmission line which includes a transportation delay) can also be reduced by a purely passive network of lumped elements with acceptable accuracy.

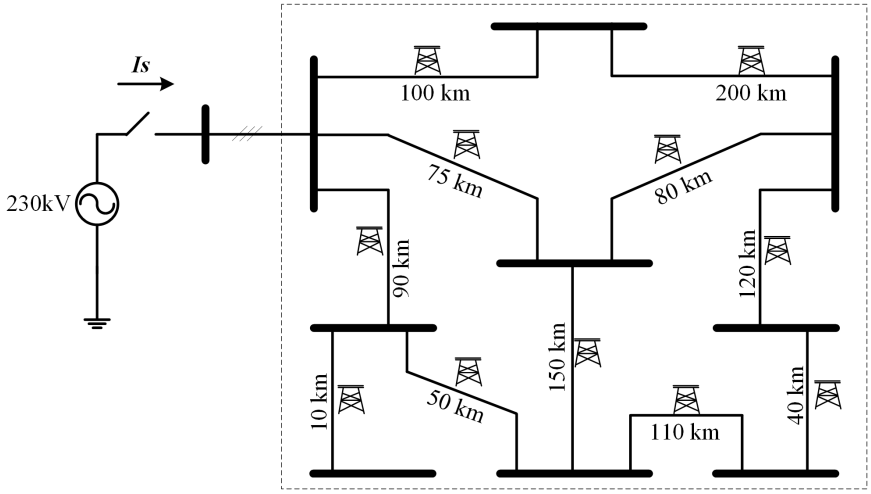

Figure 4.20: A 230 *kV* power transmission network scanned and modeled as FDNE adapted from [2].

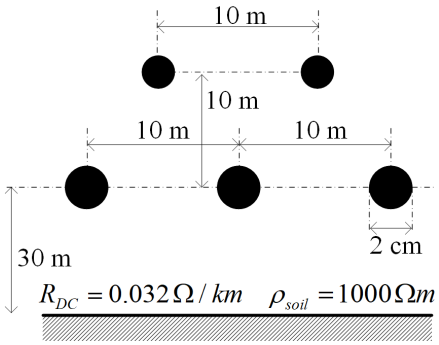

Figure 4.21: Configuration of the conductors in transmission lines of the 230 *kV* network

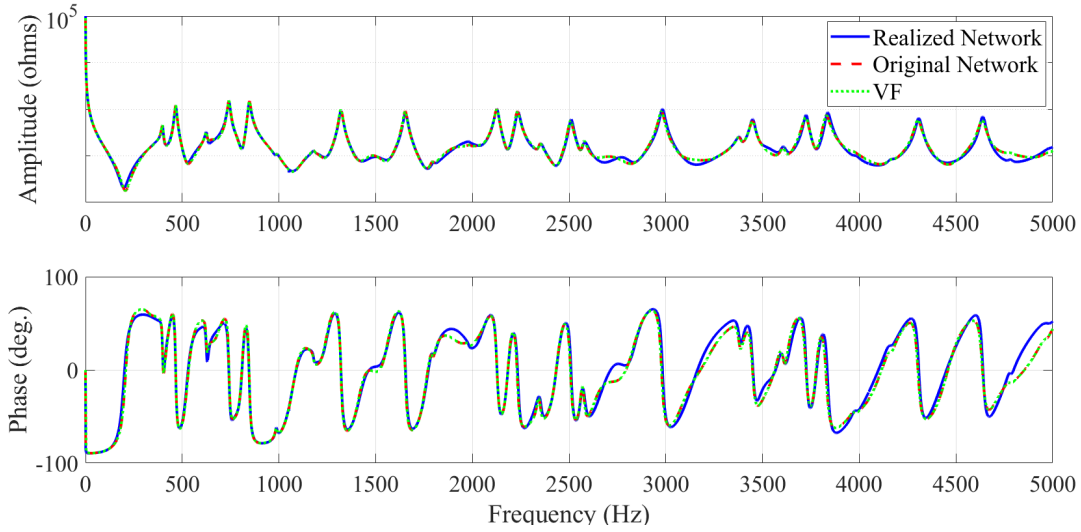

Figure 4.22: Frequency response comparison of the original network versus fitted circuit and VF. (Z_{11})

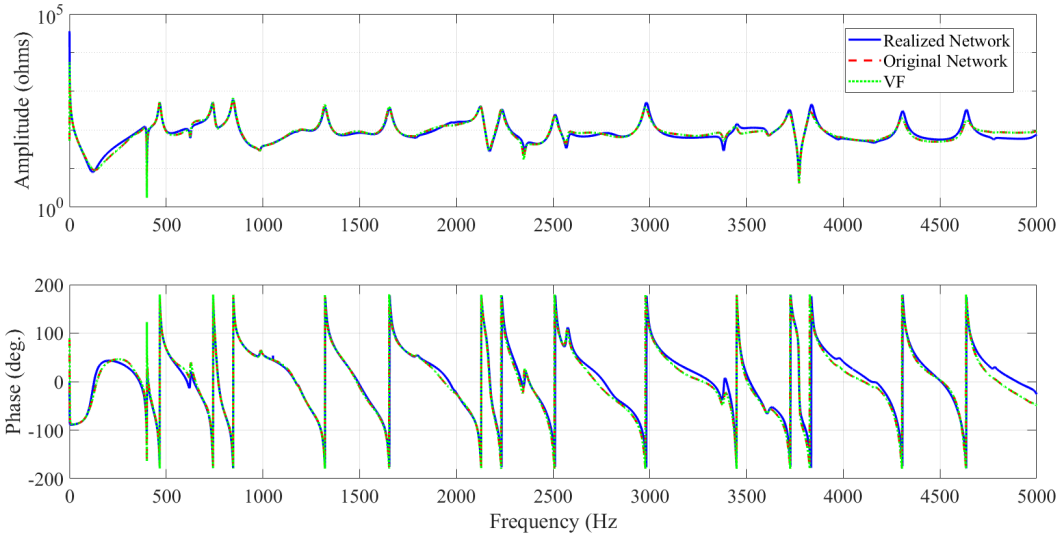

Figure 4.23: Frequency response comparison of the original network versus fitted circuit and VF. (Z_{12})

The time-domain implementation of the realized networks in this chapter is presented in Chapter 5 and comparisons between the realized and the original network is also presented.

4.6 Limitations of the Proposed Method and Differences with the Vector Fitting

The proposed method is an adaption of Brune's and Tellegen's network realization approaches which uses the successive procedure to develop the FDNE network, and the more the realization rounds, the better the fit. Vector fitting [37], on the other hand, is iterative, and the larger the number of iterations, the better the fit. Therefore, both methods can give arbitrarily good fitting of the data depending on how many rounds (Brune/Tellegen) or iterations (VF) are used. One of the aspects of the proposed method is that its accuracy of fitting the frequency domain data depends on the density of samples in the impedance-frequency data. This is due to the fact that each round of the Tellegen procedure realizes a portion of the network, with the round terminating after a minimum resistance value is encountered at a certain frequency. The realized network in earlier rounds remains unchanged in the future rounds which realize subsequent portions of the network. When the samples are not sufficiently dense, the actual minimum resistance can lie in between two frequency points, creating a slight error in the fitting. As there is no opportunity to correct the realized elements in future rounds, this error remains. This is different from vector fitting, in which all parameters of the fitted transfer function get re-calculated at each iteration. Potential approaches to overcome the above-mentioned limitation of the proposed method could include interpolating data samples in between original data points, post-fitting accuracy improvement using perturbation of the network values, etc. However, these are left as recommendations for future work.

4.7 Summary

In this chapter, an adaptation of Tellegen's network realization (which itself is an extension to Brune's method) was introduced for numerical implementation. It was proved via a theorem that to investigate poles of impedance matrices on the imaginary axis, looking into diagonal elements is sufficient. The realization algorithm was automated in a computer program.

Through a case study, it was shown that some improvements to Tellegen's original approach were necessary, in order to be able to handle complicated tabulated functions and high order FDNE cases. Therefore, the algorithm was modified accordingly by changing the realization ports at each round of the procedure.

Industrial case studies were conducted to verify the functionality of the method. It was shown that the proposed method also was able to realize a passive fitting when imperfect data (non-passive data) is given.

As compared to VF, the proposed method always provides a passive realization while VF can not. Therefore, a post fitting process becomes necessary for VF to enforce the passivity. But it was observed that VF in some cases can provide more accurate fitting than the proposed method. This was found to be due to limitations in the resolution of the data.

Chapter 5

Implementation of The Realized Network in EMT Programs

In the previous chapters, numerical implementation of Brune's synthesis and Tellegen's extension are introduced. The realized networks consist of several sub-circuits of a known structure. Therefore they can be algorithmically implemented in EMT simulation using either state space representation or companion circuit models (for smaller cases).

5.1 State Space Approach

The proposed approach, by following some repetitive steps, results in a network that is a cascade connection of several sub-circuits (with positive R, L, and C components and/or ideal transformers and thus guaranteed passive) with a well-defined topology for each sub-circuit.

Automating the inclusion of the realized FDNE topology into an EMT program's data file may be difficult and could require human intervention. Therefore, an alternative approach was developed in the thesis which converts the realized network into a state space form which can be interfaced with the EMT solver straightforwardly. Directly implementing the circuit in the EMT program also results in the EMT algorithm calculating the internal voltages of the FDNE, which are of no interest from the terminal behavior's point of view. Converting

to SV also allows a more compact and numerically efficient solution. This can be done by modeling each of the sub-circuits in the form of a Differential Algebraic Equations (DAEs) and then connecting them together to yield a state space model of the whole network.

In this section, a procedure is proposed to generate a state space model of a large network made up of several cascade sub-circuits whose configurations and thus DAEs are already known. The state space representation can then be easily implemented in an EMT solver.

In addition to the current FDNE application, it is possible to apply the proposed state space generation of cascaded sub-circuits in several applications. These include transmission cascaded pi sections [25], cross-bonded cables with cascaded segments [86], finite difference time domain models of a multiple segment cable transmission system [87] and nonuniform transmission line systems [88].

5.1.1 State Space Generation Procedure

Figure 5.1 shows a schematic representation of the above mentioned cascaded network made up of N sub-circuits. For convenience, the left hand side of a sub-circuit in Figure 5.1 is referred to as the "sending end" and the right side as the "receiving end".

In both single port and multi-port network realization, the last sub-circuit to be realized is a resistance or a resistive network shown by scalar or matrix R_{end} respectively. In Figure 5.1, the first (1^{st}) sub-circuit is considered as a resistive network with the terminal voltage and current relation of $v_S^1 = R_{end}\ i_S^1$. Where v_S^1 is $n \times 1$ vector of the voltages, i_S^1 is $n \times 1$ vector of the currents and R_{end} is a $n \times n$ resistance matrix.

To create the state space equations, a variety of approaches are available including modified nodal analysis (MNA) [89] or the conventional tree and co-tree method [85]. In this work, the equations are derived using a slightly modified tree and co-tree method applied to the sub-circuit in Figure 4.1 which turned out to be in the form of DAEs.

Usually, DAEs are in form of (5.1), in which the matrix E is a singular matrix [90].

$$\begin{aligned} E\dot{x}(t) &= Ax(t) + Bu(t) \quad , \quad x(0) = x_0 \\ y(t) &= Cx(t) + Du(t) \end{aligned} \tag{5.1}$$

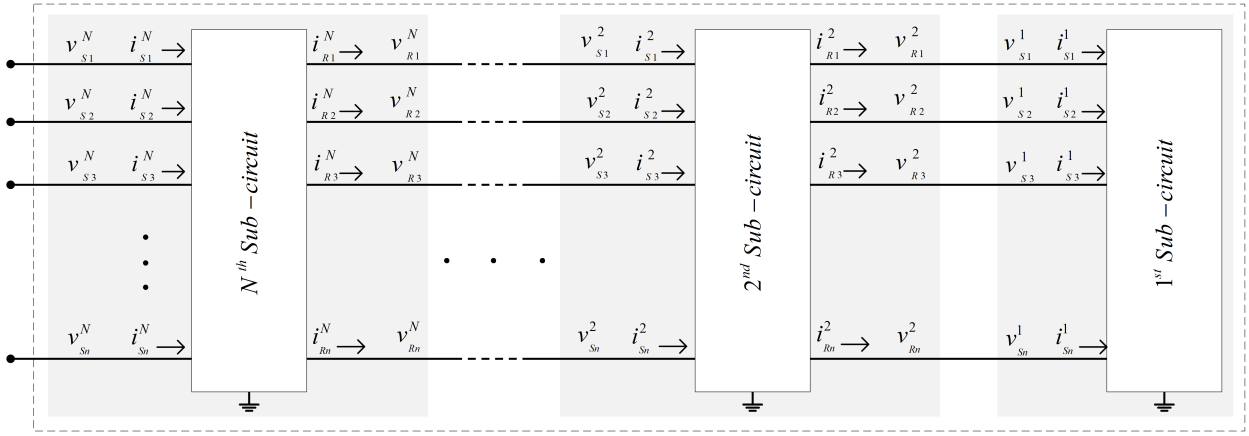

Figure 5.1: Cascade connection of N sub-circuits

For the networks realized in Chapters 3 and 4, due to the ideal transformer in the circuit, there will be a coupling between the output current equations and derivative of the state variables which forces differential equations to be in form of (5.2) in which matrix M is singular. This is a special type of DAE in which even the output relation is coupled to the state equation. The full matrices of M and N are given in the Appendix E which explains why matrix M is singular.

In (5.2), v and i are $2n \times 1$ vectors of the terminal voltages and currents and x is $ns \times 1$ vector of state variable of the k^{th} sub-circuit assuming number of its state variables to be ns. Also, $\dot{x}$ indicates derivative of x. If matrix M is non-singular, it can be inverted and thus the equation turns into classical state space form.

As Figure 5.1 shows, the sending end of the k^{th} sub-circuit directly connects to the receiving end of the $(k-1)^{th}$ sub-circuit. Therefore, the sending end voltages and currents of the k^{th} sub-circuit are the same as the receiving end voltages and currents of the $(k-1)^{th}$ sub-circuit and by eliminating all of these internal node voltages and currents, only the sending terminal of the N^{th} sub-circuit will remain which is the driving point terminal of the whole network.

$$M^k \begin{bmatrix} \dot{x}^k \\ i^k \end{bmatrix} = N^k \begin{bmatrix} x^k \\ v^k \end{bmatrix} \quad where \quad x^k = \begin{bmatrix} x_1^k \\ x_2^k \\ \vdots \\ x_{ns}^k \end{bmatrix} \quad , \quad i^k = \begin{bmatrix} i_{S1}^k \\ i_{S2}^k \\ \vdots \\ i_{Sn}^k \\ i_{R1}^k \\ i_{R2}^k \\ \vdots \\ i_{Rn}^k \end{bmatrix} \quad , \quad v^k = \begin{bmatrix} v_{S1}^k \\ v_{S2}^k \\ \vdots \\ v_{Sn}^k \\ v_{R1}^k \\ v_{R2}^k \\ \vdots \\ v_{Rn}^k \end{bmatrix} \tag{5.2}$$

In order to start the internal node elimination process, equation (5.2) is broken into two parts shown in (5.3 a and b).

$$\begin{matrix} a) \\ \\ b) \end{matrix} \quad \left(\begin{array}{ccc} M_{11}^k & | & M_{12}^k \\ -- & -|- & - \\ M_{21}^k & | & M_{22}^k \end{array}\right) \begin{bmatrix} \dot{x}^k \\ i_S^k \\ - \\ i_R^k \end{bmatrix} = \left(\begin{array}{ccc} N_{11}^k & | & N_{12}^k \\ -- & -|- & - \\ N_{21}^k & | & N_{22}^k \end{array}\right) \begin{bmatrix} x^k \\ v_S^k \\ - \\ v_R^k \end{bmatrix} \tag{5.3}$$

To make the formulation more compact, the vectors $[\dot{x}^k \quad i_S^k]^T$ and $[x^k \quad v_S^k]^T$ are renamed as $\dot{X}_{is}^2$ and X_{vs}^2 respectively.

Starting from the 2^{nd} sub-circuit, the receiving end currents and voltages (i_R^2 and v_R^2 which are equal to i_S^1 and v_S^1) must be eliminated in the formulation. Knowing that, $v_S^1 = R_{end}\ i_S^1$ and using (5.3a) i_R^2 and v_R^2 can be found by solving the following set of equations;

$$\begin{cases} v_S^1 = R_{end}\ i_S^1 \quad \Rightarrow \quad v_R^2 = R_{end}\ i_R^2 \\ M_{21}^2 \dot{X}_{is}^2 + M_{22}^2 i_R^2 = N_{21}^2 X_{vs}^2 + N_{22}^2 v_R^2 \end{cases} \tag{5.4}$$

Which gives i_R^2 and v_R^2 in (5.5):

$$\begin{bmatrix} i_R^2 \\ v_R^2 \end{bmatrix} = \begin{pmatrix} -R_{end} & I \\ M_{22}^2 & -N_{22}^2 \end{pmatrix}^{-1} \begin{pmatrix} 0 & 0 \\ -M_{21}^2 & N_{21}^2 \end{pmatrix} \begin{bmatrix} \dot{X}_{is}^2 \\ X_{vs}^2 \end{bmatrix} \tag{5.5}$$

Equation (5.5) can be simplified as

$$\begin{cases} i_R^2 = K_{11}\dot{X}_{is}^2 + K_{12}X_{vs}^2 \\ v_R^2 = K_{21}\dot{X}_{is}^2 + K_{22}X_{vs}^2 \end{cases} \tag{5.6}$$

where the matrix K is given by (5.7)

$$\begin{pmatrix} K_{11} & K_{12} \\ K_{21} & K_{22} \end{pmatrix} = \begin{pmatrix} -R_{end} & I \\ M_{22}^2 & -N_{22}^2 \end{pmatrix}^{-1} \begin{pmatrix} 0 & 0 \\ -M_{21}^2 & N_{21}^2 \end{pmatrix} \tag{5.7}$$

Now by substituting i_R^2 and v_R^2 from (5.7) into (5.3b), we get:

$$M_{11}^2\dot{X}_{is}^2 + M_{12}^2(K_{11}\dot{X}_{is}^2 + K_{12}X_{vs}^2) = N_{11}^2X_{vs}^2 + N_{12}^2(K_{21}\dot{X}_{is}^2 + K_{22}X_{vs}^2) \tag{5.8}$$

Again, (5.8) can be simplified as :

$$\dot{X}_{is}^2 = P^{-1}QX_{vs}^2 \tag{5.9}$$

where;

$$\begin{cases} P = M_{11}^2 + M_{12}^2K_{11} - N_{12}^2K_{21} \\ Q = N_{11}^2 + N_{12}^2K_{22} - M_{12}^2K_{12} \end{cases} \tag{5.10}$$

Now, the state space form can be found by unwrapping (5.9) into (5.11). Where A^2, B^2, C^2 and D^2 are the state space matrices of the first 2 sub-circuits.

$$\begin{bmatrix} \dot{x}^2 \\ - \\ i_S^2 \end{bmatrix} = P^{-1}Q \begin{bmatrix} x^2 \\ - \\ v_S^2 \end{bmatrix} \quad \Rightarrow \quad \begin{bmatrix} \dot{x}^2 \\ - \\ i_S^2 \end{bmatrix} = \left(\begin{array}{c|c|c} A^2 & | & B^2 \\ - & -|- & - \\ C^2 & | & D^2 \end{array}\right) \begin{bmatrix} x^2 \\ - \\ v_S^2 \end{bmatrix} \tag{5.11}$$

Equation (5.11) gives the state space and output equations of combination of the 2^{nd} and 1^{st} sub-circuits together. In order to add the 3^{rd} and subsequent sub-circuits, a similar procedure is repeated. To do so, the receiving end currents and voltages of the third sub-circuit and later (i_R^k and v_R^k which are equal to i_S^{k-1} and v_S^{k-1}) must be eliminated.

Assume that the state space form of all the $(k-1)$ sub-circuits together is given by (5.12). $x_T^{k-1}$is a vector, including all the state variables of the previous $(k-1)$ sub-circuits.

$$\begin{matrix} a) \\ \\ b) \end{matrix} \quad \begin{bmatrix} \dot{x}_T^{k-1} \\ - \\ i_S^{k-1} \end{bmatrix} = \begin{pmatrix} A^{k-1} & | & B^{k-1} \\ -- & -|- & - \\ C^{k-1} & | & D^{k-1} \end{pmatrix} \begin{bmatrix} x_T^{k-1} \\ - \\ v_S^{k-1} \end{bmatrix} \tag{5.12}$$

Now using (5.3b) and (5.12), the following set of two equations yields i_R^k and v_R^k;

$$\begin{cases} i_S^{k-1} = C^{k-1}x_T^{k-1} + D^{k-1}v_S^{k-1} \Rightarrow i_R^k = C^{k-1}x_T^{k-1} + D^{k-1}v_R^k \\ M_{21}^k \dot{X}_{is}^k + M_{22}^k i_R^k = N_{21}^k X_{vs}^k + N_{22}^k v_R^k \end{cases} \tag{5.13}$$

After solving the above-mentioned equations one obtains;

$$\begin{cases} i_R^k = T_{11}\dot{X}_{is}^k + T_{12}X_{vs}^k + T_{13}x_T^{k-1} \\ v_R^k = T_{21}\dot{X}_{is}^k + T_{22}X_{vs}^k + T_{23}x_T^{k-1} \end{cases} \tag{5.14}$$

in which matrix T is given by:

$$T = \begin{pmatrix} I & D^{k-1} \\ M_{22}^k & -N_{22}^k \end{pmatrix}^{-1} \begin{pmatrix} 0 & 0 & C^{k-1} \\ -M_{21}^k & N_{21}^k & 0 \end{pmatrix} \tag{5.15}$$

Now by substituting i_R^k and v_R^k from (5.14) in (5.3a);

$$\dot{X}_{is}^k = W^{-1}ZX_{vs}^k + W^{-1}Gx_T^{k-1} \qquad , \qquad \begin{cases} W = M_{11}^k + M_{12}^2 T_{11} - N_{12}^k T_{21} \\ Z = N_{11}^k + N_{12}^k T_{22} - M_{12}^k T_{12} \\ G = N_{12}^k T_{13} - M_{12}^k T_{23} \end{cases} \tag{5.16}$$

Equation (5.16) only includes the derivatives of the state variables of k^{th} sub-circuit. To add the derivatives of all previous $(k-1)$ sub-circuits, v_R^k from (5.14) should be substituted in (5.12a) as shown below;

$$\begin{aligned}
&\dot{x}_T^k = A^{k-1}x_T^k + B^{k-1}v_R^k \Rightarrow \\
&\dot{x}_T^k = A^{k-1}x_T^k + B^{k-1}(T_{21}\dot{X}_{is}^k + T_{22}X_{vs}^k + T_{23}x_T^{k-1}) \Rightarrow \\
&\dot{x}_T^k = (A^{k-1} + B^{k-1}T_{21}W^{-1}G + B^{k-1}T_{23})x_T^k + (B^{k-1}T_{21}W^{-1}Z + B^{k-1}T_{22})X_{vs}^k
\end{aligned} \tag{5.17}$$

Therefore, the state space equation of all k sub-circuits together becomes (5.18);

$$\begin{bmatrix} \dot{x}_T^{k-1} \\ \dot{X}_{is}^k \end{bmatrix} = \begin{pmatrix} E & F \\ W^{-1}G & W^{-1}Z \end{pmatrix} \begin{bmatrix} x_T^{k-1} \\ X_{vs}^k \end{bmatrix} \quad , \quad \begin{cases} E = A^{k-1} + B^{k-1}T_{21}W^{-1}G + B^{k-1}T_{23} \\ F = B^{k-1}T_{21}W^{-1}Z + B^{k-1}T_{22} \end{cases} \tag{5.18}$$

By unwrapping the matrices and compact parameters of (5.18), the classical state space form of entire k sub-circuit can be found as given in (5.19);

$$\begin{bmatrix} \dot{x}_T^{k-1} \\ - \\ \dot{x}^k \\ i_S^k \end{bmatrix} = \begin{pmatrix} E & | & F \\ - & -|- & - \\ W^{-1}G & | & W^{-1}Z \end{pmatrix} \begin{bmatrix} x_T^{k-1} \\ - \\ x^k \\ v_S^k \end{bmatrix} \quad \Rightarrow \quad \begin{bmatrix} \dot{x}_T^{k-1} \\ \dot{x}^k \\ - \\ i_S^k \end{bmatrix} = \begin{pmatrix} A^k & | & B^k \\ - & -|- & - \\ C^k & | & D^k \end{pmatrix} \begin{bmatrix} x_T^{k-1} \\ x^k \\ - \\ v_S^k \end{bmatrix} \tag{5.19}$$

The process of eliminating internal nodes and recursively growing the state space matrices continues to $k = N$ including all of the N sub-circuits to form A^N, B^N, C^N and D^N in (5.20) where x_T^N is the vector of state variables of the entire network.

$$\begin{bmatrix} \dot{x}_T^N \\ - \\ i_S^k \end{bmatrix} = \begin{pmatrix} A^N & | & B^N \\ - & -|- & - \\ C^N & | & D^N \end{pmatrix} \begin{bmatrix} x_T^N \\ - \\ v_S^k \end{bmatrix} \tag{5.20}$$

The state space matrices can then readily be used in the EMT program for time-domain simulation as illustrated in Appendix B.3.

This part of the work was published in [91].

5.2 Validation Using Simulation

In order to verify the state space generation method, the proposed approach is implemented in an EMT program (PSCAD) and the following simulation cases (which their frequency domain comparison were already discussed in the previous chapters) are investigated.

5.2.1 Two Port RLC Network

In the first example, state space model of the network realized for the FDNE of the two-port RLC network shown in Figure 4.4 is developed using the proposed approach. The network contains 5 sub-circuits which results in a 7^{th} order state space model.

For time-domain comparisons, a 60 Hz sinusoidal voltage of 1 kV is applied to port 1 of both the original and FDNE circuits. The voltage at port 2 and current at port 1 for the original and fitted circuit for FDNE are shown in Fig. 6. Both the frequency and time domain comparisons agree very well and confirm the functionality of the proposed method.

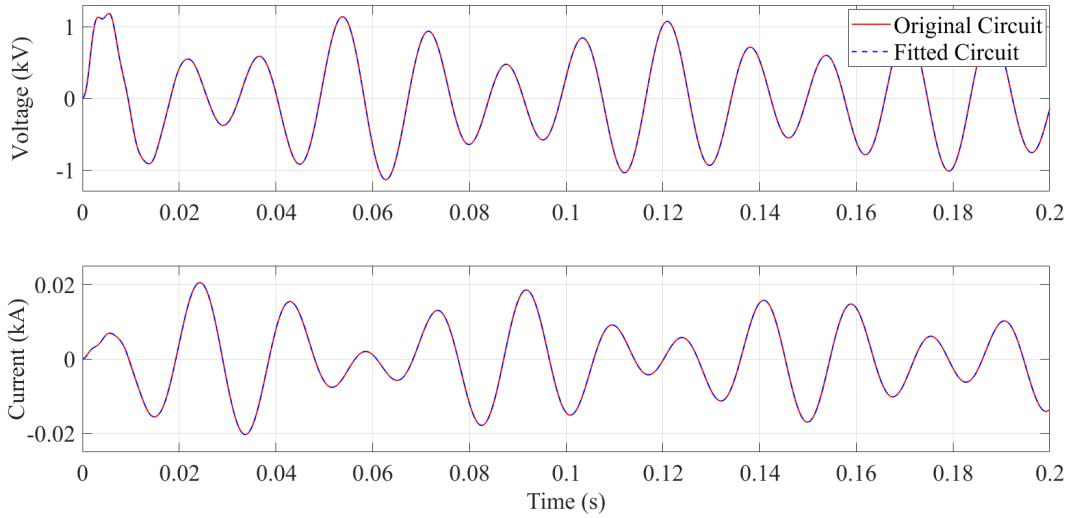

Figure 5.2: Time domain response of the original circuit two port RLC network and the realized one.

5.2.2 20 kV Distribution Network

The time-domain comparison of the 20 kV distribution network and the realized FDNE is done through energization of the capacitor bank in Figure 4.12 at $t = 0.1$ ms. Figure 5.3 shows the Phase B current after energizing the capacitor bank which a good agreement is achieved between the original network and the realized circuit of the reduced-order FDNE model. The first $0.5ms$ of the plot is zoomed-in which shows the high frequency response of the realized FDNE matches very good to that of the original network.

The simulation run-time of the original network was 12922 ms while in the realized network it was reduced to 4094 ms, providing a speed up factor of 3.16. The simulation time step was set as 0.1 µs for both networks. To implement the network in time-domain simulation, state space model of a network with 35 sub-circuit is generated in this case.

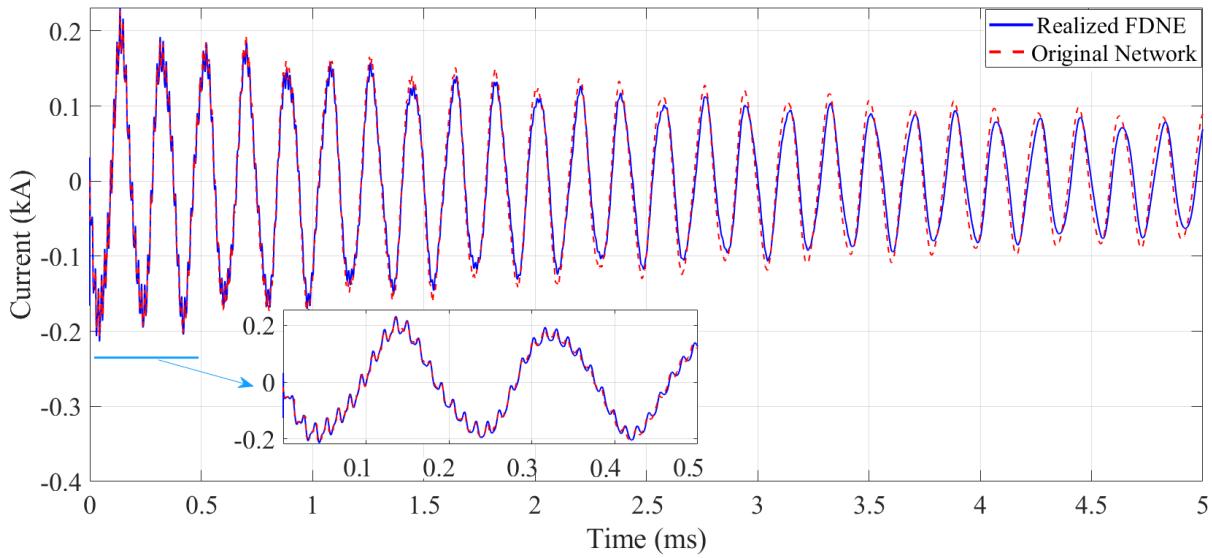

Figure 5.3: Phase B current of the original network versus fitted circuit.

5.2.3 230 kV Power Transmission Network

The FDNE of the 230 kV transmission network in Figure 4.20 had 80 sub-circuits. The state space model is generated and a 230 kV source is connected to (energized) the network. The three-phase current I_s going into the network is depicted in Figure 5.4 which shows very

good agreement between the original network and the reduced FDNE model.

With the time step of simulation set as 20 μs, the CPU run-time of the original network was 640 ms while the realized FDNE model used only 194 ms to run the case. This provides speed up factor of 3.4 for the reduced FDNE model.

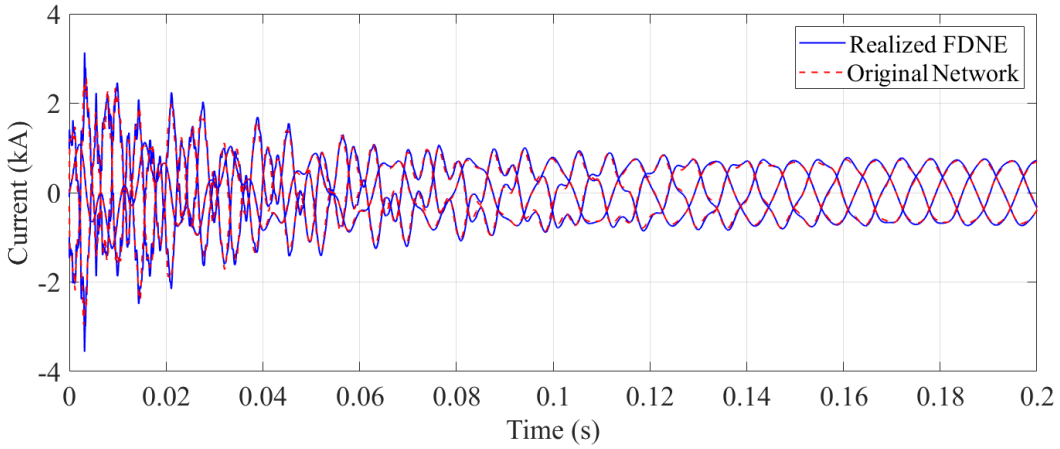

Figure 5.4: Time domain response of the original network versus realized network through energization of the network.

5.3 Summary

In this chapter, a systematic implementation of the realized networks in EMT solver was introduced. Since the Brune/Tellegen networks consist of several sub-circuits of a known structure, they were algorithmically implemented in EMT simulation by state space representation using Differential Algebraic Equations (DAEs). It was found that each of the sub-circuits is identified by a special type of DAE. To generate the state space model of the entire network, DAEs of the sub-circuits were combined by the elimination of the internal node voltage and currents in an algorithmic procedure.

Also, using the method presented in this chapter, transient simulations were conducted to provide time-domain comparison of those case studies of the earlier chapters. Transient responses showed good agreement between the original networks and that of their realized FDNEs with speed up gain in simulation time.

Chapter 6

Contributions, Conclusions, and Recommendations for Future Work

In this chapter, a brief overview of this work, the main contributions, and conclusions of the research are given. In the end, some suggestions are provided as directions for future works.

6.1 Contributions and Conclusions

- For making Frequency Dependent Network Equivalents (FDNEs) for power system electromagnetic transient (EMT) simulation, the first step is to curve fit the available frequency response data with a function that can be implemented in EMT code. Previous approaches have tried to address this issue by applying additional post-fitting procedures which perturb the fitted parameters to create a passive system. However, Passivity violation of these fitting methods has always been an important challenge in modeling FDNEs for power system simulation tools. Passivity enforcement often comes at the expense of accuracy. Also, these algorithms use passivity enforcement after an original (maybe non-passive) fitting, and enforcing passivity in a violated frequency range often leads to a loss of passivity in another range. This thesis solves the fitting problem from a different perspective. For the first time, a network realization

approach is used to directly realize a passive network for FDNEs frequency response data (given as tabulated function). Since the resulting network only includes physically realizable RLCM elements, the proposed method inherently guarantees the passivity of the fitting, thus, there is no need for post-facto passivity check and enforcement.

- In this thesis, the literature on classical network realization approaches was thoroughly reviewed. All the classical methods require a rational function in the s-domain, from which the equivalent is to be constructed, but in the case of FDNEs, usually, only a table of impedance (or admittance) values at discrete frequencies is available. The focus of this thesis was to find a network realization method to be implemented numerically on tabulated data.

- The classical network realization methods by Brune (for single port) and Tellegen (for multi-port) were also only designed for rational polynomials $Z(s)$ in s-domain, but in this thesis, it is proved that having a tabulated impedance function $Z(j\omega)$ is sufficient to perform the realization, thereby permitting the use of tabulated frequency response data. The frequency response data could be obtained from measurements on an actual network, or through scanning of an EMT model of the network.

- The Brune and Tellegen's methods were thus adapted for numerical implementation and a systematic way of implementing network realization directly from tabulated data was introduced. The algorithm was straightforward to automate and therefore easy to convert to be coded for computer application.

- Through examples and case studies, the proposed methods were validated and shown to have high accuracy in the frequency response as well as in the simulated time domain response.

  Brune's method was adapted for single port networks and validated via case studies with the following conclusions:

  - With a simple and a high order PR functions, the proposed single port FDNE real-

ization method was validated and high accuracy was achieved. It was shown that the accuracy of the proposed method depends on the resolution of the frequency sampled data. Also, the closer samples at very high and very low frequencies provide a more accurate calculation of their corresponding pole/zero residues.

– A single port network containing a cable, a filter, and two short lines was scanned and realized using the proposed method. It is shown that the procedure can be stopped at any round of realization even without reaching an exact termination criterion (the remainder having phase angle less than 5°, i.e., a resistance) an still get a passive network.

Tellegen's method was adapted for multi-port networks and validated via case studies with the following conclusions:

– Simple multi-port RLC network is chosen to verify the functionality of the proposed realization method. It was shown that the accuracy of the proposed method is highly dependent on the number of samples. Also, the type of spacing between the frequency sampled data plays an important role in the accuracy of the fitting as logarithmically spaced data provides denser resolution at lower frequencies as compared to linearly spaced data which provides closer samples at higher frequencies.

– It was found that the original Tellegen's procedure does not work generally for all tabulated functions as it only offers a connection of elements on one port of the multi-port network which gives problems for realizing very high order FDNEs.

– Hence, Tellegen's approach was modified such that it can easily handle networks of a very high order. This is achieved by a cyclical procedure, by changing the realization port at each round of the realization. The process terminates when the remnant network is almost a pure resistance or the number of rounds of realization reaches to a predetermined value. The overall network then becomes a cascade connection of several sub-circuits which are realized in each round of

the procedure.

  - FDNE of a distribution network containing several short underground cables and overhead transmission lines was studied. The proposed method realized a passive network for the FDNE while the frequency scan of the original network had a passivity violation in this case. Therefore, the proposed method is validated on the imperfect input data.
  - Also, the proposed approach is compared with the conventional vector fitting and it is shown that while the accuracy of the two methods was comparable, VF does sometimes result in the non-passive fitting.
  - A very high order transmission network containing very long overhead transmission lines was also studied and the proposed method showed a very good fitting. This example proved that a distributed network (i.e. long transmission line which includes a transportation delay) can also be reduced by a purely passive network of lumped elements with acceptable accuracy.

- The realized EMT network obtained from the FDNEs consists of a cascade connection of several sub-circuits with known topology. The state space approach is used for the EMT implementation of the network. Each of the sub-circuits has a representation in Differential Algebraic Equation (DAE) form. The overall state space model of the network is generated by combining this DAEs taking care to maintain boundary constraints between the sub-circuits. Also, the reduced-order circuit is seen to have faster simulation speed as expected from *FDNEs* comparing the original circuit.

The outcomes of this work are presented in 2 conference papers and a transactions paper under review as listed below:

- M. Ahmadi, A. M. Gole, "A New Approach to Model Frequency Dependent Network Equivalents in Transient Simulation Tools," in *International Conference on Power Systems Transients (IPST17)*, June 2017

- Meysam Ahmadi, Shengtao Fan, Huanfeng Zhao, and Aniruddha M. Gole, "Efficient Implementation of Frequency Dependent Network Equivalents using State Space Models of Cascaded Sub-Circuits," in *International Conference on Power Systems Transients (IPST19)*, June 2019

- Meysam Ahmadi, Shengtao Fan, Aniruddha M. Gole, and Jeewantha De Silva, "Network Synthesis Based Approach for Creating Multi-port Frequency Dependent Network Equivalents with Guaranteed Passivity," *submitted, under review*

6.2 Recommendations for Future Work

There are some possible paths for continuing this work which is itemized here:

- It is shown in Chapter 4 that the accuracy of the proposed method is highly dependent on the number of samples. Since the method works by looking for minimum resistance in step 3, it is always possible that the actual minimum happens between the two sample points. Therefore, if a high number of samples are not available, one approach could be a combination of circuit realization approaches and a mathematical fitting (e.g. vector fitting), to create a local fit and find more accurate location of the minimum resistance. This allows achieving better accuracy in frequency domain fitting while preserving the passivity. The properties of PR functions as well as physical networks can be used as constraints of the vector fitting.

- Brune and Tellegen's realization approaches require a large number of ideal transformers. Ideal transformers (i.e. just turns ratios) can not be implemented in the nodal analysis based EMT algorithms using regular companion circuits. Thus, the author used DAE based simulation and interfaced it to the nodal admittance based model of the remainder of the network. In future work, the alternative approach of Using modified nodal analysis to implement the network [92] enables using ideal transformers in the implemented circuit. There could be some benefits in this approach, such as further speeding up the time domain simulation

- Reduction of the mathematical order of the function can also be explored in the future. One approach to reduce the size of state space model introduced in Chapter 5 is using model order reduction techniques to get a smaller dimension for the FDNE and thus lead to an even faster simulation.

- Another direction to implement the cascaded network in the EMT program is using the nested and simultaneous solution of the sub-circuits in order to speed up the time-domain simulation.

- Making a more compact model of the entire network can be explored by eliminating the internal nodes and creating a Thevenin or Norton equivalent. This also may help simplify the whole network and benefit from the smaller size of the matrices toward speeding up the time-domain simulation.

- Implementing the algorithm of the proposed network realization approach in real-time power system simulation tools (e.g. RTDS) could be beneficial to investigate further improvements e.g. using parallel processing to speed up the time-domain simulation.

- Another idea would be to explore modeling transmission lines using the proposed method and trying to extract the travel time. Extracting the travel time will make the frequency response of transmission lines and cables smoother and thus the realized network would become smaller in size. The proposed method would help overcome passivity issues in modeling cables and transmission lines as well.

Appendix A

Positive Real Functions and Their Properties

A.1 Definition

A.1.1 Scalar Functions

A rational scalar function $z(s)$ is called a Positive Real (PR) function if and only if meets both following conditions [82, 85];

I. $z(s)$ is real for any real *'s'* .

II. $z(s)$ is analytic in the right-half of the *'s'* plane

III. The real part of $z(s)$ is non-negative when the real part of *'s'* is non-negative.

IV. Poles of $z(s)$ on the $j\omega$ axis must be simple with positive real residues.

Brune in 1931 found that any positive real function can be impedance (admittance) of a passive RLC network. He proved that the driving point impedance of any RLC circuit is also a positive real function [55].

For a better understanding, considering the complex impedance of a network $z(j\omega)$ as a positive real function, it can not have a negative real part at any frequency. This is reasonable

as it is shown in (A.1), if there is a frequency in which the real part of the impedance is negative, then P or active power will be negative at that frequency. This means the circuit can generate power at that frequency which is physically impossible.

$$S = z(j\omega).I^*I = \Re[z(j\omega)].|I|^2 + \Im[Z(j\omega)].|I|^2 = P + jQ \tag{A.1}$$

Where I^* is the complex conjugate of I.

A.1.2 Multi-port Functions

In the case of multi-port networks, a rational positive real matrix represents the relation between the voltages and currents at the terminals. For instance, it can be an impedance matrix $Z(s)$ as shown by (A.2);

$$V = Z(j\omega).I \tag{A.2}$$

In this case, the matrix $Z(s)$ is positive real if and only if [82];

1. All the elements of $Z(s)$ are real when *'s'* is real.
2. All the elements of $Z(s)$ are analytic (i.e. have no pole) in the right-half *'s'* plane.
3. The Hermitian part of $Z(j\omega)$, $Z^H(j\omega) = Z(j\omega) + Z(j\omega)^{*T}$,is positive semi-definite for all ω. In the case of symmetric matrices, the Hermitian part coincides with the real part of the matrix e.g. in the FDNEs.
4. Poles of $Z(s)$ on the $j\omega$-axis are simple and the matrices of the residues are positive semi-definite.

Positive semi-definiteness of the real part of matrix comes from the fact that for any sets of currents applied to the terminals of a passive network, the active power P in the following relation should always remain positive;

$$P = \Re\{I^*Z(j\omega)I\} = \Re\{I^*(R(\omega) + jX(\omega))I\} = \Re\{I^*R(\omega)\ I\} \geq 0 \tag{A.3}$$

In A.3, the vector I^* is transpose and conjugate of vector I. Based on the definition, it follows that the active power P will be positive if and only if the matrix $R(\omega)$ is positive semi-definite for all ω. This means all of the eigenvalues of matrix $R(\omega)$ must be non-negative for all ω. In other words, for a passive network, the real part of its impedance matrix, $R(\omega)$, should be positive semi-definite.

It is almost impossible to separate the real part of matrix $Y(j\omega)$ as a function of ω and then find the eigenvalues of that matrix as a function of ω to see whether they are always positive. Therefore, an inspection can be conducted through numerical tests at a wide range of frequencies to make sure the matrix $G(\omega)$ indeed is passive at all points of frequencies.

A.2 Properties

In this section, some properties of PR functions that are frequently used in this work are discussed. Each one of these items is proved as a theorem in [82].

I. The sum of two positive real functions is a positive real function.

II. The reciprocal of a positive real function is a positive real function.

III. A positive real function cannot have any poles in the right-half *'s'* plane.

IV. A positive real function cannot have any zeros in the right-half *'s'* plane

V. A positive real function may have poles on the $j\omega$-axis, but each must be simple and the residue at each must be positive real.

VI. Let $F(s) = M(s)/N(s)$ be a rational positive real function. Then the degree of $M(s)$ and the degree of $N(s)$ cannot differ by more than one.

VII. Let $F(s)$ be a positive real function. Let $F(j\omega) = R(\omega) + jX(\omega)$. Then $R(\omega) \geq 0$ for all ω.

Based on the theorems given above, it can be proved that the necessary and sufficient conditions for a function $F(s)$ to be positive real are:

1. $F(s)$ is real when *'s'* is real.

2. $F(s)$ is analytic in the right-half of the *'s'* plane.

3. Let $F(j\omega) = R(\omega) + jX(\omega)$. $R(\omega)$ is non-negative for all ω.

4. Poles of $F(s)$ on the $j\omega$-axis are simple with positive real residues.

Appendix B

Basic Time Domain Equivalents in an EMT Program

As mentioned earlier, an FDNE can be modeled in EMT programs by means of RLC branches or mathematical s-domain transfer functions. In this section, a brief review of the modeling of basic circuit elements, i.e., resistance, inductance, and capacitance in transient simulation is given. RLC networks can be modeled using either companion circuits or state space models. Also transforming *'s'* domain functions to time-domain transient simulation can be done using recursive convolution or state space method which are explained in this section.

B.1 RLC Branches in EMT Programs

In transient simulation, if the circuit is pure resistive, the node voltages can be computed using linear equation of (B.1) in which G is a $n \times n$ conductance matrix of the network with n nodes whose diagonal element (i,i) is the summation of all the conductances connected to node i and the off-diagonal element (i,j) is the negative of the conductance between nodes i and j. Vector V is the node voltages and vector I is the external current sources injected to the nodes [11].

$$V(t) = G^{-1} I(t) \tag{B.1}$$

When there are capacitors and/or inductors in the circuit, voltage and current relation in are not in linear form as shown in (B.2). Hence, to implement these integrals in EMT programs, the integrals can be solved numerically in small time steps Δt and get a linear matrix form as before.

$$i_L(t) = i_L(t_0) + \frac{1}{L}\int_{t_0}^{t} v_L(t)dt \qquad , \qquad v_C(t) = v_C(t_0) + \frac{1}{C}\int_{t_0}^{t} i_C(t)dt \tag{B.2}$$

There are several methods to numerically solve the above mentioned integrals in small time steps e.g. Forward Euler, Backward Euler, Trapezoidal, Runge-Kutta [93]. All these methods eventually model the equations (B.2) by a resistance in parallel with a history current source as shown in Figure B.1 [11].

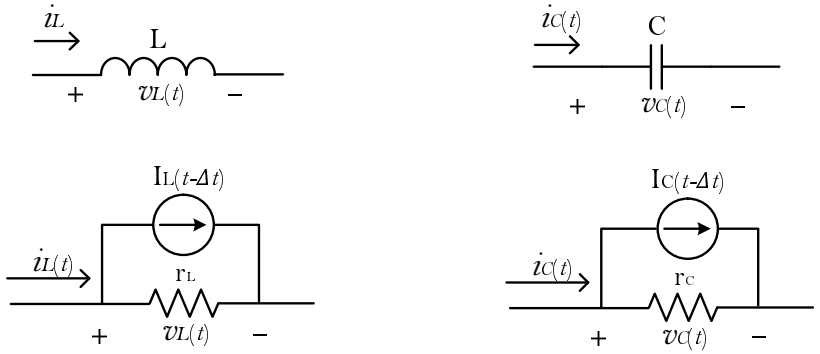

Figure B.1: Inductor and Capacitor equivalent circuits in transient simulation.

In these models, the history current sources come from the previous time step information. The relations for capacitor and inductor history current sources s and the resistances are given in (B.3) where the integrals are solved using trapezoidal rule for one time step Δt.

$$\begin{aligned} &a. \quad I_L(t-\Delta t) = v_L(t-\Delta t)/r_L + i_L(t-\Delta t) \quad , \quad r_L = \frac{2L}{\Delta t} \\ &b. \quad I_C(t-\Delta t) = -v_C(t-\Delta t)/r_C - i_C(t-\Delta t) \quad , \quad r_C = \frac{\Delta t}{2C} \end{aligned} \tag{B.3}$$

With these equivalent models of L and C, all the elements of the network will become either resistances or current sources. Then the nodal analysis of the resulted network will

give the linear equation of (B.4).

$$V(t) = G^{-1}[(I(t) - I_H(t - \Delta t)] \tag{B.4}$$

Vector $[I_H(t - \Delta t)]$ is the history current sources of capacitors and inductors which are calculated from the previous time step information as shown in (B.3).

Furthermore, by combining (B.3) and the equations of the inductor's and capacitor's currents from the Figure B.1, equations of the history current sources can be written in form of recursive equations as shown in (B.5).

$$\begin{aligned} a. \quad & I_L(t - \Delta t) = I_L(t - 2\Delta t) + 2v_L(t - \Delta t)/r_L \\ b. \quad & I_C(t - \Delta t) = -I_C(t - 2\Delta t) - 2v_C(t - \Delta t)/r_C \end{aligned} \tag{B.5}$$

B.2 Transferring '*s*' Domain Functions into an EMT Program

Has mentioned earlier, FDNEs can be fitted with some frequency (or *'s'*) domain functions and then turned into the time domain by recursive convolution.

Considering the frequency domain function $F(s)$ to be product of two frequency domain functions, in time domain it becomes convolution of their corresponding functions as shown in (B.6).

$$F(s) = P(s)Q(s) \qquad \leftrightharpoons \qquad f(t) = p(t) * q(t) \tag{B.6}$$

Where convolution of the two time domain functions is given by;

$$p(t) * q(t) = \int_0^\infty p(\tau)q(t - \tau)d\tau \tag{B.7}$$

Now, assuming $Y(s)$ is the fitted admittance function of an FDNE in the frequency domain in form of (B.8); (Later it will be shown that one of the most popular fitting methods is using this form of function)

$$Y(s) = \sum_{i=1}^{n} \frac{c_i}{s + a_i} \tag{B.8}$$

Then in time domain $y(t)$ would be in form of (B.9);

$$y(t) = \sum_{i=1}^{n} c_i e^{a_i t} \tag{B.9}$$

Now, to solve for current $i(t)$, it can be written as convolution of voltage $v(t)$ and admittance $y(t)$ as shown in (B.10);

$$i(t) = y(t) * u(t) = \int_0^{\infty} y(\tau) u(t - \tau) d\tau \tag{B.10}$$

Substituting (B.9) in (B.10) gives;

$$i(t) = \sum_{i=1}^{n} \int_0^{\infty} c_i u(t - \tau) e^{a_i \tau} d\tau \tag{B.11}$$

Solving the convolution in this form will be time consuming and needs a huge amount of computing burden. A technique is introduced in [35] that makes the convolution done accurately in a discretized and recursive manner which is explained below.

Each of every convolution in (B.11) integral of the exponential terms can be written as follows ;

$$i(t) = \int_0^{\infty} c_i u(t - \tau) e^{a_i \tau} d\tau \tag{B.12}$$

And then decomposed into two parts;

$$i(t) = \int_0^{\Delta t} c_i u(t - \tau) e^{a_i \tau} d\tau + \int_{\Delta t}^{\infty} c_i u(t - \tau) e^{a_i \tau} d\tau \tag{B.13}$$

The right hand side integral with some manipulation can be simplified as;

$$i(t) = \int_0^{\Delta t} c_i u(t - \tau) e^{a_i \tau} d\tau + \int_0^{\infty} c_i u(t - \tau - \Delta t) e^{a_i (\tau + \Delta t)} d\tau \tag{B.14}$$

Comparing (B.12) and the right hand side integral in (B.14) concludes that;

$$i(t) = \int_0^{\Delta t} c_i u(t-\tau) e^{a_i \tau} d\tau + e^{a_i \Delta t}\ i(t-\Delta t) \tag{B.15}$$

Therefore, assuming a linear change in $u(t)$ during the one time step (Δt) and solving the integral and also knowing information from the previous time step, the discretized recursive convolution can be written as [94];

$$i(t) = k_1 u(t-\tau) + k_2 u(t-\tau-\Delta t) + k_3 i(t-\Delta t) \tag{B.16}$$

Where k_1, k_2 and k_3 are given as bellow ;

$$k_1 = -\frac{c_i}{a_i}\left(1 + \frac{1-e^{a_i \Delta t}}{a_i \Delta t}\right) \quad , \quad k_2 = \frac{c_i}{a_i}\left(e^{a_i \Delta t} + \frac{1-e^{a_i \Delta t}}{a_i \Delta t}\right) \quad , \quad k_3 = e^{a_i \Delta t} \tag{B.17}$$

Using this approach, the frequency domain function multiplications can be converted to step by step convolution in time domain simulation and coded in EMT programs very fast and efficiently.

B.3 State Space Method

As mentioned before, electric networks and *'s'* domain functions can be also represented with a set of State Space equations. Then the state space equation can be solved using one of the integration methods.

In electric networks, normally capacitor voltages and inductor currents are selected as state variables. Thus all other current and voltage of the network can be derived as a function of the state variable and input as shown in (B.18).

$$\begin{aligned} a.\quad & \dot{x}(t) = Ax(t) + Bu(t) \\ b.\quad & y(t) = Cx(t) + Du(t) \end{aligned} \tag{B.18}$$

There is a relation between state space matrices ($ABCD$) and the poles (a_i) and residues (c_i) of the frequency domain function of $Y(s)$ which helps to convert it into time domain differential equations as shown in (B.19)and solve it in EMT type programs.

$$Y(s) = \sum_{i=1}^{n} \frac{c_i}{s + a_i} = C(sI - A)^{-1}B + D \tag{B.19}$$

Where

$$\sum_{i=1}^{n} \frac{c_i}{s + a_i} = \begin{bmatrix} c_1 \\ \vdots \\ c_n \end{bmatrix}^T \left(s \begin{pmatrix} 1 & 0 & 0 \\ 0 & \ddots & 0 \\ 0 & 0 & 1 \end{pmatrix} - \begin{pmatrix} a_1 & 0 & 0 \\ 0 & \ddots & 0 \\ 0 & 0 & a_n \end{pmatrix}\right)^{-1} \begin{bmatrix} 1 \\ \vdots \\ 1 \end{bmatrix} \tag{B.20}$$

To solve the differential equation of (B.18), a discrete integration method can be used. For instance, if trapezoidal integration is used, the solution of equation (B.18.a) in one time step (Δt) is given by (B.21).

$$x(t) = x(t - \Delta t) + A\frac{x(t) + x(t - \Delta t)}{2}\Delta t + B\frac{u(t) + u(t - \Delta t)}{2}\Delta t \tag{B.21}$$

Rearranging the (B.21) will result a recursive closed form of (B.22) which gives the state variables as a function of their previous values, $x(t - \Delta t)$, and the input, $u(t)$.

$$x(t) = \left[I - \frac{A\Delta t}{2}\right]^{-1} \left[I + \frac{A\Delta t}{2}\right] x(t - \Delta t) + \left[I - \frac{A\Delta t}{2}\right]^{-1} (B\Delta t)\frac{u(t) + u(t - \Delta t)}{2} \tag{B.22}$$

Equation (B.22) can be simplified as (B.23).

$$\begin{aligned} x(t) &= Gx(t - \Delta t) + Hu^*(t) \\ G &= \left[I - \frac{A\Delta t}{2}\right]^{-1} \left[I + \frac{A\Delta t}{2}\right] \\ H &= \left[I - \frac{A\Delta t}{2}\right]^{-1} (B\Delta t) \\ u^* &= \frac{u(t) + u(t - \Delta t)}{2} \end{aligned} \tag{B.23}$$

Furthermore, after having the state variables, all other voltages and currents in the network now can be calculated at each time step as given by (B.18.b).

Appendix C

Vector Fitting

To fit a tabular function using VF, a rational function $f(s)$ will be considered as given by (C.1) in which residues c_n and poles a_n are real or come in complex conjugate pairs. Also d and h are real quantities. The process of fitting is to find these quantities using the least square approximation.

$$f(s) = \sum_{n=1}^{N} \frac{c_n}{s + a_n} + d + sh \tag{C.1}$$

In order to form a linear problem to compute the unknowns, a set of pols $\overline{a}_n$ are selected and also a function $\sigma(s)$ multiplied by $f(s)$. This gives (C.2);

$$\begin{aligned} I. \qquad \sigma(s)f(s) &= \sum_{n=1}^{N} \frac{c_n}{s + \overline{a}_n} + d + sh \\ II. \qquad \sigma(s) &= \sum_{n=1}^{N} \frac{\overline{c}_n}{s + \overline{a}_n} + 1 \end{aligned} \tag{C.2}$$

Now multiplying the second equation in (C.2) by $f(s)$ yields the following relation;

$$\sum_{n=1}^{N} \frac{c_n}{s + \overline{a}_n} + d + sh = (\sum_{n=1}^{N} \frac{\overline{c}_n}{s + \overline{a}_n} + 1) f(s) \tag{C.3}$$

The relation (C.3) is now a linear problem of unknowns c_n, d, h and $\overline{c}_n$. Then it would yield a form of $Ax = B$ by calculating the (C.3) at several sample points which is an

over-determined problem. To find the unknowns in vector x, the least square problem is solved. [18]

Appendix D

Tables and Data of the Example Cases

D.1 17^{th} order PR function

Table D.1: Elements of the circuit realized for the 17^{th} order *PR* function

Elements ⇒ Block # ⇓	$R_{min}(\Omega)$	$L_z(H)$	$C_z(H)$	$L_1(H)$	$C_2(F)$	$L_2(H)$	$L_3(H)$
1	6.85e-4	∞	0	5.578e-5	1.07e-5	1.09e-4	-3.69e-5
2	0.073	∞	0	2.34e-8	7.29e-7	6.82e-7	-2.26e-8
3	0.013	∞	9.004e-6	0	0	∞	0
4	0.025	∞	0	5.03e-6	4.22e-6	1.04e-5	-3.39e-6
5	0.142	∞	0	1.28e-5	1.10e-4	1.38e-5	-6.64e-6
6	0.010	∞	0	1.97e-6	1.16e-5	3.86e-5	-1.88e-6
7	0.094	∞	0	5.54e-5	2.14e-4	7.83e-5	-3.25e-5
8	0.416	∞	0	3.78e-4	0.0014	9.07e-4	-2.17e-4
9	0.0397	0.0135	0	0	0	∞	0
10	0.078	∞	0.0092	0	0	∞	0

D.2 Portion of Electric Network

- Small T-line sections modeled as L-R circuits: $L = 50\ mH, R = 5\ \Omega$
- RL Loads: $R = 125\ \Omega, L = 180\ mH$

- Filters: 1 $MVAR$ equally distributed between 3^{rd}, 11^{th}&13^{th} double tuned and 24^{th}&26^{th} double tuned HP filters.

- Cable: Resistivity $\rho = 1.68 \times 10^{-8}$ $\Omega.m$, Relative Permittivity $\varepsilon = 4.1$ and Relative Permeability $\mu = 1$ with the configuration as shown in Figure D.1.

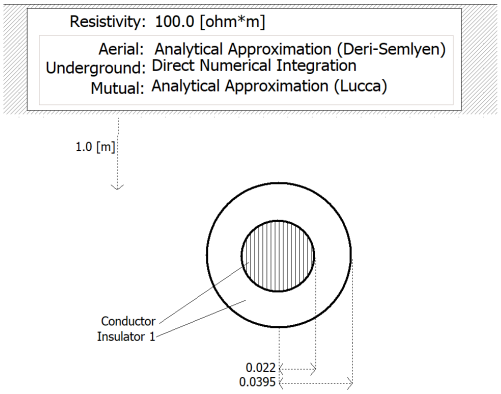

Figure D.1: Configuration of the cable in the single phase electric network example.

Table D.2: Elements of the circuit realized for the single phase network

Elements ⇒ Block # ⇓	$R_{min}(\Omega)$	$L_z(H)$	$L_1(H)$	$C_2(F)$	$L_2(H)$	$L_3(H)$
1	1.989	∞	-0.002	4.29e-7	0.021	0.0022
2	1.973	∞	-0.005	6.36e-7	0.101	0.0057
3	2.059	∞	0.00013	1.64e-6	0.010	-0.0001
4	0.225	∞	-0.0055	1.586e-6	0.057	0.006
5	24.790	∞	0.0314	4.13e-6	0.086	-0.023
6	2.877	∞	0.0333	2.97e-5	0.083	-0.024
7	6.806	∞	0.0075	2.98e-6	0.047	-0.0064
8	13.772	∞	0.0175	1.52e-5	0.066	-0.0139
9	11.172	∞	0.00084	1.88e-6	0.0397	-0.0008
10	2.112	0.0743	0	0	∞	0
11	11.291	0.0876	0	0	∞	0
12	1.216	∞	0.00137	1.57e-6	∞	-0.0013
13	4.981	∞	0.00069	1.76e-6	∞	-0.0007

D.3 Two Ports Network

Table D.3: Elements of the two ports network realized

Blocks # ⇒ Elements ⇓	**1**	**2**	**3**	**4**	**5**
$L_{sr}(H)$	66.6667	20.000	-	-	-
$t^2_{\infty p}$	1	0	-	-	-
$C_{sr}(F)$	-	-	2.5100e-04	-	-
t^2_{0p}	-	-	0.7071	-	-
$R_{min}(\Omega)$	-	-	-	5.00000	10.5537
$L_1(H)$	-	-	-	-0.0598	-0.0505
$t^2_1(H)$	-	-	-	-1	1
$L_2(H)$	-	-	-	0.5456	0.0064
$C_2(H)$	-	-	-	2.0153e-05	2.4577e-05
t^2_2	-	-	-	-5.6215e-07	-0.7036
$L_3(H)$	-	-	-	0.0598	0.1621

Appendix E

Matrices of the DAE Representation

Differential algebraic equations of the network in Figure 3.1 yield the matrix representation in (E.1) is provided here for instance. The representation of multi-port networks is analogous to this. It can be seen that rows number 8 and 9 in matrix M are linearly dependent which is making it a singular matrix.

$$
\begin{pmatrix}
1 & 0 & 0 & 0 & 0 & 0 & 0 & 0 & 0 & 0 \\
0 & C_{sh} & 0 & 0 & 0 & 0 & 0 & 0 & 0 & 0 \\
0 & 0 & C_z & 0 & 0 & 0 & 0 & 0 & 0 & m \\
0 & 0 & 0 & C_2 & 0 & 0 & 0 & 0 & 0 & 1-m \\
0 & R_{min}C_{sh} & 0 & 0 & -L_{sr} & 0 & 0 & (1-m)L & -R_{min} & 0 \\
0 & 0 & 0 & 0 & 0 & 1 & 0 & 0 & 0 & 0 \\
0 & 0 & 0 & 0 & 0 & 0 & 1 & 0 & 0 & 0 \\
0 & 0 & 0 & 0 & 0 & 0 & 0 & 1 & 0 & 0 \\
0 & 0 & 0 & 0 & 0 & 0 & 0 & m & 0 & 0 \\
0 & -C_{sh} & -C_z & 0 & 0 & 0 & 0 & 0 & 1 & -m
\end{pmatrix}
\begin{bmatrix}
\dot{v_{sr}} \\ \dot{v_{sh}} \\ \dot{v_z} \\ \dot{v_2} \\ \dot{i_{sr}} \\ \dot{i_{sh}} \\ \dot{i_z} \\ \dot{i_L} \\ i_{S1} \\ i_{R1}
\end{bmatrix} =
$$

$$
\begin{pmatrix}
0 & 0 & 0 & 0 & 1/C_{sr} & 0 & 0 & 0 & 0 & 0 \\
0 & -1/R_{min} & 1/R_{min} & 0 & 1 & -1 & 0 & 0 & 0 & 0 \\
0 & 1/R_{min} & -1/R_{min} & 0 & 0 & 0 & 1 & -1 & 0 & 0 \\
0 & 0 & 0 & 0 & 0 & 0 & 0 & 1 & 0 & 0 \\
1 & 0 & 0 & 0 & 0 & -R_{min} & 0 & 0 & -1 & 1 \\
0 & 1/L_{sh} & 0 & 0 & 0 & 0 & 0 & 0 & 0 & 0 \\
0 & 0 & 1/L_z & 0 & 0 & 0 & 0 & 0 & 0 & 0 \\
0 & 0 & 1/L & -1/L & 0 & 0 & 0 & 0 & 0 & 0 \\
0 & 0 & 0 & -1/L & 0 & 0 & 0 & 0 & 0 & 1/L \\
0 & 0 & 0 & 0 & 0 & 1 & 1 & 1 & 0 & 0
\end{pmatrix}
\begin{bmatrix}
v_{sr} \\ v_{sh} \\ v_z \\ v_2 \\ i_{sr} \\ i_{sh} \\ i_z \\ i_L \\ v_{S1} \\ v_{R1}
\end{bmatrix}
\tag{E.1}
$$

References

[1] A. Ubolli and B. Gustavsen, "Multiport frequency-dependent network equivalencing based on simulated time-domain responses," *IEEE Transactions on Power Delivery*, vol. 27, pp. 648–657, April 2012.

[2] K. Sheshyekani and B. Tabei, "Multiport frequency-dependent network equivalent using a modified matrix pencil method," *IEEE Transactions on Power Delivery*, vol. 29, pp. 2340–2348, Oct 2014.

[3] A. S. Morched, J. H. Ottevangers, and L. Marti, "Multi-port frequency dependent network equivalents for the emtp," *IEEE Transactions on Power Delivery*, vol. 8, pp. 1402–1412, July 1993.

[4] N. G. Hingorani and M. F. Burbery, "Simulation of ac system impedance in hvdc system studies," *IEEE Transactions on Power Apparatus and Systems*, vol. PAS-89, pp. 820–828, May 1970.

[5] A. Clerici and L. Marzio, "Coordinated use of tna and digital computer for switching-surge studies: Transient equivalent of a complex network," *IEEE Transactions on Power Apparatus and Systems*, vol. PAS-89, pp. 1717–1726, Nov 1970.

[6] A. Morched, L. Marti, and J. Ottevangers, "A high frequency transformer model for the emtp," *IEEE Transactions on Power Delivery*, vol. 8, pp. 1615–1626, July 1993.

[7] V. Q. Do and M. M. Gavrilovic, "An iterative pole-removal method for synthesis of power system equivalent networks," *IEEE Power Engineering Review*, vol. PER-4, pp. 42–43, Aug 1984.

[8] V. Q. Do and M. M. Gavrilovic, "A synthesis method for one-port and multi-port equivalent networks for analysis of power system transients," *IEEE Power Engineering Review*, vol. PER-6, pp. 37–38, April 1986.

[9] N. R. Watson and J. Arrillaga, "Frequency-dependent ac system equivalents for harmonic studies and transient convertor simulation," *IEEE Transactions on Power Delivery*, vol. 3, pp. 1196–1203, Jul 1988.

[10] A. Morched and V. Brandwajn, "Transmission network equivalents for electromagnetic transients studies," *IEEE Transactions on Power Apparatus and Systems*, vol. PAS-102, no. 9, p. 2984–2994, 1983.

[11] H. W. Dommel, "Digital computer solution of electromagnetic transients in single-and multiphase networks," *IEEE Transactions on Power Apparatus and Systems*, vol. PAS-88, pp. 388–399, April 1969.

[12] Y. Huangfu, L. Di Rienzo, and S. Wang, "Frequency-dependent multi-conductor transmission line model for shielded power cables considering geometrical dissymmetry," *IEEE Transactions on Magnetics*, vol. 54, pp. 1–4, March 2018.

[13] M. Cervantes, I. Kocar, J. Mahseredjian, and A. Ramirez, "Partitioned fitting and dc correction for the simulation of electromagnetic transients in transmission lines/cables," *IEEE Transactions on Power Delivery*, vol. 33, pp. 3246–3248, Dec 2018.

[14] A. Cataliotti, A. Daidone, and G. Tine, "A medium-voltage cables model for power-line communication," *IEEE Transactions on Power Delivery*, vol. 24, pp. 129–135, Jan 2009.

[15] Y. Hu, W. Wu, A. M. Gole, and B. Zhang, "A guaranteed and efficient method to enforce passivity of frequency-dependent network equivalents," *IEEE Transactions on Power Systems*, vol. 32, pp. 2455–2463, May 2017.

[16] Y. Hu, W. Wu, and B. Zhang, "A semidefinite programming model for passivity enforcement of frequency-dependent network equivalents," *IEEE Transactions on Power Delivery*, vol. 31, pp. 397–399, Feb 2016.

[17] Y. Liang, X. Lin, A. M. Gole, and M. Yu, "Improved coherency-based wide-band equivalents for real-time digital simulators," *IEEE Transactions on Power Systems*, vol. 26, pp. 1410–1417, Aug 2011.

[18] Z. Xiaofeng, Y. Shihao, Z. Desheng, and S. Jie, "Research on application of fdne based on rtds and comparison analysis of fault transient of shanghai sijing power grid," *The Journal of Engineering*, vol. 2019, no. 16, pp. 1393–1397, 2019.

[19] B. Porkar, M. Vakilian, R. Feuillet, M. Ghassemi, and A. Akhavan, "Multi-port frequency-dependent network equivalent for electromagnetic transient studies," in *Proceedings of the 37th Annual North American Power Symposium, 2005.*, pp. 287–295, Oct 2005.

[20] A. Thakallapelli and S. Kamalasadan, "Optimization based real-time frequency dependent reduced order modeling of power grid," in *2017 IEEE Power Energy Society General Meeting*, pp. 1–5, July 2017.

[21] Y. Hu, W. Wu, B. Zhang, and Q. Guo, "Development of an rtds-tsa hybrid transient simulation platform with frequency dependent network equivalents," in *IEEE PES ISGT Europe 2013*, pp. 1–5, Oct 2013.

[22] S. H. Hosseinian, B. Vahidi, and J. Bieza, "Frequency dependent network equivalents for harmonic and transient studies," in *TENCON 2006 - 2006 IEEE Region 10 Conference*, pp. 1–4, Nov 2006.

[23] M. M. Almalki, M. I. Chehardeh, and C. J. Hatziadoniu, "Capacitor bank switching transient analysis using frequency dependent network equivalents," in *2015 North American Power Symposium (NAPS)*, pp. 1–6, Oct 2015.

[24] B. Gustavsen, "Computer code for rational approximation of frequency dependent admittance matrices," *IEEE Transactions on Power Delivery*, vol. 17, pp. 1093–1098, Oct 2002.

[25] B. Gustavsen and A. Semlyen, "A robust approach for system identification in the frequency domain," *IEEE Transactions on Power Delivery*, vol. 19, pp. 1167–1173, July 2004.

[26] X. Lin, A. M. Gole, and M. Yu, "A wide-band multi-port system equivalent for real-time digital power system simulators," *IEEE Transactions on Power Systems*, vol. 24, pp. 237–249, Feb 2009.

[27] Xiao Jiang and A. M. Gole, "A frequency scanning method for the identification of harmonic instabilities in hvdc systems," *IEEE Transactions on Power Delivery*, vol. 10, pp. 1875–1881, Oct 1995.

[28] B. Gustavsen and A. Semlyen, "Simulation of transmission line transients using vector fitting and modal decomposition," *IEEE Transactions on Power Delivery*, vol. 13, pp. 605–614, April 1998.

[29] A. O. Soysal and A. Semlyen, "Practical transfer function estimation and its application to wide frequency range representation of transformers," *IEEE Transactions on Power Delivery*, vol. 8, pp. 1627–1637, July 1993.

[30] L. P. R. K. Ihlenfeld, G. H. C. Oliveira, and M. R. Sans, "A data passivity-enforcement preprocessing approach to multiport system modeling," *IEEE Transactions on Power Delivery*, vol. 31, no. 3, pp. 1351–1359, 2016.

[31] R. M. Foster, "A reactance theorem," *Bell System Technical Journal*, vol. 3, p. 259–267, November 1924.

[32] A. Semlyen and A. Dabuleanu, "Propagation of travelling waves on transmission lines - frequency dependent parameters," *IEEE Transactions on Power Apparatus and Systems*, vol. PAS-91, pp. 85–91, Jan 1972.

[33] W. Meyer and H. Dommel, "Numerical modelling of frequency-dependent transmission-line parameters in an electromagnetic transients program," *IEEE Transactions on Power Apparatus and Systems*, vol. PAS-93, no. 5, p. 1401–1409, 1974.

[34] J. R. Marti, "Accurate modelling of frequency-dependent transmission lines in electromagnetic transient simulations," *IEEE Transactions on Power Apparatus and Systems*, vol. PAS-101, pp. 147–157, Jan 1982.

[35] A. Semlyen and A. Dabuleanu, "Fast and accurate switching transient calculations on transmission lines with ground return using recursive convolutions," *IEEE Transactions on Power Apparatus and Systems*, vol. 94, pp. 561–571, Mar 1975.

[36] M. Kizilcay, "Computation of switching transients using low-order, multi-port network equivalents," in *International Conference on Power Systems Transients (IPST97)*, June 1997.

[37] B. Gustavsen and A. Semlyen, "Rational approximation of frequency domain responses by vector fitting," *IEEE Transactions on Power Delivery*, vol. 14, pp. 1052–1061, July 1999.

[38] B. Gustavsen, G. Irwin, R. Mangelrød, D. Brandt, and K. Kent, "Transmission line models for the simulation of interaction phenomena between parallel ac and dc overhead lines," in *International Conference on Power Systems Transients (IPST'99)*, June 1999.

[39] A. Morched, B. Gustavsen, and M. Tartibi, "A universal model for accurate calculation of electromagnetic transients on overhead lines and underground cables," *IEEE Transactions on Power Delivery*, vol. 14, pp. 1032–1038, July 1999.

[40] Y. Hu, W. Wu, and B. Zhang, "A fast method to identify the order of frequency-dependent network equivalents," *IEEE Transactions on Power Systems*, vol. 31, pp. 54–62, Jan 2016.

[41] B. Gustavsen, "Computer code for rational approximation of frequency dependent admittance matrices," *IEEE Transactions on Power Delivery*, vol. 17, pp. 1093–1098, Oct 2002.

[42] D. Deschrijver, B. Gustavsen, and T. Dhaene, "Causality preserving passivity enforcement for traveling-wave-type transmission-line models," *IEEE Transactions on Power Delivery*, vol. 24, pp. 2461–2462, Oct 2009.

[43] B. Gustavsen and A. Semlyen, "Enforcing passivity for admittance matrices approximated by rational functions," *IEEE Transactions on Power Systems*, vol. 16, pp. 97–104, Feb 2001.

[44] B. Gustavsen, "Frequency-dependent transmission line modeling utilizing transposed conditions," *IEEE Transactions on Power Delivery*, vol. 17, pp. 834–839, July 2002.

[45] D. Deschrijver, B. Gustavsen, and T. Dhaene, "Advancements in iterative methods for rational approximation in the frequency domain," *IEEE Transactions on Power Delivery*, vol. 22, pp. 1633–1642, July 2007.

[46] A. Ramirez, "Vector fitting-based calculation of frequency-dependent network equivalents by frequency partitioning and model-order reduction," *IEEE Transactions on Power Delivery*, vol. 24, pp. 410–415, Jan 2009.

[47] E. Medina and A. Ramirez, "Svd-based reduced-order rational approximation on specific frequency bandwidth," in *2015 North American Power Symposium (NAPS)*, pp. 1–6, Oct 2015.

[48] A. Thakallapelli and S. Kamalasadan, "An online reduced order modeling based frequency regulation adaptive control architecture for wind integrated power grid," in *2018 IEEE Industry Applications Society Annual Meeting (IAS)*, pp. 1–8, Sep. 2018.

[49] A. Thakallapelli, S. Ghosh, and S. Kamalasadan, "Real-time frequency based reduced order modeling of large power grid," in *2016 IEEE Power and Energy Society General Meeting (PESGM)*, pp. 1–5, July 2016.

[50] A. Ramirez, A. Mehrizi-Sani, D. Hussein, M. Matar, M. Abdel-Rahman, J. Jesus Chavez, A. Davoudi, and S. Kamalasadan, "Application of balanced realizations for model-order reduction of dynamic power system equivalents," *IEEE Transactions on Power Delivery*, vol. 31, pp. 2304–2312, Oct 2016.

[51] Y. Hu, W. Wu, and B. Zhang, "Compacting and partitioning-based simulation solution for frequency-dependent network equivalents in real-time digital simulator," *IET Generation, Transmission Distribution*, vol. 9, no. 16, pp. 2526–2533, 2015.

[52] B. Gustavsen, "Wide band modeling of power transformers," *IEEE Transactions on Power Delivery*, vol. 19, pp. 414–422, Jan 2004.

[53] L. Ling, S. Nai-qiu, C. Yun-ping, P. Chun-ming, and L. Min, "Study on grid-based seamless-link hybrid simulation system for power networks," in *2006 International Conference on Power System Technology*, pp. 1–4, Oct 2006.

[54] H. Bode, *Network Analysis and Feedback Amplifier Design.* New York: Van Nostrand, 1945.

[55] O. Brune, "Synthesis of a finite two-terminal network whose driving-point impedance is a prescribed function of frequency," *Journal of Math and Physics*, vol. 10, pp. 191–236, 1931.

[56] F. Mukhtar, J. A. Russer, S. Wane, D. Bajon, A. Kuo, and P. Russer, "Brune's four-port equivalent circuit models for mmmwics," in *2014 44th European Microwave Conference*, pp. 564–567, Oct 2014.

[57] F. Mukhtar, J. A. Russer, Y. Kuznetsov, and P. Russer, "Methodology for generation of brune's equivalent circuit models for linear passive reciprocal multi-ports," in *2012 International Conference on Electromagnetics in Advanced Applications*, pp. 674–677, Sept 2012.

[58] F. Mukhtar, Y. Kuznetsov, C. Hoffmann, and P. Russer, "Brune's synthesis of linear lossy distributed one-port and symmetric two-port microwave circuits," in *2011 German Microwave Conference*, pp. 1–4, March 2011.

[59] J. A. Russer, F. Mukhtar, A. Gorbunova, A. Baev, Y. V. Kuznetsov, and P. Russer, "A brune's two-port process applied to lumped element filter modeling," in *2013 IEEE MTT-S International Microwave Symposium Digest (MTT)*, pp. 1–4, June 2013.

[60] F. Mukhtar and P. Russer, "Brune's algorithm for lumped element equivalent circuit synthesis of linear lossy multiports," *AEU - International Journal of Electronics and Communications*, vol. 76, 09 2016.

[61] A. C. S. Lima, B. Gustavsen, and A. B. Fernandes, "Inaccuracies in network realization of rational models due to finite precision of rlc branches," in *International Conference on Power Systems Transients (IPST'07)*, June 2007.

[62] B. Gustavsen, "Fast passivity enforcement for pole-residue models by perturbation of residue matrix eigenvalues," *IEEE Transactions on Power Delivery*, vol. 23, pp. 2278–2285, Oct 2008.

[63] B. Gustavsen, "Passivity enforcement of rational models via modal perturbation," *IEEE Transactions on Power Delivery*, vol. 23, pp. 768–775, April 2008.

[64] B. Gustavsen, "Passivity enforcement for transmission line models based on the method of characteristics," *IEEE Transactions on Power Delivery*, vol. 23, pp. 2286–2293, Oct 2008.

[65] S. Grivet-Talocia, "Passivity enforcement via perturbation of hamiltonian matrices," *IEEE Transactions on Circuits and Systems I: Regular Papers*, vol. 51, pp. 1755–1769, Sep. 2004.

[66] J. Morales, J. Mahseredjian, K. Sheshyekani, A. Ramirez, E. Medina, and I. Kocar, "Pole-selective residue perturbation technique for passivity enforcement of fdnes," *IEEE Transactions on Power Delivery*, vol. 33, pp. 2746–2754, Dec 2018.

[67] L. P. R. K. Ihlenfeld, G. H. C. Oliveira, and M. R. Sans, "A data passivity-enforcement preprocessing approach to multiport system modeling," *IEEE Transactions on Power Delivery*, vol. 31, pp. 1351–1359, June 2016.

[68] B. Gustavsen and A. Semlyen, "On passivity tests for unsymmetrical models," *IEEE Transactions on Power Delivery*, vol. 24, pp. 1739–1741, July 2009.

[69] B. Porkar, M. Vakilian, R. Iravani, and S. M. Shahrtash, "Passivity enforcement using an infeasible-interior-point primal-dual method," *IEEE Transactions on Power Systems*, vol. 23, pp. 966–974, Aug 2008.

[70] B. D. H. Tellegen, "Synthesis of 2n-poles by networks containing the minimum number of elements," *Journal of Math and Physics*, vol. 32, pp. 1–18, Apr. 1953.

[71] W. Cauer, "Die verwirklichung von wechselstromwiderstanden vorgeschriebener frequenzabhangigkeit.","*Archiv fur Elektrotechnic*, vol. 17, pp. 355–388, 1926.

[72] S. Darlington, "Synthesis of reactance 4-poles.," *Journal of Math and Physics*, vol. 18, pp. 257–353, 1939.

[73] R. Bott and R. J. Duffin, "Impedance synthesis without use of transformers," *Journal of Applied Physics*, vol. 20, no. 8, pp. 816–816, 1949.

[74] F. M. Reza, "A supplement to the brune synthesis," *Transactions of the American Institute of Electrical Engineers, Part I: Communication and Electronics*, vol. 74, no. 1, pp. 85–90, 1955.

[75] F. Miyata, "Synthesis of a one-port utilizing lattice construction," *IEEE Transactions on Circuit Theory*, vol. 10, no. 2, pp. 227–234, 1963.

[76] B. McMillan, "Introduction to formal realizability theory.," *Bell System Technical Jour.*, vol. 31, no. 2, pp. 217–279,541–600, 1952.

[77] J. H. Westcott, "Driving-point impedance synthesis with maximally lossy elements.," in *Proceedings of the Symposium 0Synthesis, Polytechnic Institute of Brooklyn*, 1955.

[78] H. Ozaki, "Synthesis of three-terminal network without ideal transformer.," in *Technology Reports of the Osaka University,*, vol. 3, (Osaka, Japan), 1953.

[79] Y. Oono, "Synthesrs of a finite 2n-terminal network by a group of networks, each of which contains only one ohmic resistance.," *Journal of Math and Physics*, vol. 29, pp. 13–26, 1950.

[80] L. Weinberg, "New synthesis procedures for realizing transfer functions of rlc and rc networks.," tech. rep., Massachusetts Institute of Technology,Research Laboratory Electronics,, 201. 1951.

[81] M. C. Smith, "Synthesis of mechanical networks: the inerter," *IEEE Transactions on Automatic Control*, vol. 47, pp. 1648–1662, Oct 2002.

[82] O. Wing, *Classical Circuit Theory.* New York: Springer, 2008.

[83] H. K. Khalil, *Nonlinear Systems.* Upper Saddle River, N.J.: Prentice-Hall, 2002.

[84] M. Ahmadi and A. M. Gole, "A new approach to model frequency dependent network equivalents in transient simulation tools," in *International Conference on Power Systems Transients (IPST2017)*, June 2017.

[85] N. Balabanian, *Network Synthesis.* Englewood Cliffs, N.J.: Prentice-Hall, 1958.

[86] K. K. M. A. Kariyawasam, S. Fan, A. M. Gole, and H. M. J. S. P. De Silva, "Accurate validation of electromagnetic transient models of cascaded power transmission systems," in *2016 IEEE Power and Energy Society General Meeting (PESGM)*, pp. 1–5, 2016.

[87] A. Kariyawasam, *Improving the Numerical Accuracy of Models of Sector-shaped and Cross-bonded Cable Systems.* PhD thesis, University of Manitoba, Winnipeg, MB, Canada, 2016.

[88] J. A. B. Faria and R. Araneo, "Computation, properties, and realizability of the characteristic immittance matrices of nonuniform multiconductor transmission lines," *IEEE Transactions on Power Delivery*, vol. 33, no. 4, pp. 1885–1894, 2018.

[89] L. Brančík, "Modified nodal analysis and state variable descriptions for mtls systems solution in matlab," in *2013 36th International Conference on Telecommunications and Signal Processing (TSP)*, pp. 354–357, 2013.

[90] N. Banagaaya, G. Alì, and W. Schilders, *Index-aware Model Order Reduction Methods - Applications to Differential-Algebraic Equations.* Paris: Atlantis Press, 2016.

[91] M. Ahmadi, S. Fan, H. Zhao, and A. M. Gole, "Efficient implementation of frequency dependent network equivalents using state space models of cascaded sub-circuits," in *International Conference on Power Systems Transients (IPST2019)*, June 2019.

[92] Chung-Wen Ho, A. Ruehli, and P. Brennan, "The modified nodal approach to network analysis," *IEEE Transactions on Circuits and Systems*, vol. 22, pp. 504–509, June 1975.

[93] X. Fu, S. Mouhamadou Seye, J. Mahseredjian, M. Cai, and C. Dufour, "A comparison of numerical integration methods and discontinuity treatment for emt simulations," in *2018 Power Systems Computation Conference (PSCC)*, pp. 1–7, June 2018.

[94] J. D. silva, *Accuracy and Stability Improvements in the Electromagnetic Simulations of Power Transmission Lines and Cables*. PhD thesis, University of Manitoba, Winnipeg, MB, Canada, 2008.